

Developing an M₃ Antagonist for Molecular Imaging of Muscarinic Acetylcholine
Receptors in Breast Cancer

by

Maxwell Akuamoah Boateng

A thesis submitted in partial fulfillment of the requirements for the degree of

Master of Science

Department of Chemistry

University of Alberta

© Maxwell Akuamoah Boateng, 2021

Abstract

The lack of the three targeted receptors, estrogen, progesterone, and the human epidermal growth factor receptor 2, causes difficulty in treating triple negative type cancers. Most often, patients with this type of malignancy have a low chance of survival. The focus of this work will be on constructing a molecular antagonist to detect the overexpression of a receptor subtype. The category of tumor under research is the triple negative type of breast cancer. Only about 30% of women are rated to survive this class of growth, especially at the metastatic stage when the cancer has spread to various parts of the body. Studies have shown that the M₃ subtype of the muscarinic acetylcholine receptor is overexpressed at the fourth and last stages of the carcinoma. In the numerous efforts of developing an M₃ antagonist, the greatest challenge has been identifying a compound with a high selectivity towards the M₃ receptor antagonist due to its similarities with the M₂ subtype in their binding pocket. Based on an article published in the “Journal of Medicinal Chemistry” in 2002 by Ohtake and his group at the Banyu Tsukuba Research Institute, a novel molecule with structural features like previously reported nonselective muscarinic antagonists was discovered showing high selectivity for M₃ receptors over the other subtypes. The subtype of interest was that of M₂/M₃ = 98-fold.

I adopted the structural features published in the article with alterations at the cationic site and the hydrophobic region to create a library of six compounds that had properties for potential radiolabelling in a future project. The six compounds were screened against all five subtypes of the muscarinic acetylcholine receptor for radioligand binding competition assay. The IC₅₀ values to M₃ receptors of two of the compounds, **47**

(0.35 μM) and **45** (0.448 μM) had promising results. The two compounds, in particular **47**, showed high selectivity for M_3 receptors over the other muscarinic receptor subtypes: **47** ($M_1/M_3 = 66$ -fold, $M_2/M_3 = 73$ -fold, $M_4/M_3 = 62$ -fold, $M_5/M_3 = 37$ -fold) and **45** ($M_1/M_3 = 31$ -fold, $M_2/M_3 = 31$ -fold, $M_4/M_3 = 30$ -fold, $M_5/M_3 = 37$ -fold).

Preface

This thesis is an original work composed by myself, Maxwell A. Boateng, and I am responsible for all the synthesis and characterization of intermediates and target molecules. This thesis was conducted under the supervision of Dr. Frederick West and co-supervised by Dr. Frank Wuest.

All figures and schemes in Chapter 1 and Chapter 2 are taken from journals that are open access articles under the Creative Commons Attribution Licence (CC BY).

I completed the unpublished work in Chapter 2 and with the help of Dr. Atul Bhardwaj, the molecular docking experiments were carried out.

Dedicated to my Lord and Saviour Jesus Christ

and to my lovely family:

Dad, Mum, Gideon, Daniel, and Angel Rose.

Acknowledgement

First, I would like to thank my supervisor Dr. Frederick West and co-supervisor Dr. Frank Wuest for the immense support, encouragement, and guidance they provided me over the past three years. I am privileged to have had this amazing opportunity to work with extraordinary supervisors.

I would also like to thank Dr. John Vederas, a member of my committee, for the guidance and suggestions during my MSc program. In addition, Dr. Randy Whittal, Bela Reiz, Wayne Moffat, Jennifer Jones, Ed Fu, Dr. Ryan McKay, Mark Miskolzie, Cody Bergman, Dr. Jatinder Kaur, and Dr. Susan Pike for their instrumental assistance in obtaining the compound characterizations required for my project and Dr. Atul Bhardwaj for the molecular docking experiments. I am also grateful for the help from the graduate student assistant Anita Weiler.

My appreciation also goes to the incredible lab mates of the West and Wuest group for all their suggestions and help in the lab. I have learned a lot from former and current members of both groups and the experience I have gained from them will hold for a lifetime. An extra thanks to Cara Perozok and PhD candidates, Natasha Rana and James Donnelly, who helped to revise my thesis. Finally, I am thankful to my parents and siblings for their love and support throughout.

A special thanks also goes to the Kipnes Foundation and to the U of A Faculty of Graduate Studies and Research for funding this project.

Table of Contents

Chapter 1: Introduction	1
1.1 General Introduction to Muscarinic Receptors.....	2
1.1.1 Muscarinic Receptors as G Protein-Coupled Receptors.....	3
1.1.2 Acetylcholine as a Neurotransmitter	7
1.1.2.1 Acetylcholine Synthesis	9
1.1.2.2 Acetylcholine Storage	10
1.1.2.3 Acetylcholine Release.....	11
1.2 Muscarinic Acetylcholine Receptor Binding Ligands	14
1.2.1 Agonists.....	15
1.2.2 Antagonists.....	16
1.3 Neurotransmitter Receptors.....	19
1.3.1 Nicotinic	20
1.3.2 Muscarinic Binding Sites.....	21
1.3.3 Muscarinic Receptor's Role in Cancer Progression.....	23
1.3.3.1 Role of M ₃ subtype in breast cancer	24
1.4 The Hypothesis of the Thesis	27
1.4.1 Thesis Goals.....	28

Chapter 2: Results and Discussion	30
2.1 Previous Work	31
2.2 Design and Synthesis	38
2.3 Conclusions and Future Plans	57
2.4 Experimental Section.....	58
REFERENCES.....	77
APPENDIX: NMR spectra	92

List of Tables

Table 1. Binding affinities of compounds to human muscarinic receptor subtypes ⁸⁶	35
Table 2. Structures of amino acid spacers used in human muscarinic receptor subtypes binding assay	36
Table 3. Reaction conditions of the unsuccessful routes to N-(4-fluoro)butyl product ..	45
Table 4. Binding affinities of target compounds to muscarinic subtypes	53

List of Figures

Figure 1: Overall structure of a G protein-coupled receptor (GPCR), with description of the connectivity of the intracellular (IL) and extracellular (EL) loops between the helices (H)¹² 5

Figure 2: a) The crystal structure of the inactive resting state of Gtαβγ heterotrimer with GDP (Green: Gα, Cyan: Gβ, Magenta: Gγ).¹⁶ b) The crystal structure of the active Gtα subunit with GTPγS¹⁶ 6

Figure 3: Role of acetyl-CoA from glucose metabolism and choline from SDHACU²⁷ .. 10

Figure 4: ACh absorption by VAChT and storage in neurotransmitter vesicles with exchange of H⁺ for ACh²⁷ 11

Figure 5: Ca²⁺ dependent ACh release^{27, 44} 12

Figure 6: Structures of agonist (a and b) and antagonists of ACh receptors¹⁰ 14

Figure 7: a) Methacholine; b) Carbachol ; c) Pilocarpine; d) Bethanechol; direct agonists of muscarinic acetylcholine receptors..... 16

Figure 8: Nicotinic acetylcholine receptor²⁷ 20

Figure 9: Structures and binding affinities of QNB and tiotropium⁷⁵ 22

Figure 10: Comparing the active binding sites of M2R and M3R⁷⁵ 23

Figure 11: The stages of breast cancer⁸⁹ 26

Figure 12: Left: breast cancer cell fueled by hormones and protein: violet: estrogen, green: progesterone, velvet: protein HER2, red balls: inhibitors. Right: triple negative breast cancer cell lacking target hormones and protein	27
Figure 13: Expression of M ₂ and M ₃ subtypes in breast cancer ⁸⁶	28
Figure 14: Structural features of muscarinic antagonists ⁸⁶	29
Figure 15: Reported M ₂ -sparing M ₃ antagonists ⁸⁶	31
Figure 16: Structural features of muscarinic antagonists ⁸⁶	32
Figure 17: 25 carboxylic acids for the aromatic cluster position ⁸⁶	33
Figure 18: Selected hydrophobic compounds for hydrophobic site on scaffold	43
Figure 19: Enantiomers of aminomethyl piperidine	46
Figure 20: Compounds for GPCR screening of muscarinic acetylcholine receptor subtypes M ₁ – M ₅	51
Figure 21: a) superposition of all six compounds in the M ₃ receptor; b) compound 47 docked in M ₃ receptor	55
Figure 22: Interaction of lead compound 47 with muscarinic subtype M ₃ receptor. H-bonding (purple); π-π stacking (green); π-cation (red).....	55

List of Schemes

Scheme 1: Reaction scheme of the synthesis of acetylcholine	9
Scheme 2: Synthetic route using alkyl resin ⁸⁶	34
Scheme 3: Amide coupling of Boc-glycine with β -alanyl methyl ester	38
Scheme 4: Different reagents of amide coupling of boc-glycine with β -alanyl methyl ester	39
Scheme 5: Amide coupling between triphenylpropionic acid and glycine methyl ester	40
Scheme 6: Synthetic route to piperidine derivatives	41
Scheme 7: Synthesis of model compound.....	42
Scheme 8: N-alkylation of alkyl tosylate	43
Scheme 9: Unsuccessful routes to N-(4-fluoro)butyl product.....	44
Scheme 10: Reductive amination and acylation reaction with the model compound....	46
Scheme 11: Reductive amination and acylation on target compound	47
Scheme 12: Amide coupling and boc-deprotection to yield (S)-3-(aminomethyl)piperidine derivative	48
Scheme 13: Amide coupling and boc-deprotection to yield (R)-3-(aminomethyl)piperidine derivative.....	48

Scheme 14: Reductive amination and acylation on (S)-3-(aminomethyl)piperidine derivative 42	49
Scheme 15: Reductive amination and acylation on (R)-3-(aminomethyl)piperidine derivative 44	49
Scheme 16: Example of radiofluorination reaction	57

List of Abbreviations

AA: Amino acid

AChE: Acetyl cholinesterase

Ach: Acetylcholine

Acp: 6-aminohexanoic acid

CAM: Crassulacean acid metabolism

cAMP: Cyclic adenosine monophosphate

ChAT: Choline acetyltransferase

CNS: Central nervous system

CODP: Chronic obstructive pulmonary disease

DCM: Dichloromethane

DIEA: N, N-Diisopropylethylamine

ECL: Extracellular loop

EDC: 1-(3-Dimethylaminopropyl)-3-ethylcarbodiimide

EL: Extracellular

ERK: Extracellular-signal-regulated kinase

Et₃N: Triethylamine

FDA: Food and drugs administration

GABA: Gamma-aminobutyric acid

GDP: Guanine diphosphate

GPCRs: G protein coupled receptors

GTP: Guanine triphosphate

HER2: Human epidermic receptor 2

HOBt: Hydroxybenzotriazole

ICL: Intracellular loop

IL: Intracellular

mAChRs: Muscarinic acetylcholine receptors

MRAs: Muscarinic receptor antagonists

nAChRs: Nicotinic acetylcholine receptors

NMS: N-methylscopolamine

Phe: Phenylalanine

PKC: Protein kinase

PLC: Phospholipase C

PLD: Phospholipase D

PNS: Peripheral nervous system

PyBOP: Benzotriazol-1-yloxytripyrrolidinophosphonium hexafluorophosphate

QNB: Quinuclidinyl benzylate

SDHACU: Sodium-dependent high-affinity choline intake

SiRNA: Small interfering ribonucleic acid

SRC: Sarcoma

Thr: Threonine

TM: Transmembrane

Trp: Tryptophan

VACHT: Vesicular acetylcholine transporter

Val: Valine

VEGF-A: Vascular endothelial growth factor-A

Chapter 1: Introduction

1.1 General Introduction to Muscarinic Receptors

Muscarinic receptors are transmembrane receptors also known as metabotropic receptors of neuron cell bodies and other cells. They were initially categorised as two subtypes, M₁ and M₂, in relation to their differential sensitivity to pirenzepine, which is a selective antagonist to the M₁ receptor.¹ Previous research carried out based on muscarinic receptor diversity and molecular cloning technology helped to identify three more muscarinic receptor subtypes, making a total of five different homologous subtypes known as M₁, M₂, M₃, M₄, and M₅.² The subtypes facilitate the parasympathetic stimulation in the peripheral nervous system³ and each subtype is also present within the central nervous system with separate encoded genes in respect to the types of tissues.⁴ The subtype M₁ is predominantly found in the cerebral cortex, and the gastric and salivary glands,⁵ whereas M₂ and M₄ receptors are known to be the most abundant in the body with subtype M₄ mainly found in the central nervous system.⁶ M₂ receptors regulate the smooth muscles and cardiac tissues,⁷ whereas M₃ receptors, located in the exocrine glands and the vascular endothelium, ease the parasympathetic stimulation of smooth muscle contraction in the peripheral system³ and are also widely spread in the brain.⁸ The high expression of muscarinic acetylcholine receptors (mAChRs) in the organs and tissues of the body raises an interest in studying the physiological and pathophysiological roles of each individual subtype.⁶ Studies of such roles, especially the pathophysiological, are complex due to the lack of selective ligands that can block or activate specific mAChRs subtypes.⁹ The ligands that bind to muscarinic receptors are compounds that are identified as neurotransmitters released from neuronal cells to modulate signal transduction pathways in a receptor in order to produce a certain response in the cell

which depends on the muscarinic receptor subtype and the G-protein. An example of effectors modulated by muscarinic receptor subtypes M_1 , M_3 , or M_5 is phospholipase D (PLD) which is regulated by the influx of Ca^{+} ions and protein kinase C (PKC) to generate choline and phosphatidic acid. An example of a signal transduction pathway modulated by the subtypes M_2 and M_4 is the inhibition of the enzyme adenylyl cyclase which is responsible for the synthesis of cyclic adenosine monophosphate (cAMP), known to regulate the metabolism of sugar and lipid, cell growth, and differentiation. One of the main neurotransmitters that binds to this type of receptor is acetylcholine, from which the name muscarinic acetylcholine receptor is derived.

1.1.1 Muscarinic Receptors as G Protein-Coupled Receptors

Muscarinic receptors are classified as G protein-coupled receptors. At the binding of a neurotransmitter, the receptor responds by altering the cell behaviour in a series of signalling pathways that either activate or suppresses cell activity.¹⁰ The signal transduction mechanism pathway adopted by these receptors is that of the G proteins. Muscarinic acetylcholine receptors are therefore classified as G protein coupled receptors (GPCR).

GPCRs are plasma membrane receptors that play a vital role in the signalling functions of the central nervous system (CNS), neuromuscular regulation, olfactory perception, metabolism, endocrine system, and vision.¹¹ All transmembrane proteins that are known to be members of the G-protein-coupled receptor family are distinguished by a single protein molecule that spans the plasmalemma seven times, creating seven

hydrophobic transmembrane domains linked by three intracellular (IL) and three extracellular (EL) hydrophilic loops (Figure 1).^{1, 12} Experimental data obtained from a high-resolution electron diffraction of a crystallized bacteriorhodopsin showed that all of the seven transmembrane domains of GPCRs are packed in a ringlike structure to form a ligand binding pocket.¹³ The amine N-terminal, NH₂, of all GPCR members occupy the extracellular region of the membrane, whereas the carboxylic COOH terminus resides on the cytoplasmic side of the plasma membrane.¹ The G-protein-coupled receptor is also identified as a G heterotrimeric protein containing a G α , G β , and G γ subunits.¹⁴ The number of each subunit that have been identified in humans are: 21 G α , 6 G β , and 12 G γ , and they are typically classified into four main groups, G α_s , G $\alpha_{i/o}$, G $\alpha_{q/11}$, and G $\alpha_{12/13}$, on the basis of the similarities in structure, mutagenesis and bioinformatics found in the G α subunit.¹⁵

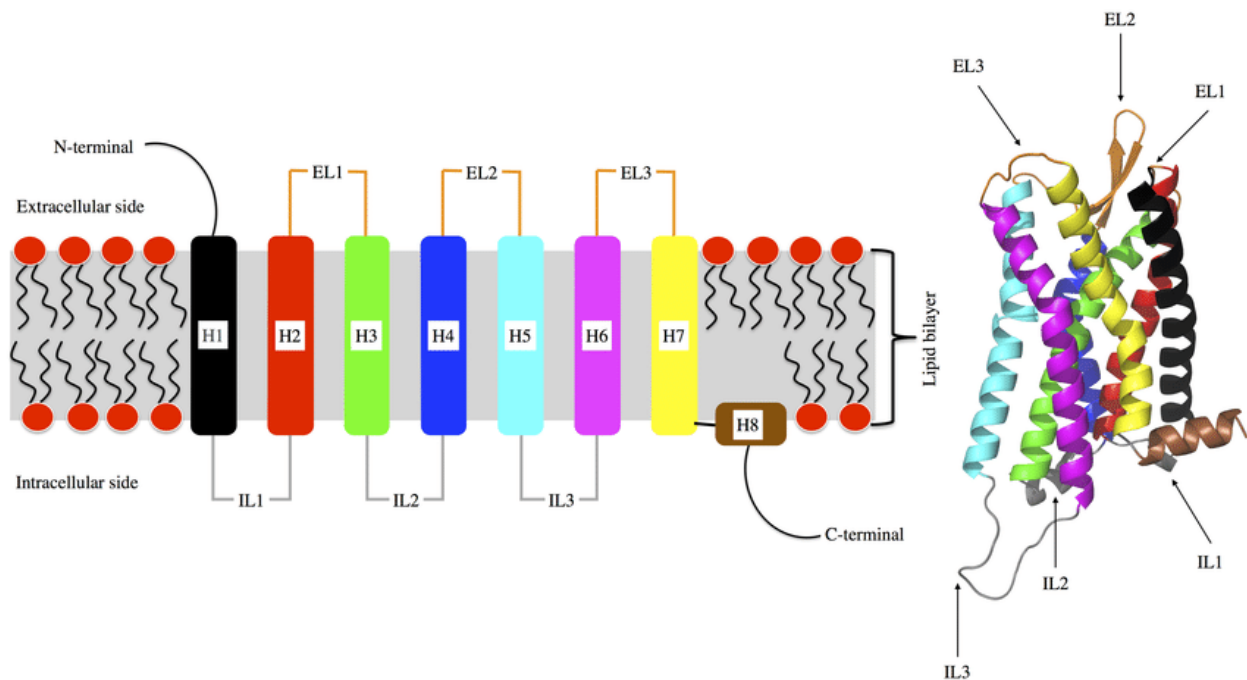


Figure 1: Overall structure of a G protein-coupled receptor (GPCR), with description of the connectivity of the intracellular (IL) and extracellular (EL) loops between the helices (H)¹²

Upon activation of GPCRs, the $G\alpha$ subunit releases guanosine diphosphate (GDP), which is then converted to guanosine triphosphate (GTP), causing the $G\alpha$ subunit to dissociate from the $G\beta\gamma$ subunits.¹⁴ After acting on an effector to modulate the desired signal transduction pathway, the activated G protein subunits return to their initial state by hydrolysis of a phosphate group on GTP to yield GDP again.¹⁴ It has been determined by high resolution X-ray crystal structures that G proteins go from an inactive (GDP-bound; Figure 2a)¹⁶ to an active (GTP γ S-bound) state with a transition state in-between (GDP•AIF-bound).^{17, 18} Results have shown the nucleotide binding pocket location and the interface in-between the $G\alpha$ protein subunit and the $G\beta\gamma$ subunits (Figure 2).¹⁶ The

binding pocket is situated between the Ras-like domain and α -helical domain of the $G\alpha$ subunit surrounded by the flexible three switch segments of the Ras-like domain and the p-loop (Figure 2b).¹⁶ The N-terminus of the $G\alpha$ subunit is known to play two important roles: as a means of attachment to the plasma membrane through its myristoylated modified region,¹⁶ and as a critical terminus for the structure and function of the subunit.¹⁹⁻²¹ The C-terminus of the $G\alpha$ subunit, on the other hand, is identified as a critical binding site to GPCRs.²² Crosslinking experiments have shown that TM6, or intracellular loop (ICL) 3 of GPCRs, is the most significant binding site for the C-terminus of the $G\alpha$ subunit.^{23,24}

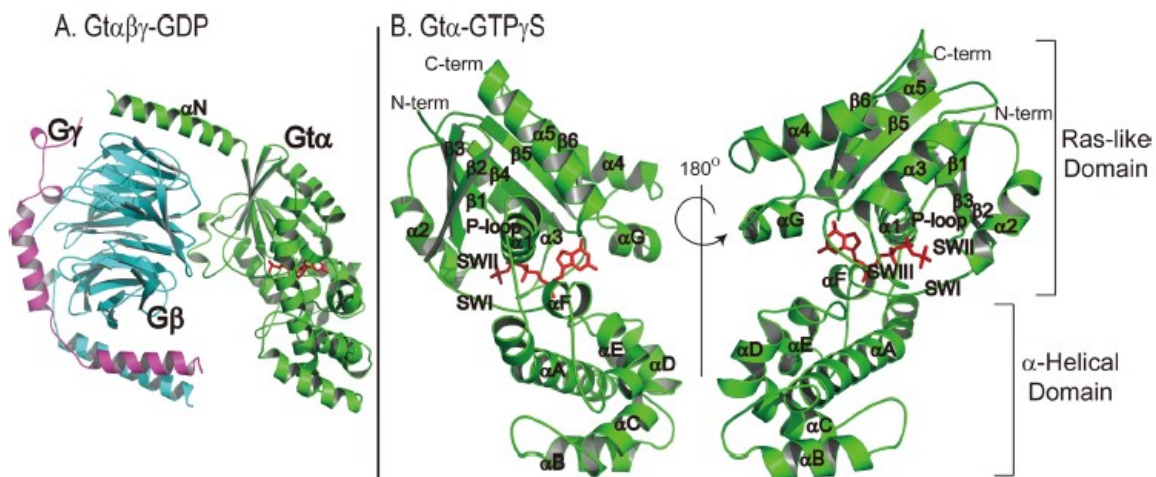


Figure 2: a) The crystal structure of the inactive resting state of G $\alpha\beta\gamma$ heterotrimer with GDP (Green: $G\alpha$, Cyan: $G\beta$, Magenta: $G\gamma$).¹⁶ b) The crystal structure of the active G α subunit with GTP γ S¹⁶

Notwithstanding the finding of the interaction between the C-terminus and the GPCR, studies have shown that there are other regions of the G protein that interact with GPCRs.¹⁶ Crosslinking experiments have shown that the αN of the $G\alpha$ subunit connects

with GPCRs in different ways based on the type of receptor.^{24, 25, 26} For the α 2-adrenergic receptor, the interaction with the α N of the G α subunit occurs with its ICL3;²⁵ Rhodopsin with its ICL1;²⁶ and the M₃ muscarinic acetylcholine receptor with its ICL2.²⁴ In the human genome, approximately 800 GPCRs have been identified with many involved in different diseases such as neurodegenerative, cancer, psychiatric, infectious diseases, cardiovascular, and metabolic disorders.¹⁶ Therefore, 40% of current drugs target GPCRs as adrenergic and angiotensin receptors to fight hypertension, opioid receptors for pain, β -adrenoceptors for heart failure, β 2-adrenoceptors for bronchial asthma, histamine receptors for peptic ulcer, and gonadorelin receptors for prostatic carcinoma.¹⁶

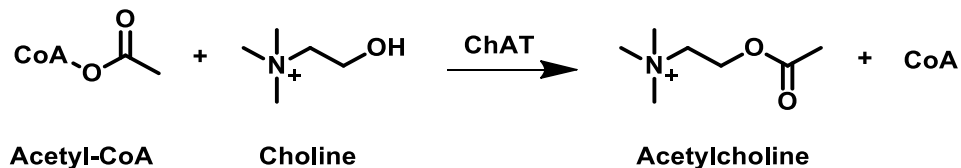
1.1.2 Acetylcholine as a Neurotransmitter

Acetylcholine (ACh) was the first neurotransmitter discovered and named as 'vagusstoff'.²⁷ The major sites of action of the neurotransmitter are at all autonomic ganglia, autonomically innervated organs, neuromuscular junctions, and in the CNS, predominantly at the synapses.²⁷ Therefore, acetylcholine can be said to be present in the central nervous system (CNS) as well as in the peripheral nervous system (PNS).²⁸ Its function is spread throughout the body where it exercises its primary role in the PNS as a neurotransmitter providing the necessary signals for every movement in the body.²⁹ In the CNS, it acts mainly as a neuromodulator, especially in many brain neurons to support mental processes such as cognition and memory.²⁸ As a neuromodulator, its neurotransmission is not directly excitatory or inhibitory,³⁰ but it changes the state of a neuron or a group of neurons so that they respond differently to stimulation in certain

environmental conditions.²⁸ Studies have suggested ACh to be critical in the course of learning as it reinforces neuronal loops and cortical dynamics by enhancing the positive reaction of the afferent inputs to the cortex, which carries the sensory information, and reducing the excitatory reaction which retrieves part of the memory.³¹ The two main sources of acetylcholine in the brain are: the projection neurons, innervating distal areas; and local interneurons, interspersed over cellular targets.²⁸ In the PNS, ACh plays important roles in both the somatic and autonomic nervous systems.³² In the somatic, it contributes to the excitatory actions leading to voluntary activation of muscles, whereas, within the autonomic system, it controls several functions by exercising actions on the neurons in both the sympathetic and parasympathetic systems.³² It also takes part in the dilation of blood vessels, the contraction of smooth muscles, a slower heart rate, and it assists body secretions.²⁹ Due to acetylcholine's important role in muscle actions, interactions with drugs that influence this neurotransmitter can affect body movements to various degrees, even unto paralysis.³² Therefore, alteration in the levels of acetylcholine in the body by drugs or substances such as pesticides and nerve gasses can result in negative effects on the body and lead to possible death.³³ Studies have shown that the venom of the black widow spider interacts with acetylcholine. When a person is bitten, it causes a rise in the levels of acetylcholine in the body leading to grave muscle contractions, spasms, paralysis, and in some cases even death.²⁸ It is also well known that Alzheimer's disease is associated with disrupted levels of acetylcholine in humans.³⁴

1.1.2.1 Acetylcholine Synthesis

The initial step to acetylcholine synthesis is the intake of choline from the extracellular space into the cytosol through a high affinity sodium-dependent uptake system known as SDHACU located at the nerve ending of cholinergic neurons.³⁵ The rate-determining step for the synthesis of acetylcholine depends on the amount of choline transferred by SDHACU into the terminals of cholinergic neurons.³⁶ The Na⁺-dependent uptake system is connected to the release and the demand of acetylcholine to be synthesised and it is suspected to express the activity status of cholinergic neurons.^{37–39} Neurotransmitters are mainly synthesised in the cytosol of nerve terminals and stored in synaptic vesicles which are small membrane sacs called vesicular ACh transporters (VAChT) which carry the neurotransmitter to the presynaptic membrane terminal bottom for exocytotic release.³⁶ The synthesis of ACh (Figure 3) occurs in a single step reaction between choline and acetyl-CoA catalyzed by the enzyme choline acetyltransferase (ChAT) which is produced in the neuronal cell body and transported through the axon to the nerve endings.²⁷



Scheme 1: Reaction scheme of the synthesis of acetylcholine

Acetyl-CoA, from glucose metabolism aided by Ca⁺, is another rate-limiting step in acetylcholine synthesis and it is upregulated from the mitochondria to react with choline as it enters the cytosol.²⁷ The free ACh in the cytoplasm that are not stored in vesicles,

undergo a metabolic reaction that converts them to choline and acetic acid.²⁷ The recycled choline is mostly used for further synthesis of acetylcholine.²⁷ Exogenous Choline can also be obtained by partaking of certain diets as it is present in foods such as egg yolk, soy, and many types of meat.⁴⁰

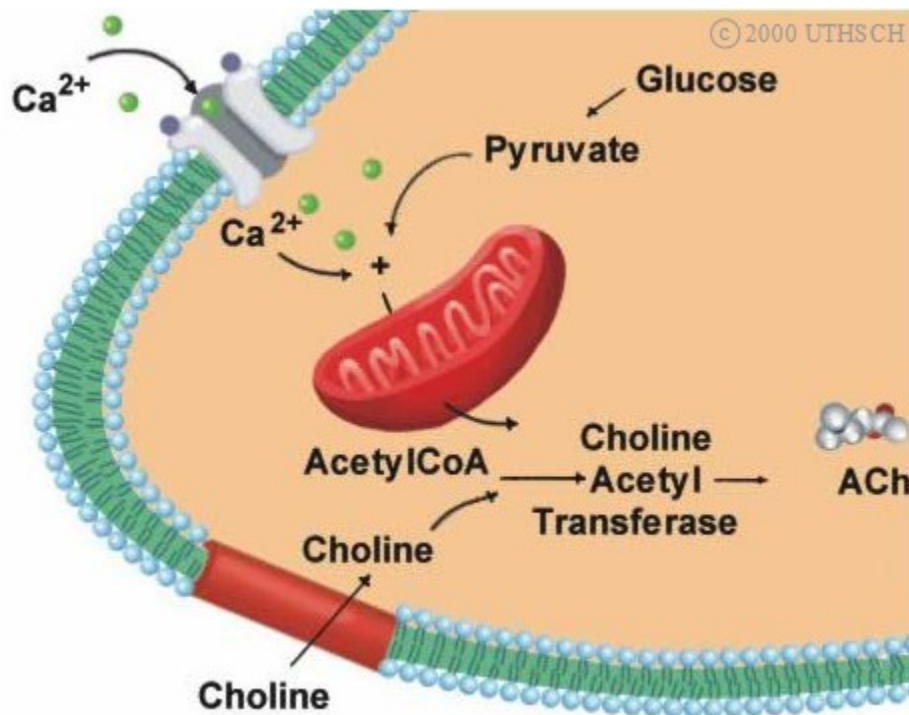


Figure 3: Role of acetyl-CoA from glucose metabolism and choline from SDHACU²⁷

1.1.2.2 Acetylcholine Storage

Synthesised acetylcholine is then stored in vesicles of 100 μm in size (Figure 4) with residual neurotransmitters in the cytosol.²⁷ The storage is enabled by an energy-dependant pump that makes the vesicles acidic.²⁷ The low pH vesicles then use the vesicular ACh transporter (VSChT) to cause an exchange of protons for acetylcholine

molecules.²⁷ These vesicles tend to be very robust to withstand any possible modification to their cholinergic function even by pharmacological agents.²⁷ The vesicle-bound acetylcholine is also not susceptible to degradation by acetylcholinesterase.²⁷

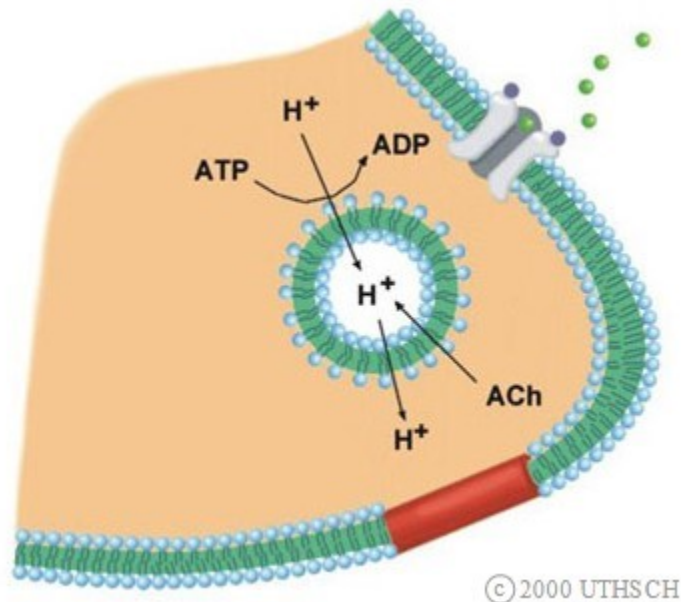


Figure 4: ACh absorption by VACHT and storage in neurotransmitter vesicles with exchange of H^+ for ACh²⁷

1.1.2.3 Acetylcholine Release

The acetylcholine stored in vesicles at the endings of cholinergic neurons is released in the peripheral nervous system through the neuromuscular junction when an impulse arrives at the terminal of a motor neuron.⁴¹ This causes neuronal depolarization which triggers voltage-gated calcium channels to open for an inflow of calcium.²⁹ The release then occurs through Ca^{2+} docking, blending, and breaking of the vesicles with the

membrane of the nerve terminal.²⁷ (Figure 5). The Soluble N-ethylmaleimide sensitive factor (NSF) attachment protein receptor (SNARE) plays a very important role in the releasing step.^{42, 43} There are two different types of this system: the synaptobrevin, referred to as a “v” SNARE which is the vesicular membrane; and SNAP-25 together with syntaxin-1 known as “t” SNAREs which are the presynaptic membrane.²⁹

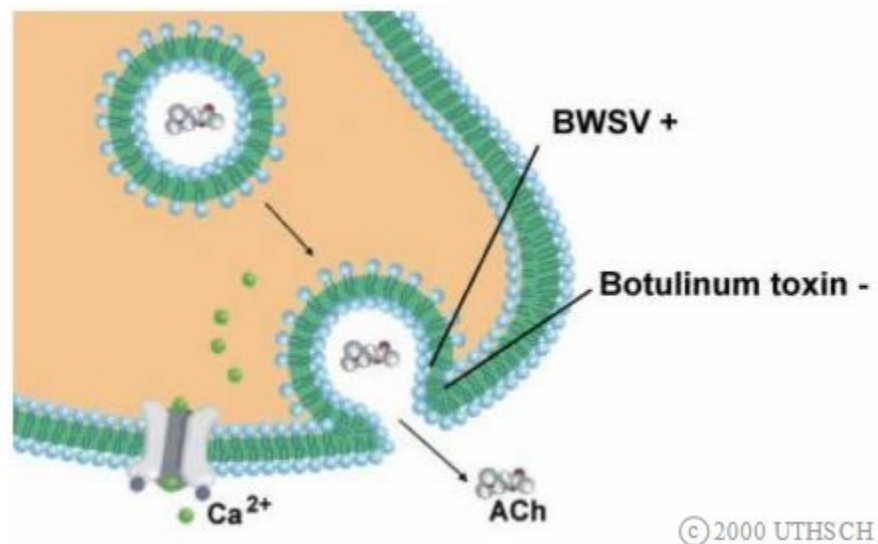


Figure 5: Ca^{2+} dependent ACh release^{27, 44}

The neuronal cell contains another vesicle-bound SNARE protein called synaptogamin that operates as the calcium sensor for the cell.²⁹ As the vesicle containing ACh comes close to the presynaptic membrane, the protein Munc 18 acts as a “clip” that attaches synaptobrevin to SNAP-25 and syntaxin-1, bringing the vesicle and the presynaptic membrane in close proximity.²⁹ The Munc 18 protein then inserts itself in the SNARE complex to stop any spontaneous fusion between the vesicle and the presynaptic membrane.²⁹ Finally, when calcium is introduced into the cell after depolarization, it binds to synaptogamin which then binds to the acidic phospholipids located in the presynaptic

membrane to cause the displacement of the fusion blocking protein.²⁹ The fusion of the vesicle and the membrane only occurs when Ca^{2+} is leached into the cell.⁴⁵ Once the fusion process is completed, Ca-ATPase pumps calcium out of the neuron while the mitochondria intakes part of the ions in the neuronal cell.²⁹ As calcium concentration decreases in the intracellular region, synaptogamin disassociates from the SNARE complex as it breaks down to get ready for the next fusion.⁴⁶

1.2 Muscarinic Acetylcholine Receptor Binding Ligands

Released acetylcholine floating in the extracellular region of the synaptic cleft binds to one of the neurotransmitter receptors which could be either muscarinic or nicotinic. Muscarinic receptors are activated by the neurotransmitter acetylcholine (Figure 6a) and the prototypical nonselective agonist muscarine (Figure 6b) mimics the effects of the chemical messenger ACh.²⁷ The overall goal of these receptors is to exert the “rest and digest” function of the parasympathetic nervous system which acts to oppose the action of the sympathetic nervous system.⁴ The muscarinic receptors provide a slow and prolonged response at the time of activation and are inhibited by anticholinergic drugs such as atropine (Figure 6c) and scopolamine (Figure 6d).¹⁰

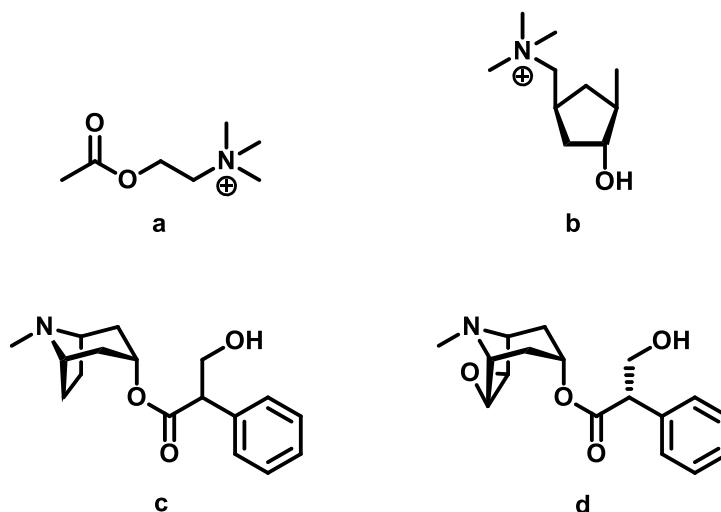


Figure 6: Structures of agonist (a and b) and antagonists of ACh receptors¹⁰

1.2.1 Agonists

Muscarinic agonists are compounds that mimic the action of acetylcholine on muscarinic receptors causing different physiological effects such as slow heart rate, increased secretion from the exocrine glandular tissue (airway mucosal and salivary gland and gastric acid), and contraction of smooth muscles (iris muscle, urethra, intestinal tract, bronchioles, and detrusor muscle).⁴⁷ The receptor agonists are divided into two classes: direct and indirect. Both cause an increase in the concentration of acetylcholine in the synapse extending the effect of the neurotransmitter on the receptor.⁴⁷

The direct agonist withstands the cleavage of acetylcholine by acetylcholinesterase.⁴⁷ For example, methacholine, (Figure 7a) which is used to diagnose asthma, excites the receptor in the airway when inhaled to stimulate bronchoconstriction and increase tracheobronchial secretion.^{47, 48} Also, carbachol (Figure 7b) is known to treat open-angle glaucoma, acute angle-closure glaucoma, and increased intraocular pressure by contracting the ciliary body muscle and opening the trabecular meshwork.^{47, 49} Other agonists, such as pilocarpine (Figure 7c) and bethanechol (Figure 7d), also follow the same principle of direct agonists.

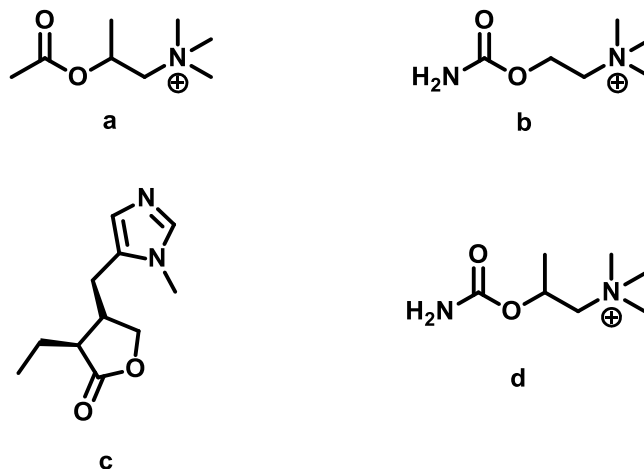


Figure 7: a) Methacholine; b) Carbachol ; c) Pilocarpine; d) Bethanechol; direct agonists of muscarinic acetylcholine receptors⁴⁷

On the contrary, indirect agonists also known as cholinesterase inhibitors, act by inhibiting the acetylcholinesterase enzyme to stop the degradation of acetylcholine.⁴⁷ Examples of indirect agonists are neostigmine, used for postoperative and neurogenic ileus and myasthenia gravis,⁵⁰ whereas galantamine, donepezil, and rivastigmine, are used for Alzheimer disease as they help with memory loss to delay the progression of the disease but do not cure it.^{51, 52} Other indirect agonists, like edrophonium and pyridostigmine, operate on the nicotinic receptor of the skeletal muscle instead of the muscarinic.⁴⁷

1.2.2 Antagonists

Muscarinic receptor antagonists (MRAs) are a class of compounds that competitively block cholinergic responses triggered by acetylcholine binding to

muscarinic receptors in the cardiac and smooth muscle cells.⁵³ Hence, MRAs operate mostly in the parasympathetic nervous system and other muscarinic receptors.⁵³ A group of lung diseases such as emphysema, bronchiectasis, asthma, and chronic bronchitis are labelled under the name of chronic obstructive pulmonary disease (COPD) sharing the same pathophysiological effect as airway obstruction.⁵³ This is due to the high parasympathetic activity via the vagus nerve that causes an increase in ACh secretion.⁵³ The excessive levels of acetylcholine on submucosal glandular cells and bronchial smooth muscles results in increased bronchial inflammation, bronchial smooth muscle constriction, and mucus plugging.⁵³ Therefore, the therapeutic pathway of COPD blocks the flow of ACh on the muscarinic receptors of the bronchial smooth muscles in the airway.⁵³ Muscarinic receptor antagonists, such as tiotropium and ipratropium, competitively inhibit muscarinic receptors on the bronchial smooth muscles to reduce the airway obstruction caused by the increased parasympathetic activity of the vagus nerve.^{54–56}

Another group of chemicals that leads to a hyperstimulation of nicotinic and muscarinic receptors due to increased levels of ACh are organophosphates.⁵³ They are toxic and induce the same effects as acetylcholinesterase inhibitors with common symptoms of diarrhea, increased urination, miosis, bronchospasm, emesis, lacrimation, and salivation.⁵³ The toxicity of organophosphates can also cause the increase of nicotinic receptor hyperstimulation that could result in muscle paralysis.⁵³ An immediate therapeutic agent approved by the FDA is the drug atropine which treats cholinergic muscarinic side effects and eases the signs and symptoms of cholinergic muscarinic

organophosphate toxicity.^{57, 58} MRAs are used for other treatments such as Parkinson disease, nausea, urinary incontinence, motion sickness, and irritable bowel syndrome.⁵³

1.3 Neurotransmitter Receptors

The neurotransmitter ACh is selective to two classes of cholinergic receptors: metabotropic muscarinic receptor (mAChRs) and ionotropic nicotinic receptor (nAChRs).^{59, 60} Therefore, after release from the presynaptic membrane, it proceeds into the synaptic cleft where it can either bind to the nicotinic or muscarinic cholinergic receptors.²⁹ The function of ACh on any given circuit is based on the concentration of the neurotransmitter in the extracellular space and the pattern by which mAChRs and nAChRs respond specifically to stimulus.²⁸ These two membrane protein receptors are grouped as either ligand-gated ion channels or G-protein-coupled receptors, and differ in both structure and functionality.⁶¹ The ligand-gated ion channel is structured with five protein subunits that assemble themselves to form a pore.⁶¹ At the binding of a neurotransmitter, the pore is opened to directly prompt ion fluxes.⁶¹ On the other hand, GPCRs, alters the conformation of the receptor protein and causes changes to the associated G proteins to induce a variety of signalling pathways.⁶¹ Hence, these receptors carry out either the excitatory or inhibitory effect based on the neurotransmitter that binds to them. Some known examples are glutamate, triggering an excitation of the receptor in the central nervous system; GABA (γ -aminobutyric acid), triggering an inhibition effect of the receptor in the adult vertebrate brain; and glycine, also causing inhibition of the receptor in the spinal cord.⁶² Neurotransmitter receptors are also identified to be rapid in inducing changes as they happen within a few milliseconds.⁶³ This characteristic is very important in the nervous system as rapid responses are required to carry out daily human activities.

1.3.1 Nicotinic

The nicotinic acetylcholine receptor is characteristic to its name in that it binds to nicotine which mimics the effects of ACh.²⁷ This receptor is a ligand-gated ion channel consisting generally of two α subunits and one of each β , σ , and γ (Figure 8) that intakes both K^+ and Na^+ ions.⁶³ It has also been reported that there are 17 individual subunits described by the Greek letters $\alpha 1$ – $\alpha 10$, $\beta 1$ – $\beta 4$, σ , ϵ , and γ .⁶⁴ Due to the number and difference in subunits, the nAChR subtypes are grouped into two broad categories: heteromeric subtypes having both α and β subunits and homomeric subtypes made of α subunits only.⁶⁴

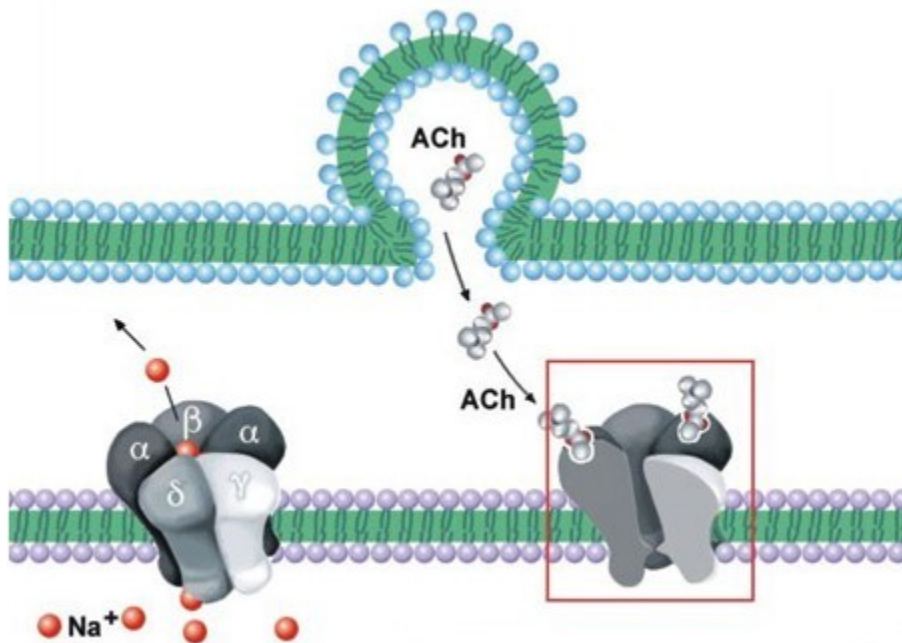


Figure 8: Nicotinic acetylcholine receptor²⁷

The nAChR is also classified into two types of receptors, the muscular type (N1) and the neuronal type (N2).⁶¹ N1 is specifically found on the outside of muscle cells at the neuromuscular junction, whereas N2 is present in the peripheral and central nervous system and can be specifically found in the adrenal medulla, on the postsynaptic cell bodies of neurons in the sympathetic and parasympathetic nervous system.⁶³ Despite its numerous locations in the neuronal regions of the body, the most important and well-studied role of the nicotinic acetylcholine receptor is that of its synapses between motor neurons and skeletal muscle cells.⁶⁵ Studies carried out through patch-clamping has shown that at the binding of acetylcholine to the nicotinic receptor of muscle plasma membranes, the cationic channel opens up to admit 15,000 – 30,000 Na⁺ or K⁺ ions per millisecond.⁶⁵

1.3.2 Muscarinic Binding Sites

Muscarinic receptors are also located in both CNS and PNS and are identified as metabotropic G protein coupled receptors. Their two main functions are to recognize the neurotransmitter acetylcholine and initiate a physiological response. Attempts to characterize muscarinic receptors have been of great interest and were facilitated by the introduction of high-affinity radioactive ligands such as tritium-labeled quinuclidinyl benzylate ([³H]QNB)⁶⁶ and N-methylscopolamine ([³H]NMS)⁶⁷ acting as antagonists. Both ligands bind to the receptor membrane with high affinity with the equilibrium dissociation constant of 15–80pM for [³H]QNB and 50–700pM for [³H]NMS.⁶⁸ Thus, the affinity of other compounds to bind muscarinic receptors was measured by their ability to compete with the two ligands.⁶⁹ Studies also showed that the distribution of muscarinic receptors in the body is roughly parallel to the uptake of choline into the neuronal cell for the synthesis of

acetylcholine.^{70, 71} These results suggested that a great portion of the neurotransmitter receptors in the brain are muscarinic and their affinity for specific antagonists varies from tissue to tissue.⁷² However, their affinities towards atropines [³H]QNB, and [³H]NMS are similar.⁶⁹

Further X-ray crystallography studies (Figure 10) of the binding pocket of the structures of different subtypes of the muscarinic acetylcholine receptors, in particular the M2R and the M3R, showed some interactions with QNB and tiotropium respectively (Figure 9).^{73,74} The key interaction of the two molecules with their respective receptors was through hydrogen bonding between Asn^{6.52} and the hydroxyl and ester moieties,⁷⁵ whereas the cationic ammonium ion pairs interacted with Asp^{3.32} in both receptors and were both surrounded by an aromatic cage made of Tyr^{3.33}, Tyr^{6.51}, Tyr^{7.39}, and Tyr^{7.43}.⁷⁵

The figure 10 shows the stacking of ring A with Tyr^{3.33}, Trp^{4.57}, and Val^{3.40}, while ring B is directed towards the extracellular vestibule and shows interaction with Thr^{5.39}, Tyr^{3.33}, and Trp^{4.57}.⁷⁵ The only difference that was found between the two receptors was the interaction of ring B with Phe181^{ECL2} in the M2R and with Leu225^{ECL2} in the M3R.⁷⁵

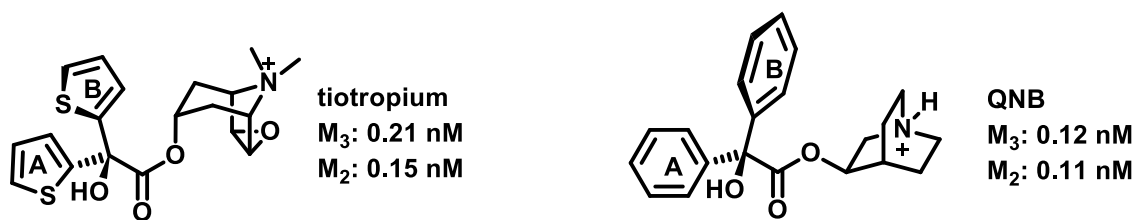


Figure 9: Structures and binding affinities of QNB and tiotropium⁷⁵

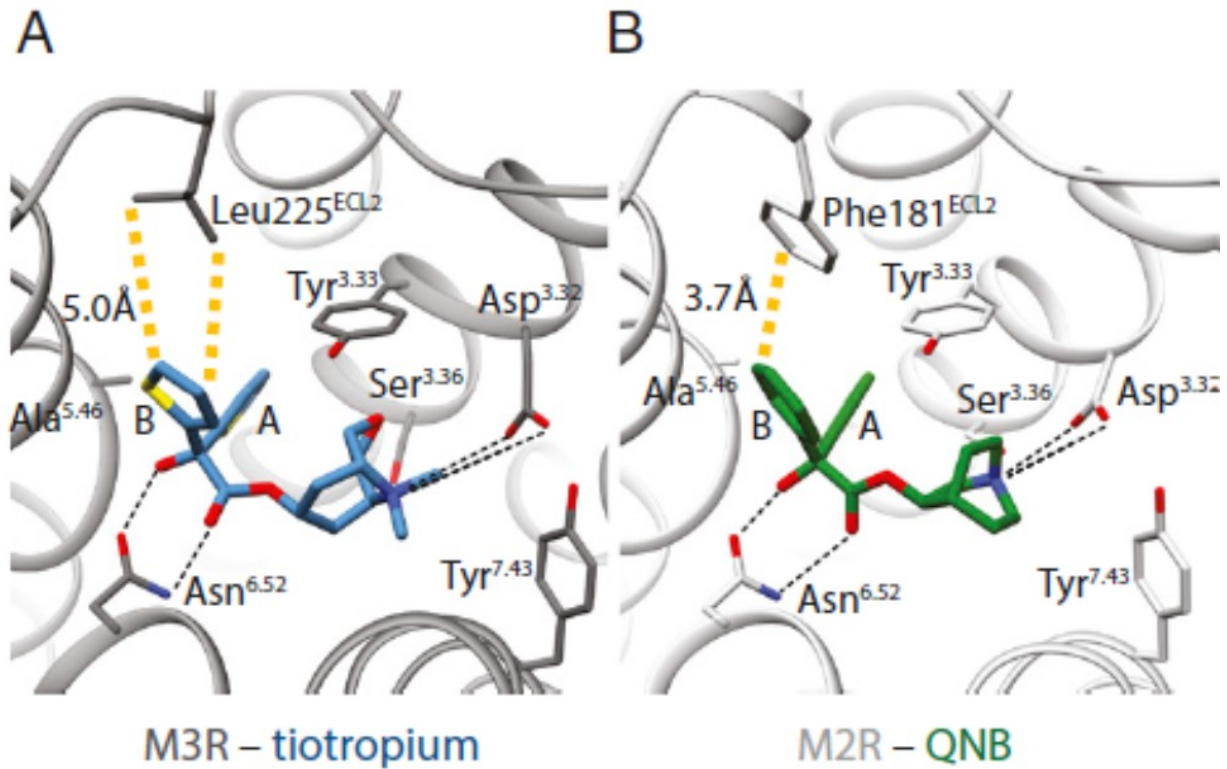


Figure 10: Comparing the active binding sites of M2R and M3R⁷⁵

1.3.3 Muscarinic Receptor's Role in Cancer Progression

Muscarinic acetylcholine receptors are expressed in most tumors originating from epithelial and endothelial cells.⁷⁶ These type of tumors also release ACh to drive their cell proliferation both in the presence or absence of ChAT and acetyl cholinesterase AChE.⁷⁶ If these two mechanisms are lacking, ACh is still derived from other tissues like neuronal, endocrine or paracrine to activate mAChRs and nAChRs present in tumors.⁷⁶ When subtypes M₁, M₃, and M₅ are activated and coupled with G_q proteins, cell viability is increased.⁷⁶ M₃ receptors in particular are mostly involved in tumor growth and invasion

during cell development through a particular metabolic signalling pathway.⁷⁶ Head (glioblastomas) and neck (larynx squamous) carcinomas have shown to have both M₂ and M₃ receptor subtypes whereas lung⁷⁷⁻⁷⁹ and gastric⁸⁰⁻⁸² tumors have been found to have high expression of only the M₃ subtype. The latter is also widely expressed in digestive tract cancer and is known to play a fundamental role in tumor proliferation, differentiation, transformation, and carcinogenesis.⁸⁰⁻⁸³ M₃ has also been identified in other tumors such as melanoma, colon cancer, gastric cancer, and prostate cancer.⁷⁶

1.3.3.1 Role of M₃ subtype in breast cancer

Regarding breast cancer, studies have shown that selective M₃ antagonists, p-F-HHSiD and atropine, have inhibition properties towards cell growth and that antagonists, in general, could be used as therapeutic tools in cancer cells.^{84, 85} Breast cancer is a very frequent cause of death in women, especially if the type of cancer is known to be triple negative or, in other words, it lacks the specific targets for chemotherapy.⁸⁶ Results from Western blot analysis performed on breast tumors showed a major expression of M₂ and M₃ subtypes.⁷⁶ Studies carried out on the expression and function of mAChRs in human breast tumor cell lines (MCF-7 cell line) extracted from human luminal breast adenocarcinoma (based on estrogen) specifically expressed M₃ and M₄ receptor subtypes of mAChRs.⁸⁷ On the contrary, normal breast tissue and non-tumorigenic mammary cell line (MCF-10A) showed the absence of mAChRs.^{86, 87}

Results from treating MCF-7 cell lines with the agonist carbachol for short periods of time, caused proliferation of the cell via the M₃ receptor triggering PLC/PKC/calcium-

dependant nitric oxide synthetase 1 and 2.⁷⁶ Further stimulation of the receptor also in the same cell line also induced malignant angiogenesis with up-regulation of vascular endothelial growth factor-A (VEGF-A) expression and high number of tumor blood vessels.⁷⁶ The increased expression of VEGF-A could be totally reversed by the antagonist methoctramine and pirenzepine whereas the increased blood level formation can be stopped by 4-DAMP.⁸⁸ Also, siRNA studies have shown that proliferation of cancer cells in MCF-7 breast cancer cell lines is mediated by M₃ receptors leading to ERK 1 and ERK 2 activation by partial dependence on SRC and CAM Kinase pathways.⁸⁹

Breast cancer develops and spreads in 5 stages (Figure 11). It starts at stage 0 where the cancer cells are in a non-invasive phase.⁹⁰ In other words, they are present in the ducts but have not spread around breast tissues.⁹⁰ In stages 1A, 1B, and 2A, the size of the tumor is smaller than 5cm and has not spread to more than 3 lymph nodes.⁹⁰ When the size is larger than 5cm, there is a high chance that the cancer may have spread to more than 3 lymph nodes. At this stage, the tumor is classified as stages 2B, 3A, 3B, and 3C.⁹⁰ The last stage, which is the hardest to fight, is stage 4 where the cancer is said to have metastasized or spread into other parts of the body which may include, brain, heart, spinal cord, and other organs in the body. At this stage M₃ receptors continue to induce signalling pathways in the cancerous tissues in the different organs, cell proliferation and angiogenesis.⁹⁰

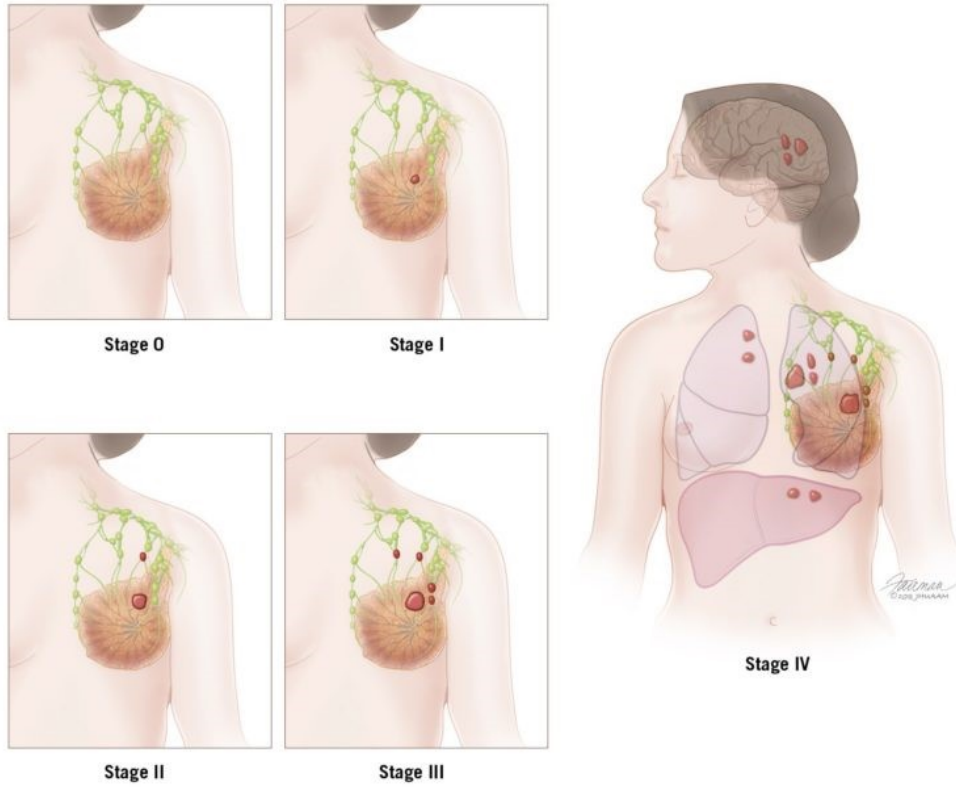


Figure 11: The stages of breast cancer⁹¹

1.4 The Hypothesis of the Thesis

The metastatic stage of breast cancer holds a death rate of 30% of all breast cancer patients. With current therapies, patients have an average survival rate between 2-3 years. These alarming numbers call for new lines of treatment to fight metastatic breast cancer, especially in cases of highly aggressive triple-negative breast cancer where the usual chemotherapeutic target receptor of the hormones, estrogen and progesterone and the protein HER2, are lacking (Figure 12).

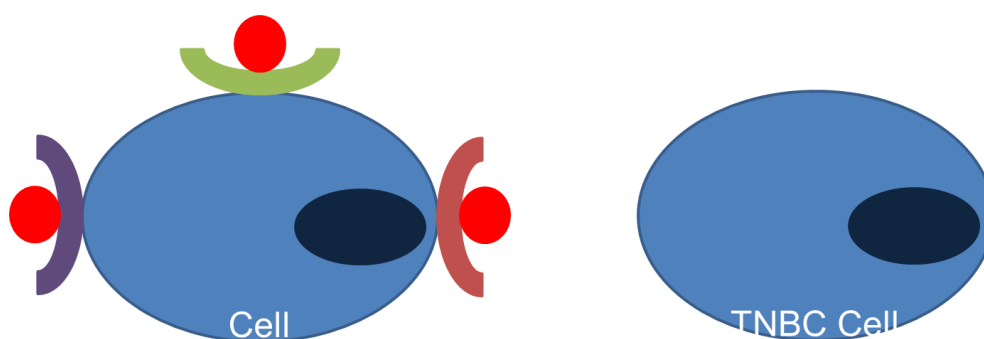


Figure 12: Left: breast cancer cell fueled by hormones and protein: violet: estrogen, green: progesterone, velvet: protein HER2, red balls: inhibitors. Right: triple negative breast cancer cell lacking target hormones and protein

Studies have shown that M₃ receptors of the muscarinic acetylcholine receptor family are significantly overexpressed (Figure 13) at the transcriptional and translational levels in metastatic triple-negative breast cancer.⁹² Despite the extensive synthetic efforts that have been made to identify a selective antagonist against M₃, the need of a more selective compound towards M₃ is essential due to similarities that have been shown of the binding pockets of M₂ and M₃ subtype receptors.⁹² Previously reported antagonists,

such as darifenacin and atropine, are known to be non-selective muscarinic antagonists as they can bind to M₂ subtypes as well as M₃ subtype receptors.

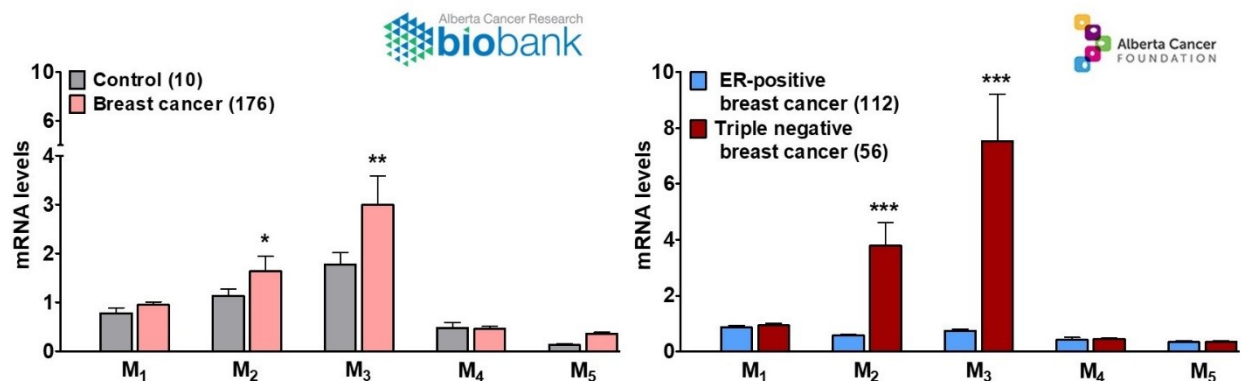


Figure 13: Expression of M₂ and M₃ subtypes in breast cancer⁸⁶

1.4.1 Thesis Goals

The purpose of this project is to synthesize a selective compound towards the M₃ subtype based on a strategic combinatorial chemistry adopted by Ohtake and his group to effectively yield a series of different antagonist structures.¹⁰ Based on the structural features of the compound that showed potent binding affinity ($K_D = 0.31$ nM) with a 98-fold M₃/M₂ in selectivity (Figure 14), I decided, along with my collaborators, to make a library of compounds that retained most of the structural features of their compounds that yielded positive result. Alterations were made at the hydrophobic site to include a fluorine-containing compound for future radiolabelling of the most potent compounds. These radiofluorinated probes could then serve as leads in the development of highly sensitive PET tracers for detection of metastatic TNBC.

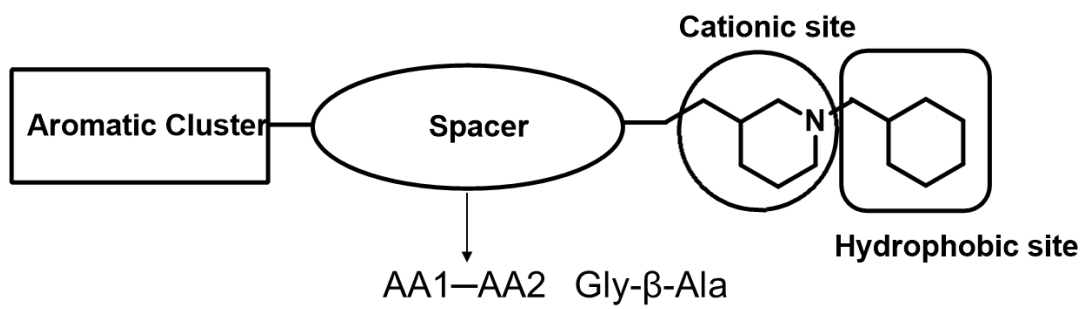


Figure 14: Structural features of muscarinic antagonists⁸

Chapter 2: Results and Discussion

2.1 Previous Work

The design of our library of compounds followed the principles that were adopted by Ohtake's group. Using previously reported structural features of darifenacin and derivatives (Figure 15),⁹³ they proposed that a bulky aromatic cluster, a cationic part containing an amine that will be protonated at physiological pH, and a hydrophobic moiety located as a nitrogen substituent on the cationic ammonium part, were all necessary in the pharmacophore for M₃ potency (Figure 16).¹⁰

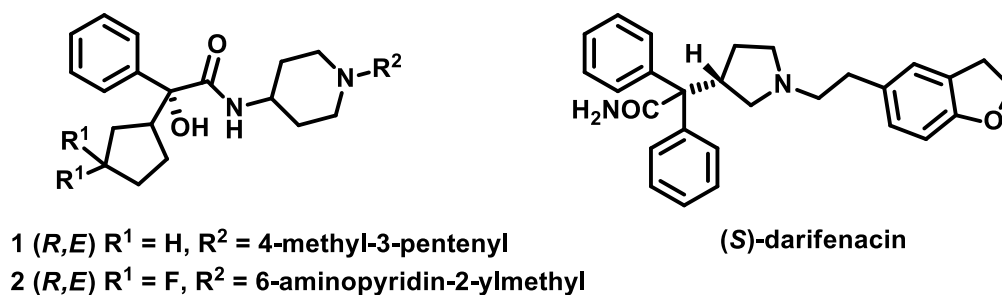


Figure 15: Reported M₂-sparing M₃ antagonists¹⁰

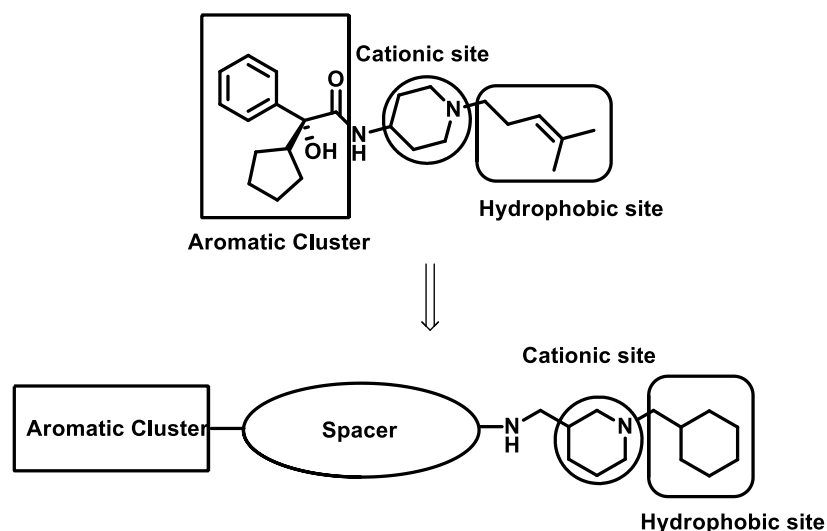


Figure 16: Structural features of muscarinic antagonists¹⁰

Furthermore, studying the spatial disposition and the positioning of pharmacophores for M_3 antagonists, they hypothesized that increasing the molecular size and the spatial flexibility of the reported muscarinic antagonist could lead to a higher selectivity in binding to the M_3 receptor over the other subtypes. Based on these predictions, they used a combinatorial chemistry approach to incorporate a spacer group between the bulky aromatic cluster and the cationic site.¹⁰ Following the designed structure (Figure 16), the region of the spacer was altered with different commercially available amino acids to make a library of compounds containing various sizes of the peptides, including both natural and unnatural amino acids. The tertiary amine, 1-cyclohexylmethyl-3-aminomethylpiperidine, was used as the cationic site. At the aromatic cluster position, 25 different cyclic commercially available aromatic, acyclic carboxylic acids, cycloalkyl, and heteroaromatic compounds were tested (Figure 17).¹⁰

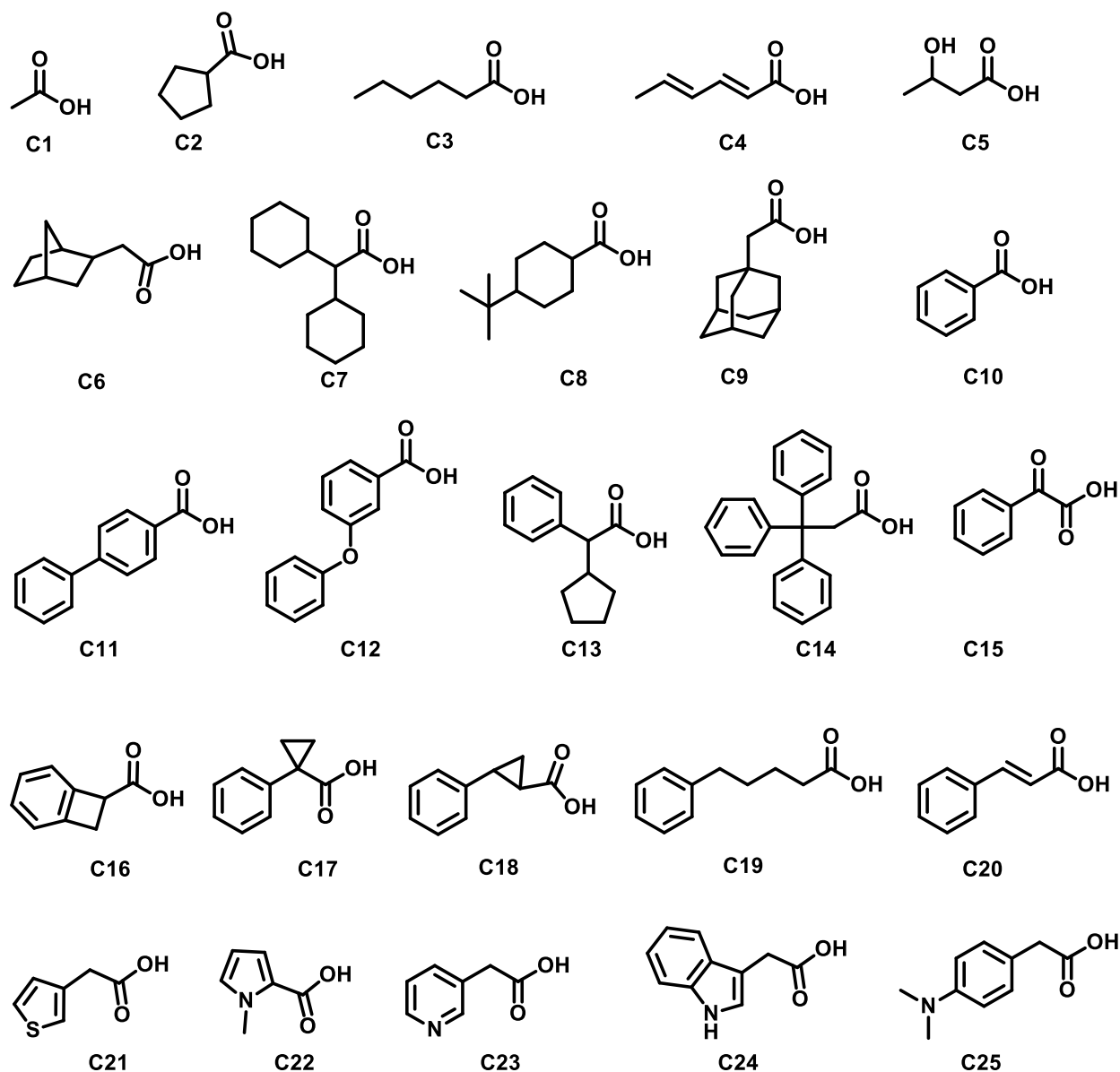
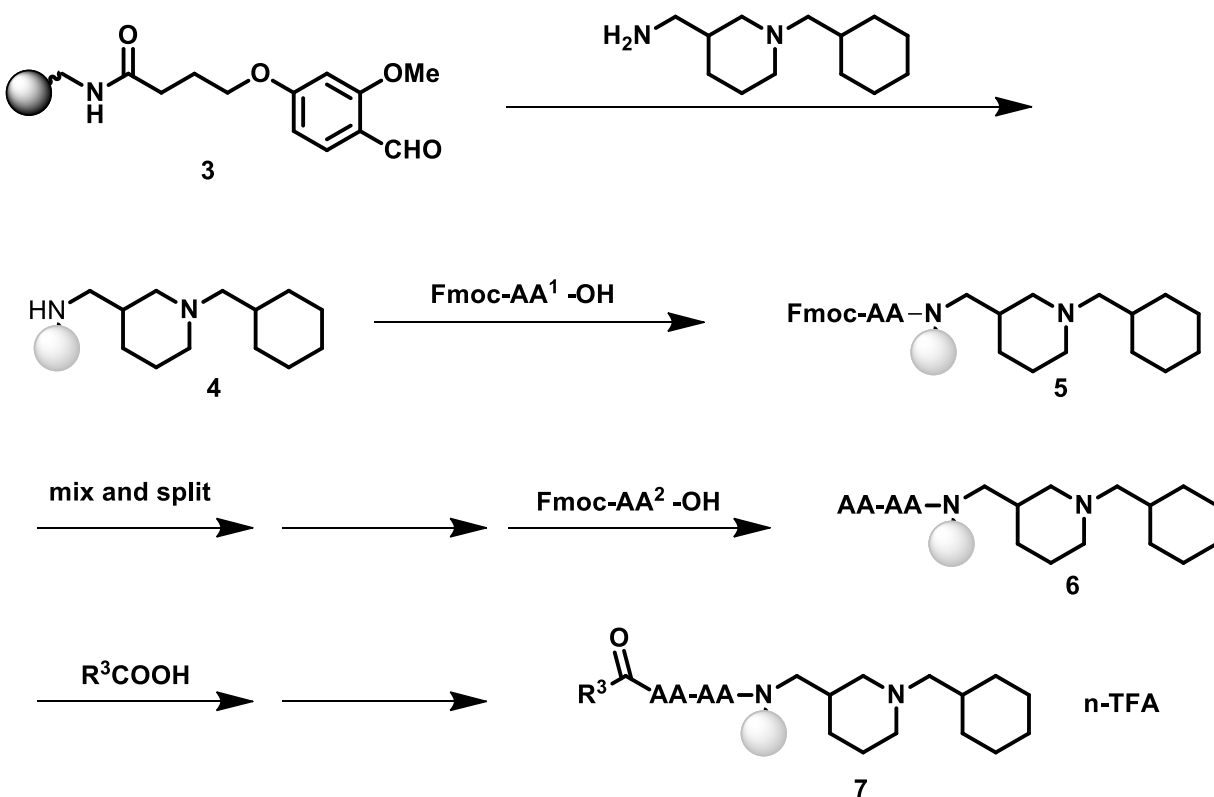


Figure 17: 25 carboxylic acids for the aromatic cluster position¹⁰

The synthetic route adopted by this group was the use of an alkyl resin (Scheme 2).⁹⁴ After introducing the aminomethyl piperidine core on the *o*-formyl resin by reductive amination, compound **4** in the scheme below was acylated with the first spacer (Fmoc-AA¹-OH) by PyBOP-DIEA method.⁹⁵ Six pools of compound **5** were made with six different amino acids of the first spacer (Gly, β -Ala, GABA, Acp, L-Pro, and D-Pro), mixed,

and split into seven groups. The Fmoc group was deprotected from each spacer to allow the acylation of the same six amino acids and one null (Gly, β -Ala, GABA, Acp, L-Pro, D-Pro, and null) of the second spacer (Fmoc-AA²-OH).¹⁰ The groups of diamide derivatives formed (compound **6**) were further divided into 25 subgroups and coupled with the 25 different commercially available carboxylic acids through a general amide coupling procedure to finally synthesize a total of 1050 compounds that were cleaved from the resin by treatment with 80% TFA/DCM and structurally confirmed by HPLC and mass spectral analysis.¹⁰



Scheme 2: Synthetic route using alkyl resin¹⁰

Their first screening was to confirm binding of the reported muscarinic antagonist [³H]-NMS ([³H]N-methyl scopolamine) (1 μ M) to the human M₃ receptor expressed in

CHO cells.¹⁰ Their synthesized compounds were then tested for binding affinities against each of the five muscarinic subtypes ($M_1 - M_5$) and to determine the selectivity, the K_D values of the muscarinic subtypes were divided with the dissociation constant value of M_3 being the denominator. Among the different spacers examined, as partly shown in Table 1, the two amino acids that produced satisfactory M_3 binding affinity and selectivity compared to the other subtypes were those of **9** in Table 1, in combination with triphenylpropionic acid acting as the aromatic cluster from the pool of carboxylic acids; chiral (*3R*)-3-aminomethylpiperidine proven to be more effective than the symmetrical 3-aminomethylpiperidine shown in scheme 2 in the role of the cationic site; and cyclohexylmethyl as hydrophobic site acting as the *N*-substituent.¹⁰

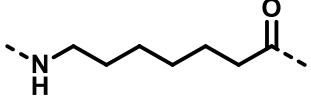
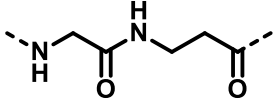
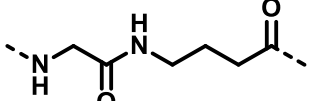
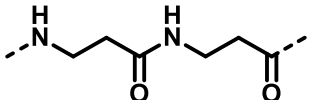
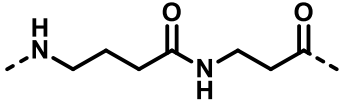
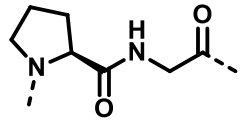
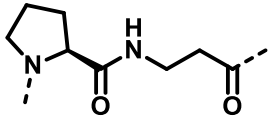
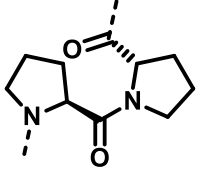
Table 1. Binding affinities of compounds to human muscarinic receptor subtypes¹⁰

no.	AA ²	AA ¹	binding affinity (K_D , nM)					selectivity			
			M_3	M_1	M_2	M_4	M_5	M_1/M_3	M_2/M_3	M_4/M_3	M_5/M_3
8	null	Acp	1.0	110	72	30	210	110	72	30	200
9	Gly	β-Ala	0.31	120	30	14	37	380	98	45	120
10	Gly	GABA	3.3	300	270	74	1100	90	82	22	320
11	β -Ala	β -Ala	0.76	36	44	31	30	48	58	41	40
12	GABA	β -Ala	2.1	77	17	60	200	37	8.2	29	95
13	L-Pro	Gly	2.2	150	13	43	2000	66	5.7	19	890
14	L-Pro	β -Ala	0.27	150	12	11	58	550	45	42	210
15	L-Pro	D-Pro	0.25	14	0.82	2.3	150	54	3.3	9.0	580

Different replacements at the glycyll and β -alanyl positions of **9** either showed improvement in the binding affinity or selectivity but not in both parameters. For example, substitution of the glycyll with the β -alanyl group, **11**, showed a moderate M_2/M_3 selectivity, whereas substitution with the γ -aminobutyryl group, **12**, showed a poor selectivity of M_2/M_3 .¹⁰ Performing substitution at the β -alanyl position in the spacer also caused reduction in the binding affinity and selectivity parameters as seen in **10** where the

replacement of the β -alanyl group with γ -aminobutyryl reduced the binding affinity in M_3 by 10-fold and decreased the selectivity in M_1/M_3 by 4-fold but retained similar selectivity in M_2/M_3 .¹⁰ Compound **9** was also more efficient in both binding affinity and selectivity as compared to the known non selective muscarinic antagonists, atropine and darifenacin.

Table 2. Structures of amino acid spacers used in human muscarinic receptor subtypes binding assay

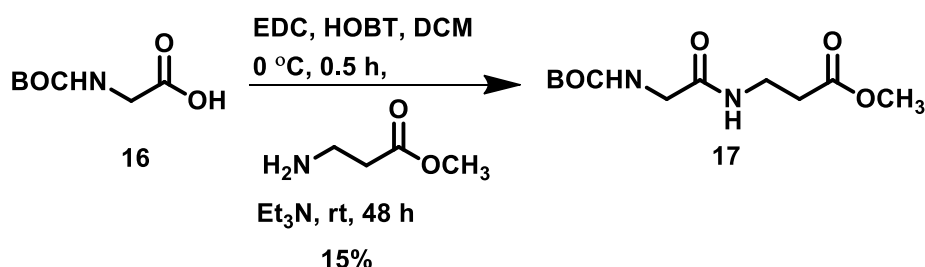
no	AA ²	AA ¹	Structures
8	null	Acp	
9	Gly	β -Ala	
10	Gly	GABA	
11	β -Ala	β -Ala	
12	GABA	β -Ala	
13	L-Pro	Gly	
14	L-Pro	β -Ala	
15	L-Pro	D-Pro	

Despite the promising results from the binding assays performed by Ohtake's group, they were unable to clarify the type of interactions between any of the class of compounds they synthesized with the muscarinic subtype receptors.

2.2 Design and Synthesis

Based on the results from the previous work, I decided to retain the triphenylpropionic acid aromatic cluster, the glycyl and β -alanyl spacer, and perform modifications at the cationic site and the hydrophobic region. For the former, I chose to use 1-Boc-4-(aminomethyl)piperidine instead of the 1-Boc-3-(aminomethyl)piperidine they used in their publication. Whereas, for the hydrophobic region, I decided to use fluorine containing derivatives with a goal of modifying the synthesis of the best inhibitors to incorporate radiofluorination.

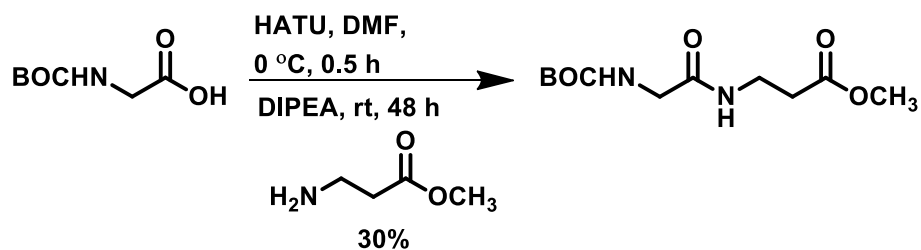
Following the established synthetic route used by Ohtake's coworkers, I started my synthesis by first reacting a Boc-glycine with β -alanyl methyl ester to build the spacer using previously reported experimental procedures for amide coupling,¹⁰ resulting in **17** (Scheme 3).



Scheme 3: Amide coupling of Boc-glycine with β -alanyl methyl ester¹⁰

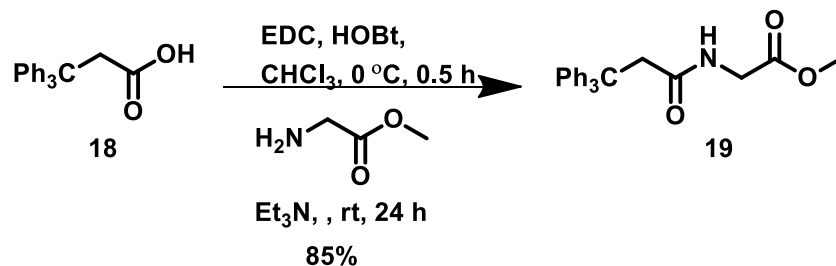
The first percentage yield of product **17** obtained was low with a high reaction time, hence, I altered the reaction conditions by refluxing the mixture after the addition of the coupling agents. The modification showed improvement in the yield by increasing the percentage of product to 45% but still required the same amount of time to see traces of the product

on the TLC together with both reactants. Changing the solvent from dichloromethane (DCM) to chloroform showed a substantial increase in the amount of the final product as the percentage yield spiked to 86%, but no effect was noticed on the reaction time. The coupling reagents were also changed in a suitable solvent (Scheme 4), but no significant improvements were recorded.



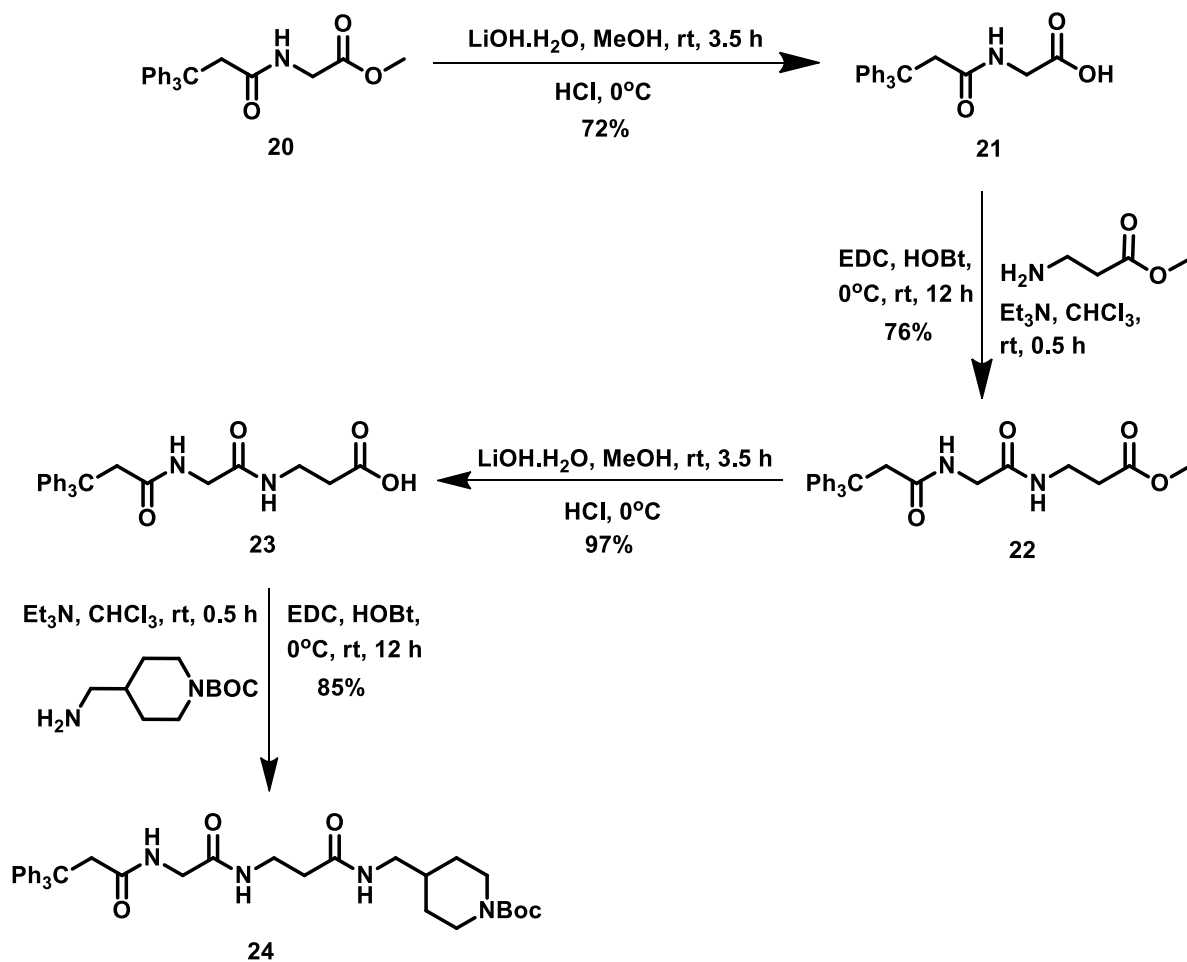
Scheme 4: Different reagents of amide coupling of boc-glycine with β -alanyl methyl ester⁹⁶

Thus, I decided to change the beginning of the building block of the scaffold by reacting the triphenylpropionic acid, **18**, with glycine methyl ester in the presence of the coupling agents 1-(3-dimethylaminopropyl)-3-ethylcarbodiimide (EDC) and hydroxybenzotriazole (HOBt) which has been found to be independent to the reaction rate but rather produces activated esters which react with amines to form amides. HOBt also contributes to reducing racemization during peptide coupling by attacking on one side of the molecule to force the nucleophile to substitute on the other side of the molecule.⁹⁷ However, since achiral carboxylic acids were employed in this route, racemization was not taken into account as an issue to be avoided. These conditions were therefore used to synthesize **19**, in the presence of triethylamine (Scheme 5).



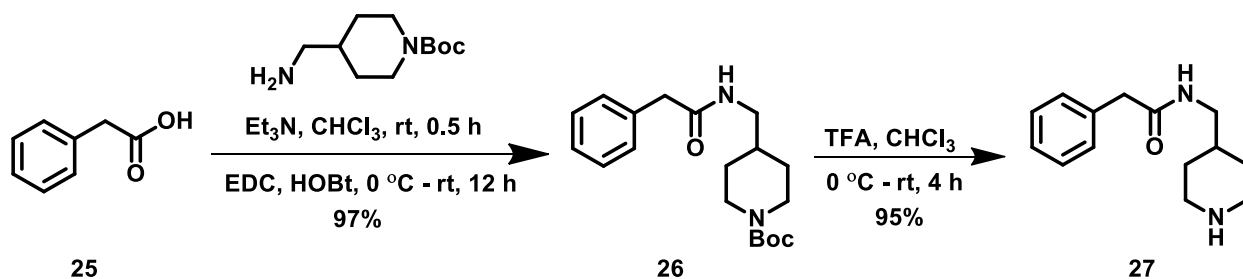
Scheme 5: Amide coupling between triphenylpropionic acid and glycine methyl ester

The reaction completed over night with a satisfactory percentage yield of 85%. Further optimization of the reaction was carried out to reduce the reaction time to 12 hours by changing the solvent to chloroform. The glycine methyl ester derivative, **20**, was then hydrolyzed, **21**, and coupled to the β -alanyl methyl ester, to yield a diamide, **22**, which was again hydrolyzed, **23**, and subsequently coupled to the achiral aminomethyl piperidine derivatives 1-Boc-4-(aminomethyl)piperidine, to form the protected product **24** (Scheme 6).



Scheme 6: Synthetic route to piperidine derivatives

Thus, compound **24** was prepared and prior to deprotection, a model compound was synthesized containing a reduced aromatic cluster to one phenyl ring, **25**, (phenylpropionic acid) and the cationic site of **24** (1-Boc-4-(aminomethyl)piperidine) for testing and optimization of the coupling of the final compounds for the hydrophobic region. The synthesis of these compounds followed the same amide coupling procedure already adopted (Scheme 7) to yield protected aminomethyl piperidine derivative **26** which via TFA was deprotected to give the free amine **27**.



Scheme 7: Synthesis of model compound

A group of hydrophobic compounds were selected as fluorine containing motifs to be connected to the aminomethyl piperidine derivative of the model compound before performing the same reactions on the target Boc-protected compounds.

I initially selected aliphatic and aromatic compounds to be used as N-substituents. Straight chains, such as propyl and butyl with a fluoro substituent at positions 3 and 4 respectively and a good leaving group at position 1 in both cases (Figure 18) were selected to make one pool of hydrophobic sites on the scaffold. Another pool was made up of aryl compounds, such as 4-fluorobenzaldehyde and 4-fluorobenzoylchloride (Figure 18). Having already examined the results of Ohtake *et al*, I decided to remove from my library cyclohexylmethyl derivative that they had adopted at the hydrophobic region because the results for such scaffold was already reported in their studies.

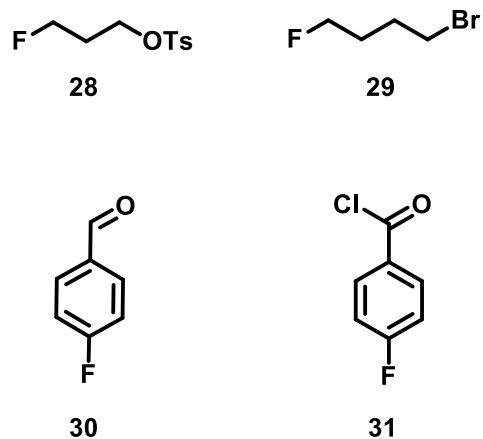
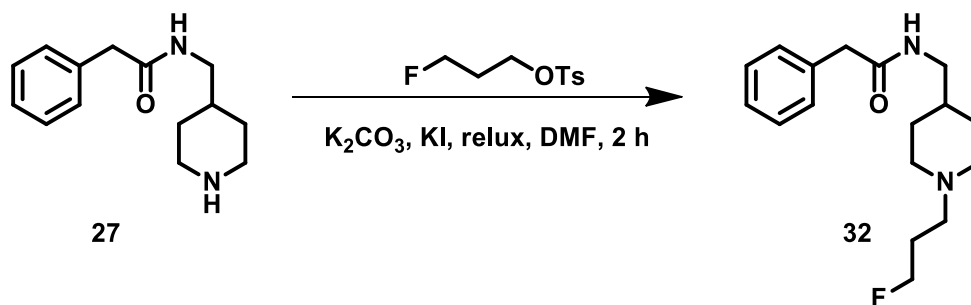
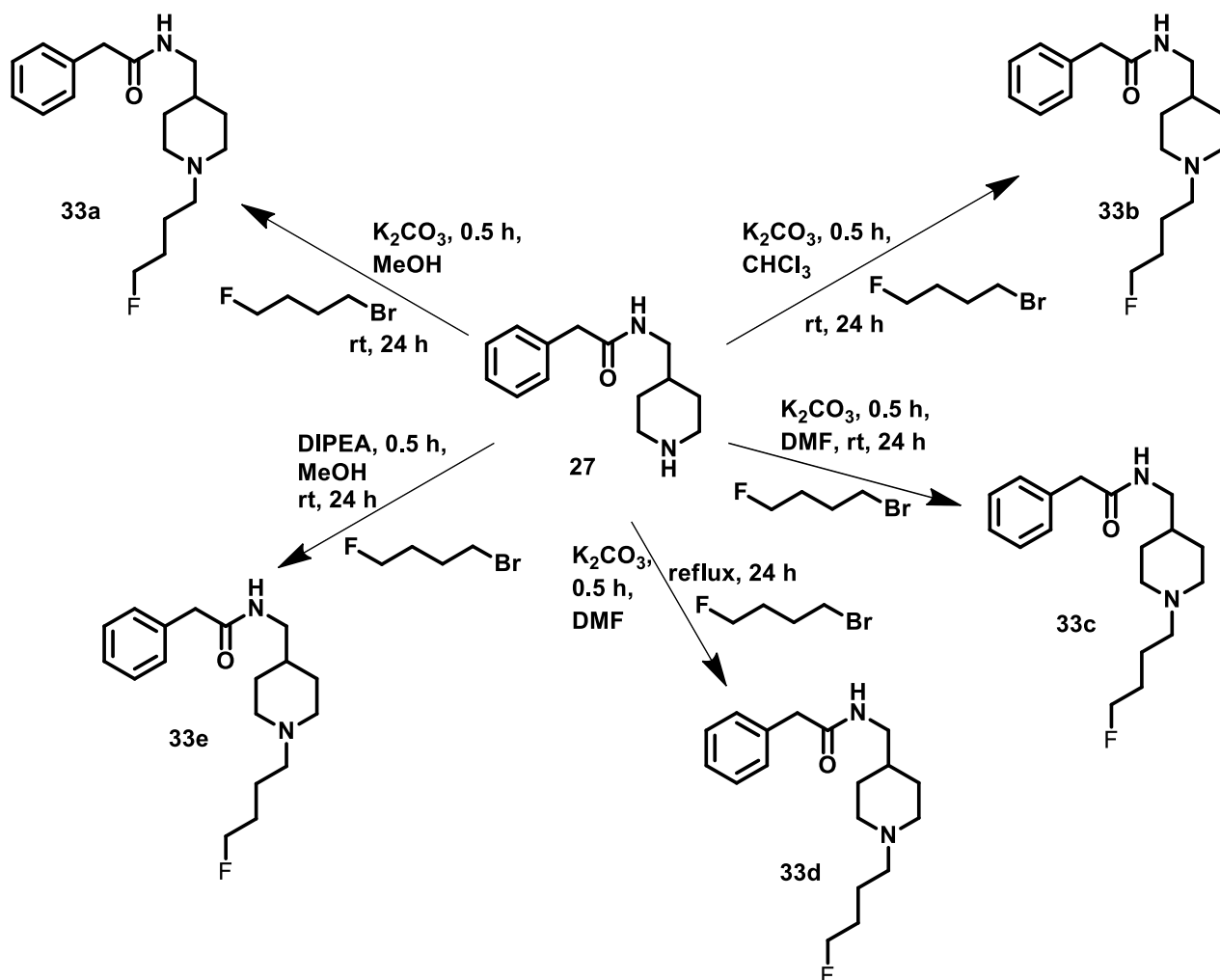


Figure 18: Selected hydrophobic compounds for hydrophobic site on scaffold

Different N-alkylation synthetic methods were selected for the combining of the two alkyl derivatives to the free amine of the model compound, especially in the synthesis with the starting material **29** (Scheme 9). Because of the high cost of starting material, only one attempt was made for the synthesis of **32** starting from **27** (Scheme 8), but the reaction resulted to be unsuccessful with decomposition of the product.



Scheme 8: N-alkylation of alkyl tosylate⁹⁸



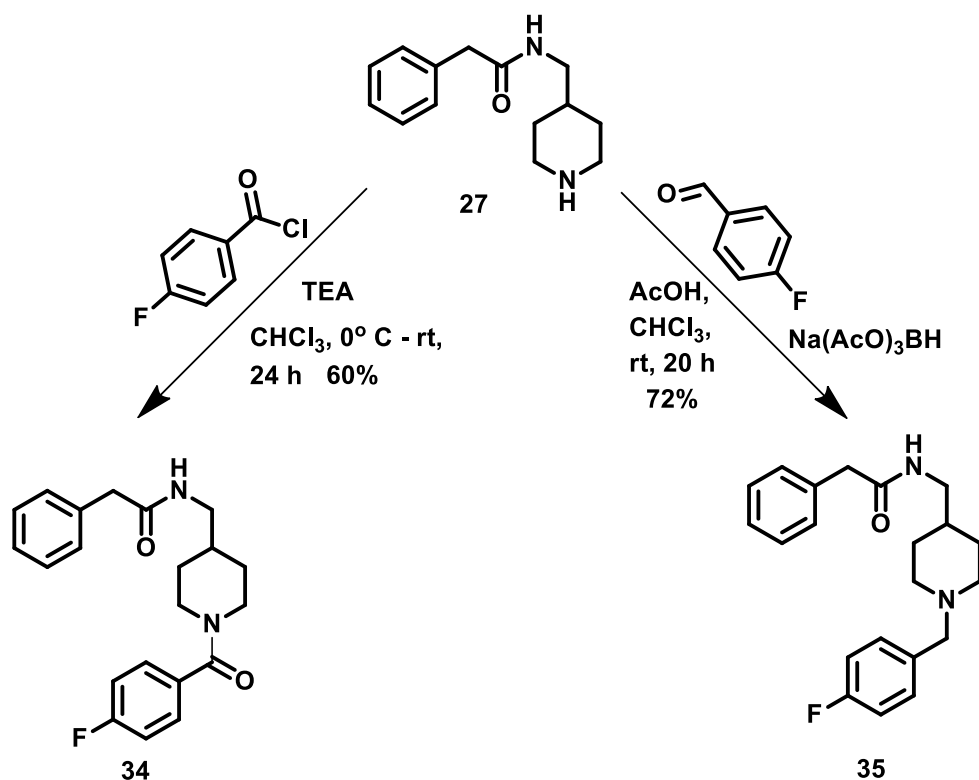
Scheme 9: Unsuccessful routes to N-(4-fluoro)butyl product⁹⁹

As shown in Table 2, most of the reactions performed with 1-bromo-4-fluorobutane as the starting material were unsuccessful. Overalkylation was observed from characterization studies of some of the products but most of the reactions showed either starting materials or decomposition. Only in the case **33a** was trace of product detected, but it was impossible to be isolated.

Table 3. Reaction conditions of the unsuccessful routes to N-(4-fluoro)butyl product

Compound	Compound 32 (equivalents)	1-bromo-4-fluorbutane (equivalents)	Observation
33a	1	1	Trace of Product
	2	1	Starting materials
33b	1	1	Starting materials
33c	1	1.5	Overalkylation
33d	1	1	Decomposition
33e	1	1	Decomposition

More positive results were obtained from the reductive amination and the nucleophilic acyl substitution reaction (Scheme 10) using the same model compound. In the first reaction, the starting material, **27**, was reacted with 4-fluorobenzoyl chloride in the presence of triethylamine to yield 60% of tertiary amide product, **34**. Whereas in the second reaction, **27** was reductively alkylated with 4-fluorobenzaldehyde and Na(AcO)₃BH to produce the targeted product **35** with a yield of 72%.



Scheme 10: Reductive amination and acylation reaction with the model compound^{100,101}

Due to the lack of positive results from the N-alkylation reactions, the library of compounds I initially selected was reduced to two compounds. Thus, I decided to add to the library the same chiral variation that Ohtake and his group applied at the cationic site by inserting the enantiomers (*R*)-1-Boc-3-(aminomethyl)piperidine, **36**, and (*S*)-1-Boc-3-(aminomethyl)piperidine, **37** (Figure 19), and performing both reductive alkylation and nucleophilic acyl substitution on each of the enantiomers.

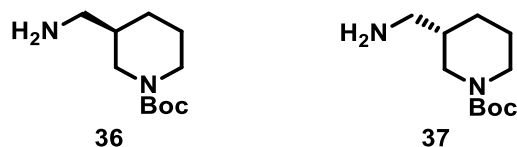
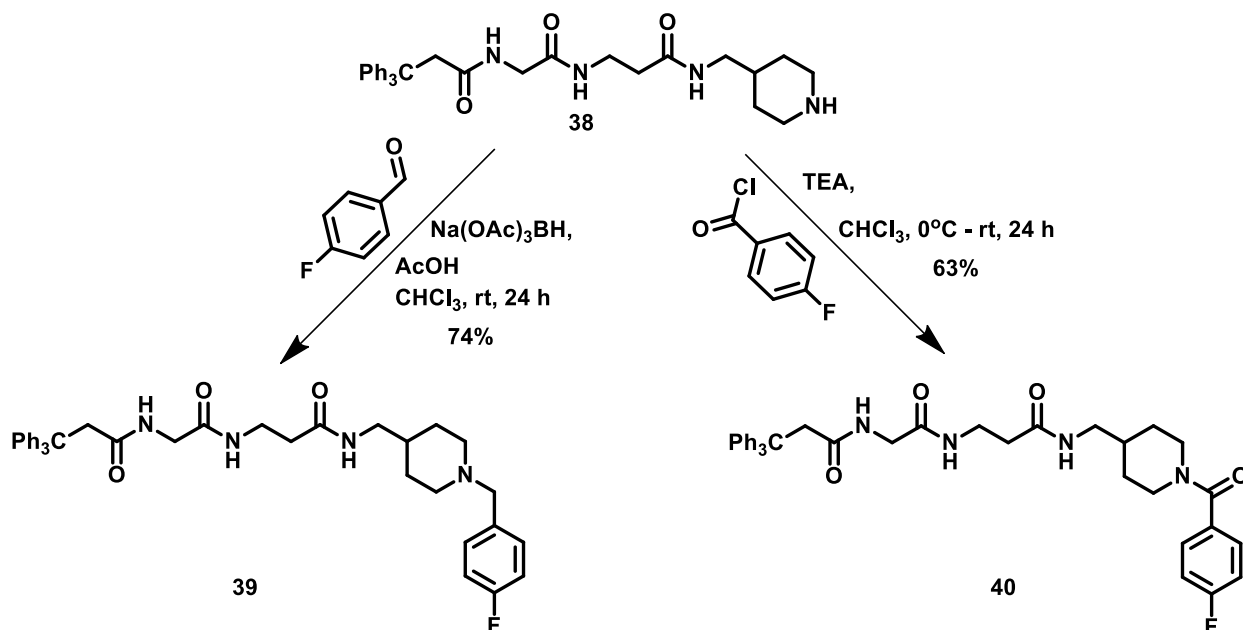


Figure 19: Enantiomers of aminomethyl piperidine

Because I already performed the chemistry of coupling the achiral 1-Boc-4-(aminomethyl)piperidine to the model compound with successive acylation and amination, I decided to move directly to my Boc-protected target compound instead of testing them first on the model compound.

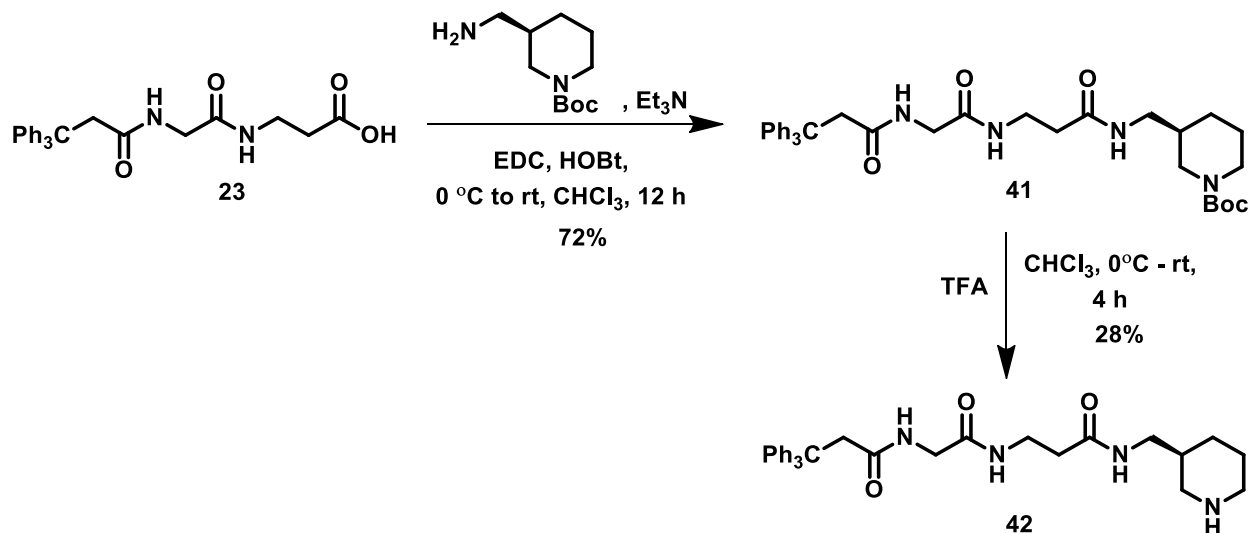
The Boc aminomethyl piperidine derivative, **24**, was deprotected with the same deprotection procedure adopted when testing the model compound to give **38** as a free amine. Following the same reductive amination and acylation procedures, 4-fluorobenzaldehyde and 4-fluorobenzoyl chloride were coupled respectively to yield **39** and **40** (Scheme 11).



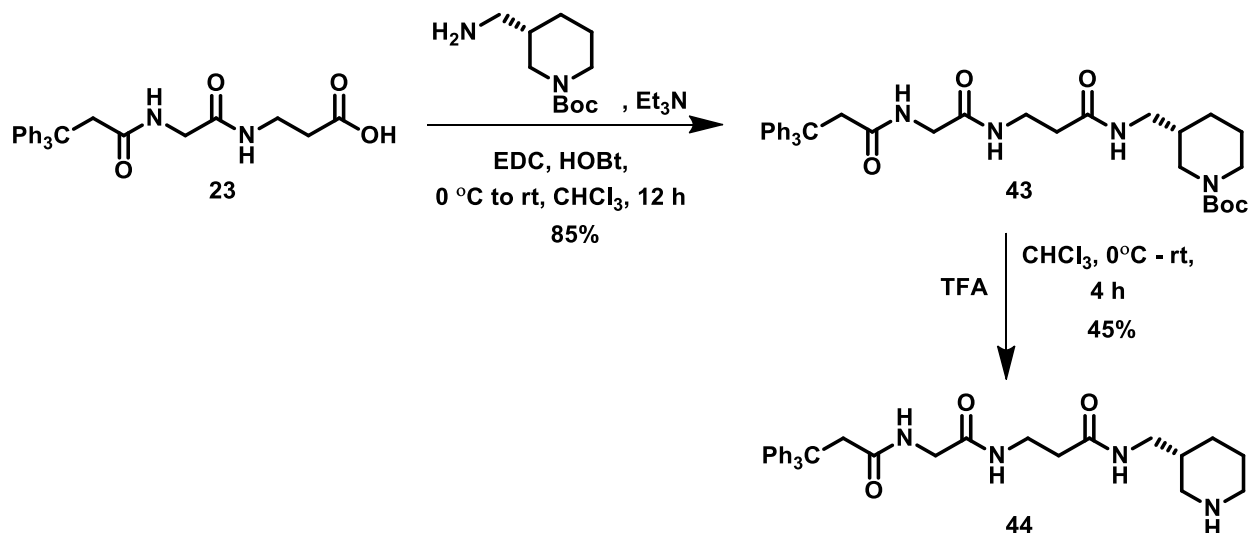
Scheme 11: Reductive amination and acylation on target compound

Following the same experimental procedures, the enantiomeric aminomethyl piperidines, **36** and **37**, were attached to the β -alanyl derivative to yield **41** (Scheme 12), and **43** (Scheme 13) followed by deprotection to give **42** (Scheme 12) and **44** (Scheme 13) for

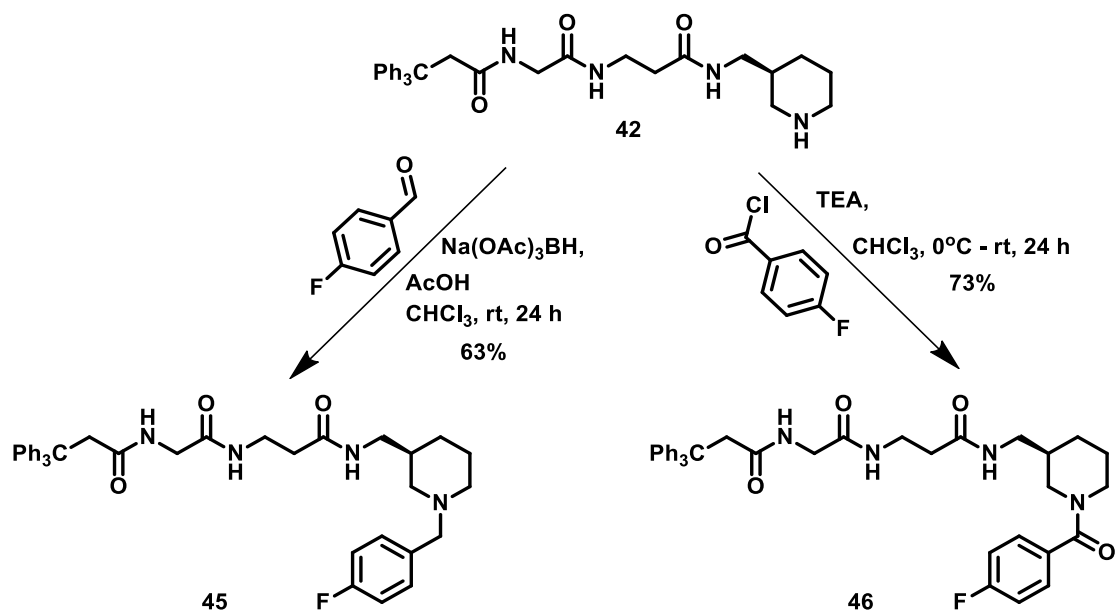
further coupling of each with both **30** and **31** to synthesise **45** and **46** (Scheme 14), and **47** and **48** (Scheme 15).



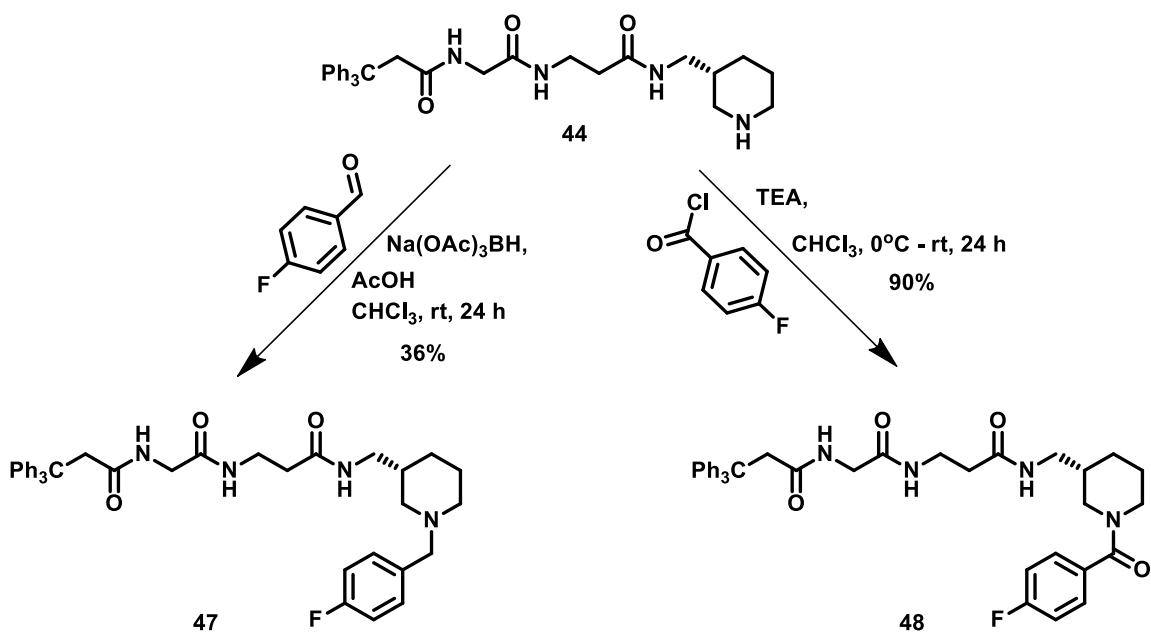
Scheme 12: Amide coupling and boc-deprotection to yield (S)-3-(aminomethyl)piperidine derivative



Scheme 13: Amide coupling and boc-deprotection to yield (R)-3-(aminomethyl)piperidine derivative



Scheme 14: Reductive amination and acylation on (*S*)-3-(aminomethyl)piperidine derivative **42**



Scheme 15: Reductive amination and acylation on (*R*)-3-(aminomethyl)piperidine derivative **44**

To ensure that the compounds prepared were pure and matched the expected structures drawn as products, different characterization techniques such as ¹H NMR, ¹³C NMR, FTIR, MS, and LCMS were used to identify the product as shown in the appendix section. For the products containing a chiral centre, an optical rotation experiment was conducted on the enantiomeric starting materials (*R*)-1-Boc-3-(aminomethyl)piperidine, **36**, and (*S*)-1-Boc-3-(aminomethyl)piperidine, **37**, (Figure 19) to confirm their enantiomeric purity based on the specific rotation of plane polarized light. The results acquired certified an opposite rotation of the plane polarized light for each compound; -51.99 for (*S*)-1-Boc-3-(aminomethyl)piperidine, **37**, and 49.87 for (*R*)-1-Boc-3-(aminomethyl)piperidine, **36**. With these results, it was possible to predict that compounds **45**, **46**, **47**, and **48** were going to be enantiomerically pure besides previously mentioned characterization techniques adopted. However, attempts were made to confirm the enantiomeric purity of the final compounds by mixing an equal amount of R and S enantiomers to study their retention time by chiral column chromatography. Due to the lack of the correct type of column the experiment was unsuccessful. Therefore, I predicted that if both starting materials, were optically pure then the products would also be optically pure. I also expected that if the final compounds were not enantiomerically pure the binding affinity values between R and S enantiomers would be similar. But on the contrary, the results from the binding affinity experiments showed difference in values and in some cases one enantiomer appeared to show inhibition while the other enantiomer showed none.

Thus, a library of six compounds were prepared (Figure 20) for GPCR screening of muscarinic acetylcholine receptor subtypes M₁ – M₅.

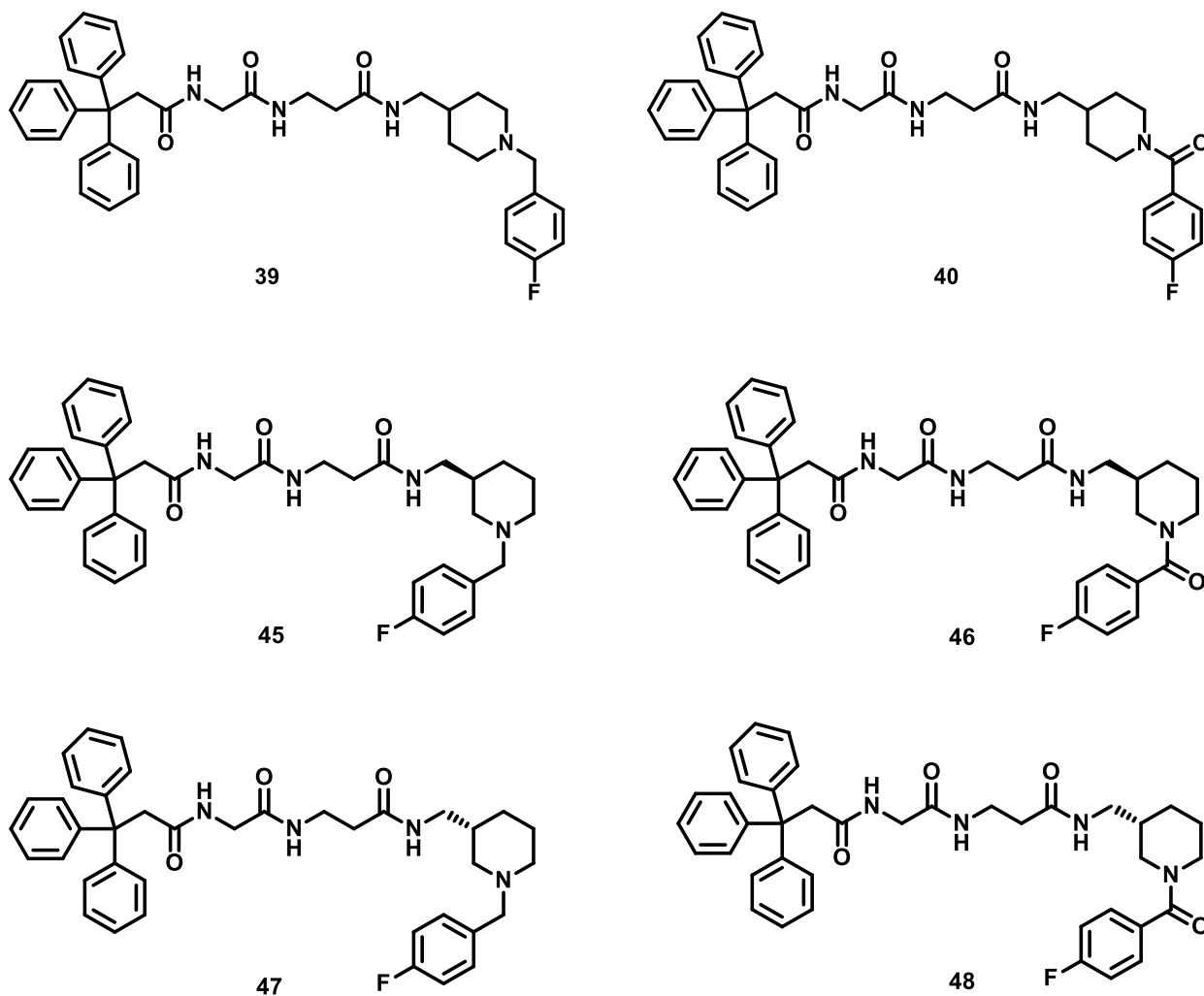
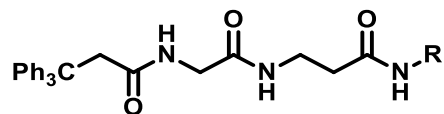


Figure 20: Compounds for GPCR screening of muscarinic acetylcholine receptor subtypes $M_1 - M_5$

About 5mg of each compound was submitted to EuroscreenFast in Belgium to conduct an 8 and 10 dose-response testing of each compound for the determination of IC_{50} values for each muscarinic subtype receptor. The IC_{50} values obtained from the binding assay experiments (Table 4), showed compounds **47** and **45** to have a higher binding affinity to M_3 compared to the other targeted compounds. It could also be observed that structures **40** and **48** did not show any binding inhibition to any of the subtypes, however, compound

46 was found to be highly selective to the subtype M₃ but with a poor binding affinity. Structure **39**, on the other hand, proved to be poorly selective to any of the subtypes with unsatisfactory binding affinities as well. Therefore, comparing the two most promising compounds, **47** and **45**, **47** had a higher affinity to the muscarinic acetylcholine receptor subtype M₃ and much lower affinity to the subtype M₂ as the ratio confirms in Table 4. Compound **45** also showed a good selectivity to the subtype M₃ compared to the other subtypes with a slightly lower binding affinity in contrast with **47**.

Table 4. Binding affinities of target compounds to muscarinic subtypes

No.	R	IC ₅₀ (μM)					IC ₅₀ Ratio M ₂ :M ₃
		M ₁	M ₂	M ₃	M ₄	M ₅	
39		5.88	6.38	15.11	11.63	35.11	1:2
45		13.96	13.78	0.448	13.54	16.41	31:1
46		No inhibition	No inhibition	55.62	No inhibition	No inhibition	1:56
47		23.15	25.51	0.35	21.55	13.11	73:1

Compounds **40** and **48** were not included in this table because they show no inhibition to any of the muscarinic receptor subtypes.

Knowing that all six compounds had a diverse spatial arrangement and knowing the challenging problem of developing an M₂-sparing M₃ antagonist, it was in my interest to investigate, through docking experiments, the interactions on these compounds with the muscarinic subtypes M₃ and M₂. With the help of Dr. Atul Bhardwaj, a research associate at the University of Alberta in the oncology department working in the group of Dr. Frank Wuest, we were able to perform a molecular docking study.

Superposition of predicted binding modes of all compounds indicate that all six compounds attained, overall, similar binding modes in the M₃ receptor binding pocket as shown on the left in Figure 21. A more detailed representation of the interactions between the lead compound **47** and M₃ subtype receptor is shown in Figure 22 where compound **47** indicated H-bonding and hydrophobic interactions with the key residues of the M₃ receptor (docking score = -10.11kcal/mol). It was noticed that one of the O-atom of the carbonyl group showed H-bonding interactions (purple) with Tyr 506 (d =1.95 Å), while two of the terminal phenyl groups showed π-π stacking (green) with Trp 525 and a π-cation interaction (red) with Lys 522 and one of the phenyl rings. The 4-fluoro-benzyl was found to be located in a deep pocket lined by Cys 532, Tyr 513, Val 155, and indicated π-π stacking with Tyr 506. Moreover, the docking analyses of the lead compound **47** did not generate a favorable binding mode to the M₂ receptor, as the only difference in their binding pocket was Phe181^{ECL2} in the M₂ receptor and Leu225^{ECL2} in the M₃ receptor.

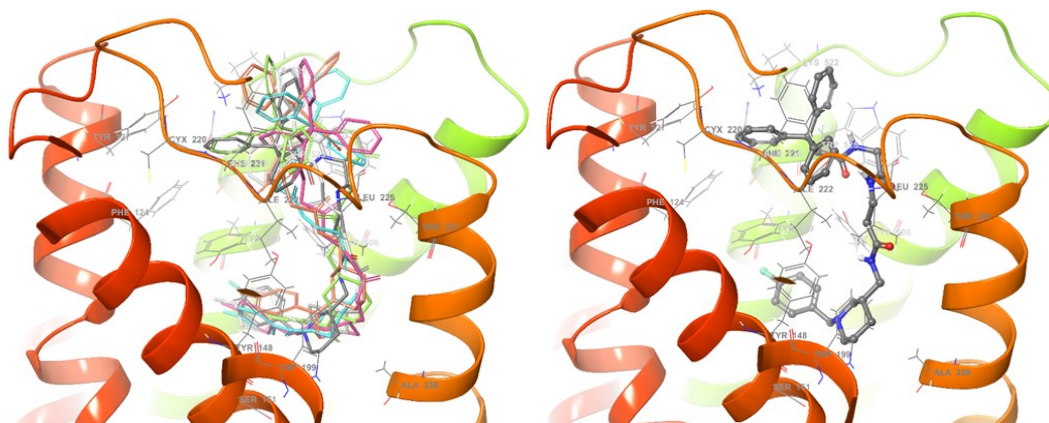


Figure 21: a) Superposition of all six compounds in the M₃ receptor; b) Compound **47** docked in M₃ receptor

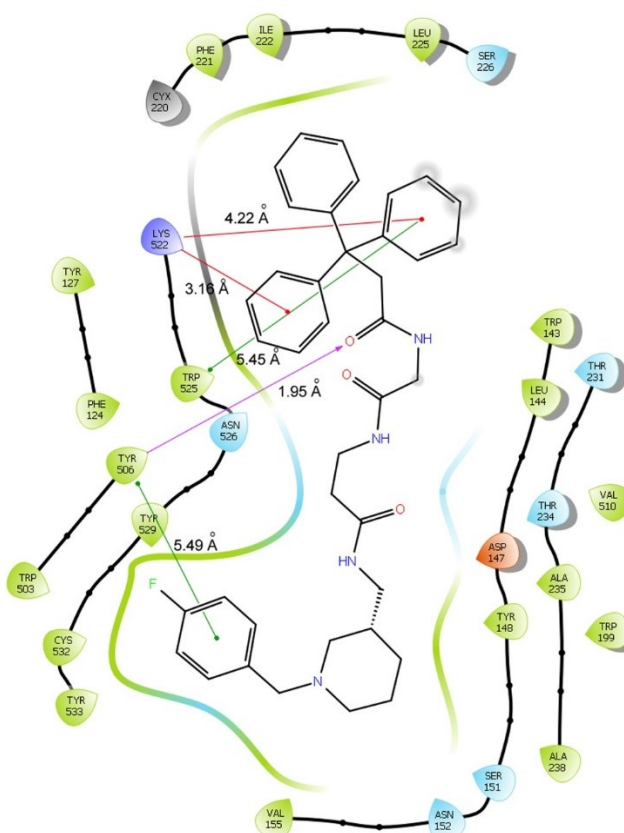


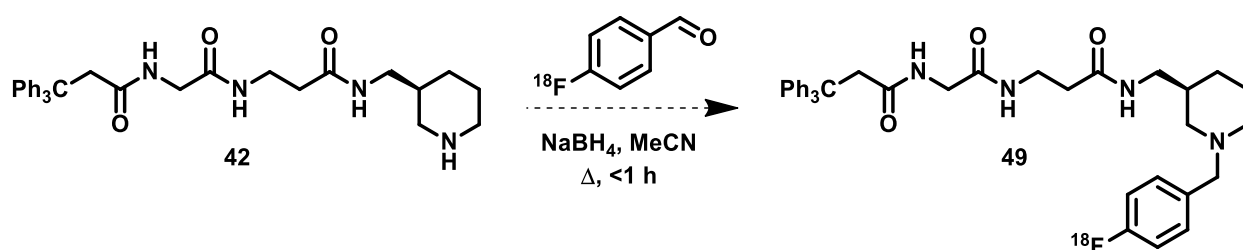
Figure 22: Interaction of lead compound **47** with muscarinic subtype M₃ receptor. H-bonding (purple); π - π stacking (green); π -cation (red)

Hence, through peptide coupling, reductive amination, and acylation chemistry, compounds containing both achiral and chiral centres were developed to study in detail their interactions with the different class of muscarinic receptor subtypes and to search for selectivity especially between the subtypes M₂ and M₃.

2.3 Conclusions and Future Plans

In conclusion, we were able to design and synthesise our six peptide compounds and perform screening for their binding to muscarinic acetylcholine receptor subtypes M₁ – M₅. These compounds were all fluorinated in such a way that radiofluorination could be considered to develop PET tracers in the event that one or more showed high affinity and selectivity. Of the two most promising compounds, **45** and **47**, compound **47** showed high affinity for the M₃ receptor (0.35 μ M) and high selectivity compared to other subtypes. Moreover, in docking experiments, clear differences in binding interactions of **47** could be seen in the M₂ and M₃ binding pockets, and a much more defined binding to the M₃ receptor subtype. This proved that the modifications made at hydrophobic region of the molecules were effective in generating positive results in the binding assay and molecular docking experiments.

With these exciting results, compounds **45** and **47** will be further subjected to radiopharmaceutical and animal testing to study their activity in detail. The synthesis of both structures could also be optimised to improve the chemistry for the half-life of future radiofluorination experiments as shown in an example in the scheme below (Scheme 16).



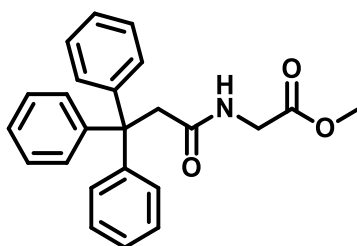
Scheme 16: Example of radiofluorination reaction¹⁰²

2.4 Experimental Section

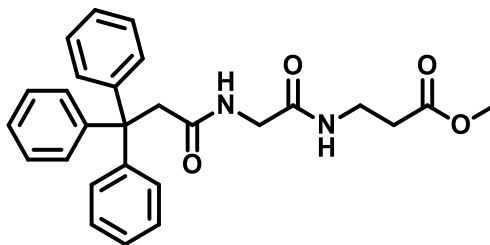
General Methods: All reagents and solvents used in these experiments were bought from MilliporeSigma, Oakwood Chemicals and Combi Block Chemicals without any purification. Progress of reactions was monitored by TLC using MilliporeSigma silica gel 60 F254 glass-backed plates. All reactions were conducted under nitrogen atmosphere with exception of the Boc-deprotection reaction. Compounds were purified by silica gel column chromatography using SiliaFlash® Irregular Silica Gel from SiliCycle. The solvent systems used were solvent A CHCl_3 and a linear gradient elution of solvent B from 2% to 10% of CH_3OH . Purity check of compounds and purification of some final products were done using reversed phase HPLC with C18 column: Phenomenex Luna® 10u C18(2) 250 x 10 mm 100 Å. A gradient elution of 30% to 95% of CH_3CN in water was used to elute the compounds over 35 minutes at a flow rate of 2 mL/min. Product retention time was recorded in minutes. Compounds were characterized by ^1H NMR and ^{13}C NMR: Agilent/Varian Inova four-channel 500 MHz, Agilent/Varian VNMRS two-channel 500 MHz, and Agilent VNMRS four-channel, dual receiver 700 MHz spectrometers. The deuterated solvents used for spectral analysis were CDCl_3 and CD_3OD . High resolution mass spectra were obtained using an Agilent Technologies 6220 oaTOF using electrospray ionization (ESI) technique and the IR spectra was acquired using Nicolet 8700 IR spectrometer.

General Procedure: Amide Coupling

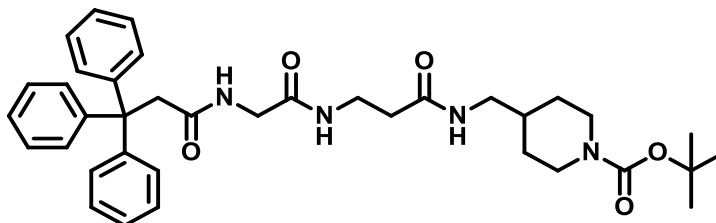
A primary amine derivative (3.31 mmol) was dissolved in CHCl_3 (11 mL), and triethylamine (6.95 mmol) was added. The reaction was stirred for 30 min at room temperature. To the mixture was added the acid derivative (3.31 mmol), EDC (4.30 mmol), and HOBT (4.30 mmol) at 0°C . The reaction was stirred for 20 h and monitored by TLC at room temperature until starting material was consumed. The reaction was quenched with saturated aqueous NaHCO_3 (15 mL), and the mixture was extracted with CHCl_3 (20 mL). The organic layer was washed with water (15 mL) and brine (15 mL). Chloroform layer was dried over MgSO_4 , filtered, and concentrated under vacuo. The residue was purified by silica gel column chromatography ($\text{MeOH}/\text{CHCl}_3$).



Methyl 2-(3,3,3-triphenylpropanamide)acetate. Purification by silica gel column chromatography (gradient elution 1 – 5% $\text{MeOH}/\text{CHCl}_3$) afforded the desired product as a pale yellow semi-solid (1.05 g, 85%). ^1H NMR (498 MHz, CDCl_3) σ 7.29 – 7.24 (m, 12H), 7.24 – 7.19 (m, 3H), 5.35 (br s, 1H), 3.72 (d, $J = 5.0$ Hz, 2H), 3.65 (s, 3H), 3.63 (s, 2H); ^{13}C NMR (126 MHz, CDCl_3) σ 170.6, 169.8, 146.2, 129.1, 128.1, 126.5, 56.2, 52.1, 48.4, 41.4; IR (cast film) 3317, 3031, 2950, 1753, 1660, 1540, 1206 cm^{-1} ; HRMS (+ESI) m/z $[\text{M}+\text{H}]^+$ calcd for $\text{C}_{24}\text{H}_{24}\text{NO}_3$ 374.1751, found 374.1757.

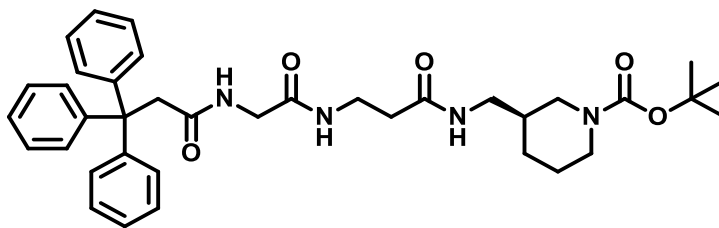


Methyl 3-(2-(3,3,3-triphenylpropanamido)acetamido)propanoate. Purification by silica gel column chromatography (gradient elution 1 – 3% MeOH/CHCl₃) afforded the desired product as a white solid (m. p. 184 – 187 °C, 0.283 g, 76%). ¹H NMR (498 MHz, CDCl₃) σ 7.29 – 7.24 (m, 12H), 7.25 – 7.19 (m, 3H), 6.11 (br s, 1H), 5.43 (br s, 1H), 3.68 (s, 3H), 3.64 (s, 2H), 3.53 (d, *J* = 5.5 Hz, 2H), 3.39 (q, *J* = 6.2 Hz, 2H), 2.45 (t, *J* = 6.3 Hz, 2H); ¹³C NMR (126 MHz, CDCl₃) σ 172.5, 171.1, 168.5, 146.1, 129.1, 128.1, 126.5, 56.2, 51.8, 48.3, 43.6, 34.8, 33.7; IR (cast film) 3315, 3067, 2947, 1733, 1636, 1526, 12.39 cm⁻¹; HRMS (+ESI) *m/z* [M+H]⁺ calcd for C₂₇H₂₉N₂O₄ 467.1941, found 467.1940.



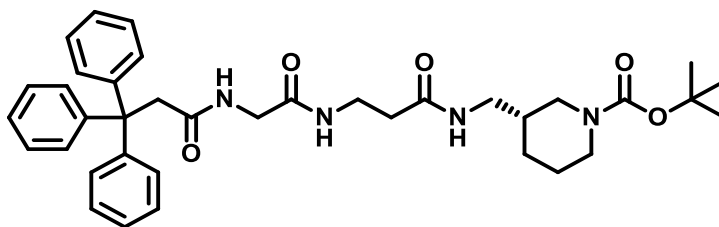
tert-Butyl 4-((3-(2-(3,3,3-triphenylpropanamido)acetamido)propanamido)methyl)piperidine-1-carboxylate. Purification by silica gel column chromatography (gradient elution 1 – 5% MeOH/CHCl₃) afforded the desired product as a white semi-solid (1.05 g, 85%). ¹H NMR (498 MHz, CDCl₃) σ 7.33 – 7.27 (m, 12H), 7.24 – 7.19 (m, 3H), 6.13 (d, *J*

= 6.4 Hz, 1H), 5.85 (t, $J = 6.1$ Hz, 1H), 5.55 (t, $J = 5.4$ Hz, 1H), 4.08 (s, 2H), 3.64 (s, 2H), 3.51 (d, $J = 5.5$ Hz, 2H), 3.38 (q, $J = 6.1$ Hz, 2H), 3.10 (s, 2H), 2.66 (s, 2H), 2.30 (t, $J = 6.1$ Hz, 2H), 1.63 (s, 1H), 1.61 – 1.58 (m, 2H), 1.45 (s, 9H), 1.13 – 1.04 (m, 2H). ^{13}C NMR (126 MHz, CDCl_3) σ 171.3, 171.2, 169.1, 154.8, 146.4, 129.1, 128.0, 126.4, 79.4, 77.3, 56.1, 48.0, 44.8, 43.4, 36.2, 35.9, 35.7, 29.7, 28.4; IR (cast film) 3315, 3057, 1657, 1543, 1227 cm^{-1} ; HRMS (+ESI) m/z $[\text{M}+\text{H}]^+$ calcd for $\text{C}_{37}\text{H}_{47}\text{N}_4\text{O}_5$ 627.3541, found 627.3544.

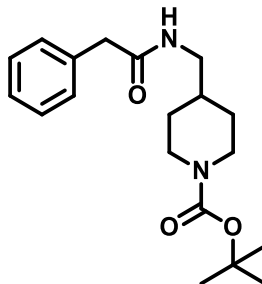


(S)-tert-Butyl 3-((3-(2-(3,3,3-triphenylpropanamido)acetamido)propanamido)methyl)piperidine-1-carboxylate. Purification by silica gel column chromatography (gradient elution 1 – 6% $\text{MeOH}/\text{CHCl}_3$) afforded the desired product as a white semi-solid (0.316 g, 72%). ^1H NMR (498 MHz, CDCl_3) σ 7.27 – 7.22 (m, 12H), 7.24 – 7.19 (m, 3H), 6.82 (br s, 1H), 6.62 (br s, 2H), 3.82 – 3.76 (m, 2H), 3.75 (d, $J = 3.7$ Hz, 1H), 3.67 (d, $J = 15.0$ Hz, 1H), 3.64 – 3.58 (m, 2H), 3.49 (dd, $J = 16.3, 5.5$ Hz, 1H), 3.40 (d, $J = 4.9$ Hz, 1H), 3.35 (t, $J = 7.3$ Hz, 1H), 3.08 – 2.99 (m, 2H), 2.84 (ddd, $J = 14.1, 10.9, 3.0$ Hz, 1H), 2.48 (s, 1H), 2.37 – 2.27 (m, 2H), 1.72 (d, $J = 13.0$ Hz, 1H), 1.67 – 1.57 (m, 2H), 1.41 (s, 9H), 1.17 – 1.05 (m, 1H). ^{13}C NMR (126 MHz, CDCl_3) σ 171.3, 169.9, 155.0, 146.6, 129.2, 127.9, 127.8, 126.2, 79.6, 77.3, 66.5, 56.1, 47.6, 47.2, 45.0, 43.5, 42.1, 36.2, 36.1, 28.4,

24.5. IR (cast film) cm^{-1} 3315, 3057, 2930, 1657, 1543. HRMS (+ESI) m/z $[\text{M}+\text{H}]^+$ calcd for $\text{C}_{37}\text{H}_{47}\text{N}_4\text{O}_5$ 627.3541, found 627.3544.



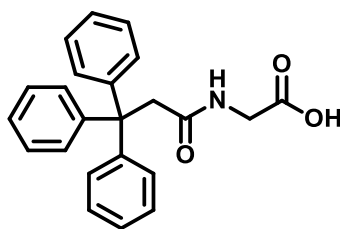
(S)-tert-Butyl 3-((3-(2-(3,3,3-triphenylpropanamido)acetamido)propanamido)methyl)piperidine-1-carboxylate. Purification by silica gel column chromatography (gradient elution 1 – 6% MeOH/ CHCl_3) afforded the desired product as a white semi-solid (0.370 g, 85%). ^1H NMR (498 MHz, CDCl_3) σ 7.28 – 7.23 (m, 12H), 7.24 – 7.19 (m, 3H), 6.88 (s, 1H), 6.67 (s, 2H), 3.84 – 3.77 (m, 2H), 3.76 (d, $J = 3.8$ Hz, 1H), 3.67 (d, $J = 15.0$ Hz, 1H), 3.65 – 3.57 (m, 2H), 3.48 (dd, $J = 16.3, 5.5$ Hz, 1H), 3.39 (q, $J = 6.2, 5.3$ Hz, 1H), 3.37 – 3.27 (m, 1H), 3.10 – 2.98 (m, 2H), 2.84 (ddd, $J = 13.8, 10.9, 3.1$ Hz, 1H), 2.48 (s, 1H), 2.41 – 2.27 (m, 2H), 1.76 – 1.68 (m, 1H), 1.66 – 1.55 (m, 2H), 1.42 (s, 9H), 1.11 (q, $J = 11.7, 10.4$ Hz, 1H). ^{13}C NMR (126 MHz, CDCl_3) σ 171.3, 170.2, 155.0, 146.7, 129.2, 127.8, 127.9, 126.2, 79.6, 77.4, 62.2, 56.1, 47.6, 47.3, 45.0, 43.5, 42.1, 36.2, 36.1, 28.4, 24.5. IR (cast film) cm^{-1} 3316, 3059, 2933, 1656, 1546. HRMS (+ESI) m/z $[\text{M}+\text{H}]^+$ calcd for $\text{C}_{37}\text{H}_{47}\text{N}_4\text{O}_5$ 627.3541, found 627.3544.



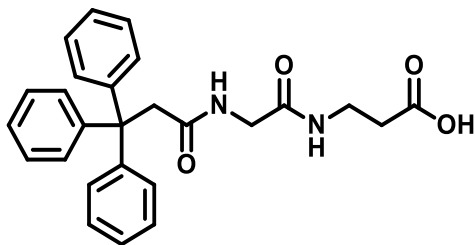
Tert-butyl 4-((2-phenylacetamido)methyl)piperidine-1-carboxylate. Purification by silica gel column chromatography (gradient elution 1 – 5% MeOH/CHCl₃) afforded the desired product as a pale-yellow powder (m. p. 84 – 87 °C, 5.69 g, 97%). ¹H NMR (498 MHz, CDCl₃) σ 7.40 – 7.35 (m, 2H), 7.34 – 7.30 (m, 1H), 7.29 – 7.27 (m, 2H), 5.47 (s, 1H), 4.07 (s, 2H), 3.60 (s, 2H), 3.11 (br s, 2H), 2.64 (br s, 2H), 1.65 – 1.56 (m, 1H), 1.54 (dt, J = 13.9, 3.3 Hz, 2H), 1.46 (br s, 9H), 1.10 – 0.98 (m, 2H). ¹³C NMR (126 MHz, CDCl₃) σ 171.1, 154.7, 134.9, 129.4, 129.1, 127.4, 79.3, 45.0, 43.9, 41.4, 36.2, 29.6, 28.4; IR (cast film) cm⁻¹ 3303, 3065, 2929, 1692, 1550; HRMS (+ESI) m/z [M+H]⁺ calcd for C₁₉H₂₉N₂NaO₃ 355.1992, found 355.1993.

General Procedure: Hydrolysis

To a stirred solution of methyl ester (1.00 mmol) in CH₃OH (3 mL), was LiOH (1.50 mmol) in H₂O (1 mL) added and the reaction was stirred at room temperature for 4 h and monitored by TLC until starting material was consumed. The solvent was removed under vacuo and the residue was acidified with 1 N HCl until pH was between 2 and 3 at 0 °C. The mixture was extracted with EtOAc (5 x 50 mL), dried over MgSO₄, filtered, and concentrated under vacuo. No purification was required.



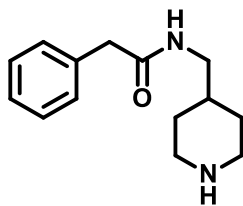
2-(3,3,3-Triphenylpropanamido)acetic acid. Purification was not required. Product was afforded as a white solid (m. p. 131 – 139 °C, 1.29 g, 72%). ¹H NMR (498 MHz, CD₃OD) σ 7.29 – 7.20 (m, *m*-, 12H), 7.20 – 7.13 (m, 3H), 3.70 (s, 2H), 3.57 (d, *J* = 4.8 Hz, 2H). ¹³C NMR (126 MHz, CD₃OD) σ 173.3, 172.9, 148.2, 130.5, 128.7, 127.1, 57.4, 48.1, 41.8. IR (cast film) cm⁻¹ 3290, 3055, 2926, 1722, 1656, 1599. HRMS (+ESI) *m/z* [M-H]⁻ calcd for C₂₃H₂₀NO₃ 358.1449, found 358.1445.



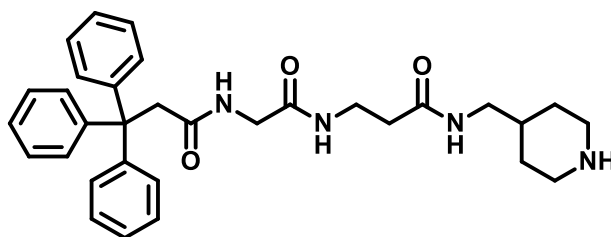
3-(2-(3,3,3-triphenylpropanamido)acetamido)propanoic acid. Purification was not required. Product was afforded as a white solid (m. p. 88 – 93 °C, 5.690 g, 97%). ^1H NMR (498 MHz, CDCl_3) σ ^1H NMR (498 MHz, CD_3OD) δ 7.29 – 7.22 (m, 12H), 7.21 – 7.14 (m, 3H), 3.72 (s, 2H), 3.47 (d, J = 4.9 Hz, 2H), 3.35 (t, J = 6.8 Hz, 2H), 2.44 (t, J = 6.8 Hz, 2H). ^{13}C NMR (126 MHz, CD_3OD) σ 173.9, 172.1, 170.1, 146.8, 129.1, 127.2, 125.7, 56.0, 46.7, 42.1, 34.8, 33.1. IR (cast film) cm^{-1} 3292, 3058, 2935, 1723, 1649, 1531. HRMS (+ESI) m/z $[\text{M}-\text{H}]^-$ calcd for $\text{C}_{26}\text{H}_{25}\text{N}_2\text{O}_4$ 429.182, found 429.1821.

General Procedure: Boc-deprotection

The Boc-protected piperidine derivative (1.40 mmol) was treated in CHCl_3 (5 mL) and was used in the deprotection of the model compound at 0 °C with TFA (3 mmol). After 30 min, the reaction was raised to room temperature and stirred for 5 h. TLC was used to monitor the progress of the reaction. The pH of the reaction mixture was adjusted to 10 with aqueous 5M NaOH and extracted with CHCl_3 (5 x 30 mL). The organic layer was dried over MgSO_4 , filtered, and concentrated under vacuo. Purification was not required.

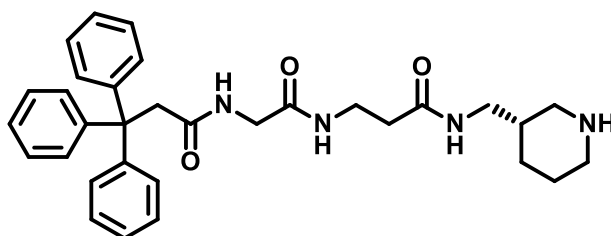


2-phenyl-N-(piperidin-4-ylmethyl)acetamide. Purification was not required. Product was afforded as a pale-yellow semi-solid (0.146 g, 95%). ^1H NMR (498 MHz, CDCl_3) σ 7.36 – 7.31 (m, 2H), 7.30 (t, $J = 7.3$ Hz, 1H), 7.26 – 7.23 (m, 2H), 5.42 (s, 1H), 3.58 (s, 2H), 3.08 (t, $J = 6.3$ Hz, 2H), 3.03 (dt, $J = 12.4, 3.2$ Hz, 2H), 2.53 (t, $J = 12.1$ Hz, 2H), 1.84 – 1.79 (m, 1H), 1.54 (dt, $J = 14.0, 3.2$ Hz, 2H), 1.04 (tt, $J = 12.8, 6.2$ Hz, 2H). ^{13}C NMR (126 MHz, CD_3OD) σ 173.1, 135.5, 128.6, 128.2, 126.5, 43.7, 43.4, 42.4, 33.8, 26.2. IR (cast film) cm^{-1} 3063, 2934, 1644, 1549. HRMS (+ESI) m/z $[\text{M}+\text{H}]^+$ calcd for $\text{C}_{14}\text{H}_{21}\text{N}_2\text{O}$ 233.1648, found 233.1650.



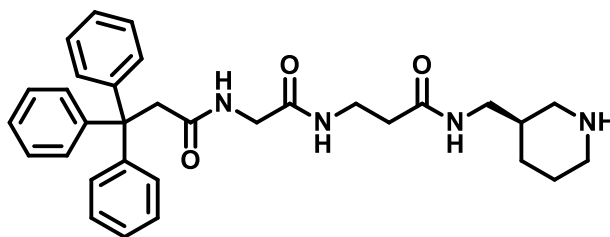
N-(2-oxo-2-((3-oxo-3((piperidin-4-ylmethyl)amino)propyl)amino)ethyl)-3,3,3-triphenylpropanamide. Purification was not required. Product was afforded as a pale-yellow semi-solid (0.727 g, 98%). ^1H NMR (498 MHz, CDCl_3) σ 7.30 – 7.26 (m, 12H), 7.21 (tt, $J = 5.7, 2.6$ Hz, 3H), 6.48 (t, $J = 5.5$ Hz, 1H), 6.31 (t, $J = 6.0$ Hz, 1H), 6.04 (t, $J = 6.2$

Hz, 1H), 3.61 (s, 2H), 3.53 (d, $J = 5.5$ Hz, 2H), 3.36 (q, $J = 6.1$ Hz, 2H), 3.11 (t, $J = 5.9$ Hz, 2H), 3.01 (dt, $J = 12.2, 3.1$ Hz, 2H), 2.54 (td, $J = 12.1, 2.4$ Hz, 2H), 2.32 (t, $J = 6.2$ Hz, 2H), 1.63 – 1.56 (m, 2H), 1.56 – 1.50 (m, 1H), 1.26 (s, 1H), 1.11 (qd, $J = 12.3, 4.2$ Hz, 2H). ^{13}C NMR (126 MHz, CD_3OD) σ 173.9, 173.7, 171.7, 148.3, 130.5, 128.7, 127.2, 57.4, 48.0, 45.0, 44.8, 43.7, 37.1, 36.7, 35.3, 27.6. IR (cast film) cm^{-1} 3300, 3058, 2945, 1782, 1664, 1560. HRMS (+ESI) m/z $[\text{M}+\text{H}]^+$ calcd for $\text{C}_{32}\text{H}_{39}\text{N}_4\text{O}_3$ 527.3017, found 527.3021.



(S)-N-(2-Oxo-2-((3-oxo-3((piperidin-3-ylmethyl)amino)propyl)amino)ethyl)-3,3,3-triphenylpropanamide. Purification was not required. Product was afforded as a pale-yellow semi-solid (0.029 g, 45%). ^1H NMR (498 MHz, CDCl_3) σ 7.25 – 7.20 (m, 12H), 7.19 – 7.14 (m, 3H), 6.98 (q, $J = 5.1, 3.7$ Hz, 2H), 6.86 (t, $J = 5.5$ Hz, 1H), 3.60 (s, 2H), 3.53 – 3.41 (m, 2H), 3.36 – 3.24 (m, 2H), 3.02 – 2.97 (m, 2H), 2.95 (dd, $J = 13.6, 3.9$ Hz, 1H), 2.87 (dt, $J = 13.1, 3.8$ Hz, 1H), 2.47 (td, $J = 11.8, 3.0$ Hz, 1H), 2.25 (t, $J = 6.6$ Hz, 2H), 2.22 – 2.17 (m, 1H), 1.69 (dd, $J = 13.1, 4.0$ Hz, 1H), 1.64 – 1.52 (m, 2H), 1.36 (td, $J = 10.8, 10.1, 5.5$ Hz, 1H), 1.25 (s, 1H), 1.08 – 0.97 (m, 1H). ^{13}C NMR (126 MHz, CDCl_3) σ 171.4, 171.4, 169.3, 146.6, 129.2, 127.9, 126.3, 56.1, 49.8, 47.7, 46.2, 43.2, 42.8, 36.6,

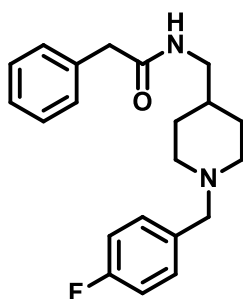
36.0, 35.8, 28.5, 25.0. IR (cast film) cm^{-1} 3301, 3058, 2928, 1651, 1547. HRMS (+ESI) m/z $[\text{M}+\text{H}]^+$ calcd for $\text{C}_{32}\text{H}_{39}\text{N}_4\text{O}_3$ 527.3017, found 527.3011.



(R)-N-(2-oxo-2-((3-oxo-3((piperidin-3-ylmethyl)amino)propyl)amino)ethyl)-3,3,3-triphenylpropanamide. Purification was not required. Product was afforded as a pale yellow semi-solid (0.062 g, 30%). ^1H NMR (498 MHz, CDCl_3) σ 7.26 – 7.21 (m, 12H), 7.20 – 7.15 (m, 3H), 6.86 – 6.80 (m, 1H), 6.78 – 6.72 (m, 1H), 6.65 (t, $J = 5.6$ Hz, 1H), 3.61 (s, 2H), 3.55 – 3.42 (m, 2H), 3.36 – 3.28 (m, 2H), 3.05 – 2.96 (m, 2H), 2.94 (d, $J = 11.3$ Hz, 1H), 2.88 (d, $J = 12.2$ Hz, 1H), 2.52 – 2.44 (m, 1H), 2.25 (t, $J = 6.5$ Hz, 2H), 2.21 (d, $J = 11.4$ Hz, 1H), 1.70 (d, $J = 12.7$ Hz, 1H), 1.65 – 1.52 (m, 2H), 1.36 (d, $J = 12.4$ Hz, 1H), 1.25 (s, 1H), 1.10 – 0.98 (m, 1H). ^{13}C NMR (126 MHz, CDCl_3) σ 171.3, 171.3, 169.2, 146.5, 129.2, 128.0, 126.4, 56.2, 50.1, 47.9, 46.4, 43.3, 42.9, 36.8, 35.9, 35.8, 28.7, 25.3. IR (cast film) cm^{-1} 3302, 3058, 2928, 1650, 1547. HRMS (+ESI) m/z $[\text{M}+\text{H}]^+$ calcd for $\text{C}_{37}\text{H}_{47}\text{N}_4\text{O}_5$ 527.3017, found 527.3012.

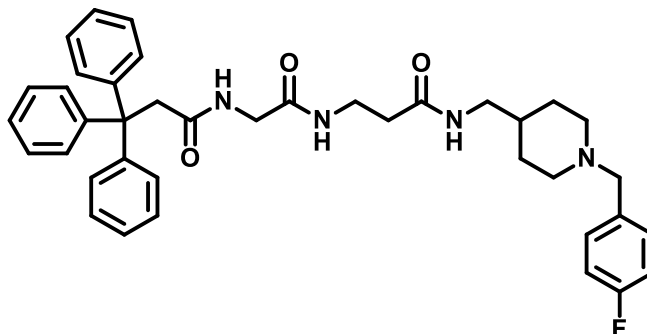
General Procedure: Reductive Amination

4-Fluorobenzaldehyde (0.09 mmol) and piperidine derivative (0.14 mmol) were dissolved in CHCl_3 (0.5 mL) at room temperature. $\text{Na}(\text{OAc})_3\text{BH}$ (0.45 mmol) and acetic acid (0.18 mmol) were added. The mixture was stirred for 20 h and monitored by TLC until starting material was consumed. The suspension was quenched with NaHCO_3 (2 mL), and the aqueous layer was extracted with CHCl_3 (4 x 5 mL). The organic layers were combined, dried over MgSO_4 , filtered, and concentrated under vacuo. The crude product was purified by silica gel column chromatography ($\text{MeOH}/\text{CHCl}_3$).

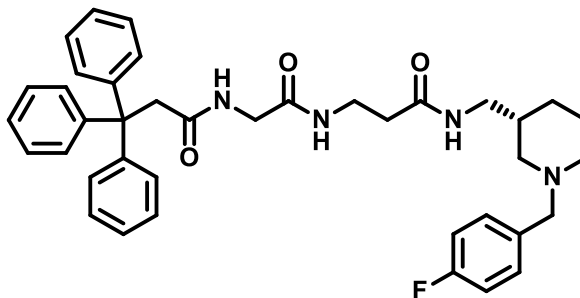


***N*-((1-(4-fluorobenzyl)piperidin-4-yl)methyl)-2-phenylacetamide.** Purification by silica gel column chromatography (gradient elution 1 – 5% $\text{MeOH}/\text{CHCl}_3$) afforded the desired product as a pale yellow solid (m. p. 133 – 136 °C, 0.295 g, 72%). ^1H NMR (498 MHz, CDCl_3) σ 7.35 (t, J = 7.4 Hz, 2H), 7.29 (t, J = 7.3 Hz, 1H), 7.26 – 7.19 (m, 4H), 6.98 (t, J = 8.5 Hz, 2H), 5.38 (s, 1H), 3.57 (s, 2H), 3.42 (s, 2H), 3.09 (t, J = 6.4 Hz, 2H), 2.81 (d, J = 11.1 Hz, 2H), 1.89 (t, J = 11.6 Hz, 2H), 1.52 (d, J = 12.9 Hz, 2H), 1.47 – 1.40 (m, 1H), 1.18 (d, J = 11.7 Hz, 2H). ^{19}F NMR (468 MHz, CDCl_3) σ -116.19. ^{13}C NMR (126 MHz, CDCl_3) σ 170.9, 135.0, 130.5 (d, J = 10.9 Hz, 1C), 129.4, 129.0, 127.4, 120.5, 115.0 (d, J = 20.5 Hz, 2C), 103.2, 62.4, 53.1, 45.1, 43.9, 35.8, 29.8. IR (cast film) cm^{-1} 3291, 3066,

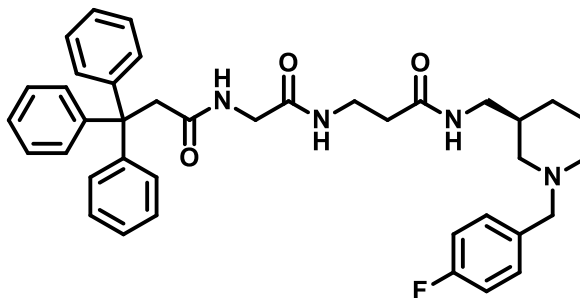
3030, 2920, 1644, 1508. HRMS (+ESI) m/z $[M+H]^+$ calcd for $C_{21}H_{26}FN_2O$ 341.2024, found 341.2021.



***N*-(2-((3-((1-(4-Fluorobenzyl)piperidin-4-yl)methyl)amino)-3-oxopropyl)amino)-2-oxoethyl)-3,3,3-triphenylpropanamide.** Purification by silica gel column chromatography (gradient elution 1 – 10% MeOH/ $CHCl_3$) afforded the desired product as a white semi-solid (0.042 g, 74%). 1H NMR (498 MHz, $CDCl_3$) σ 7.33 – 7.29 (m, 12H), 7.28 – 7.27 (m, 2H), 7.25 – 7.20 (m, 3H), 7.05 – 6.97 (m, 2H), 6.35 (d, J = 6.3 Hz, 1H), 6.02 (s, 1H), 5.90 (s, 1H), 3.65 (s, 2H), 3.53 (d, J = 5.5 Hz, 2H), 3.47 (s, 2H), 3.38 (q, J = 6.2 Hz, 2H), 3.12 (t, J = 6.2 Hz, 2H), 2.88 (dd, J = 11.5, 3.6 Hz, 2H), 2.31 (t, J = 6.2 Hz, 2H), 1.95 (td, J = 11.6, 2.5 Hz, 2H), 1.63 (d, J = 12.9 Hz, 2H), 1.51 – 1.42 (m, 1H), 1.29 – 1.27 (m, 2H). ^{19}F NMR (468 MHz, $CDCl_3$) σ -115.78, ^{13}C NMR (126 MHz, $CDCl_3$) σ 171.2, 171.0, 168.9, 146.4, 135.4, 130.9 (d, J = 8.4 Hz, 1C), 129.1, 127.9, 126.3, 115.2 (d, J = 21.4 Hz, 2C), 102.4, 61.8, 56.2, 52.9, 48.2, 46.0, 44.4, 43.5, 35.9, 35.6, 29.1. IR (cast film) cm^{-1} 3309, 3057, 2924, 1645, 1508. HRMS (+ESI) m/z $[M+H]^+$ calcd for $C_{39}H_{44}FN_4O_3$ 635.3392 found 635.3389.



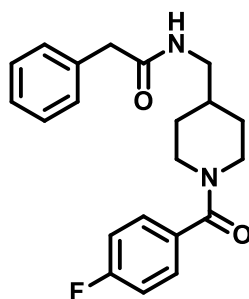
(R)-N-(2-((3-(((1-(4-Fluorobenzyl)piperidin-3-yl)methyl)amino)-3-oxopropyl)amino)-2-oxoethyl)-3,3,3-triphenylpropanamide. Purification by silica gel column chromatography (gradient elution 1 – 10% MeOH/CHCl₃) afforded the desired product as a white semi solid (0.013 g, 36%). ¹H NMR (498 MHz, CDCl₃) σ 7.37 – 7.32 (m, 2H), 7.31 – 7.28 (m, 12H), 7.25 – 7.19 (m, 3H), 7.07 – 6.99 (m, 2H), 6.58 (s, 1H), 6.33 (s, 1H), 6.03 (s, 1H), 3.68 – 3.64 (m, 2H), 3.58 – 3.54 (m, 2H), 3.51 (d, *J* = 12.2 Hz, 1H), 3.42 – 3.35 (m, 2H), 3.14 – 3.08 (m, 2H), 2.93 (br s, 1H), 2.78 (br s, 1H), 2.30 (t, *J* = 6.2 Hz, 2H), 2.17 – 2.13 (m, 1H), 2.04 – 1.95 (m, 1H), 1.90 (br s, 1H), 1.74 – 1.67 (m, 2H), 1.67 – 1.56 (m, 2H), 1.08 – 0.96 (m, 1H). ¹⁹F NMR (468 MHz, CDCl₃) σ -124.97. ¹³C NMR (126 MHz, CDCl₃) σ 174.6, 171.4, 169.1, 146.3, 131.3 (d, *J* = 8.9 Hz, 1C), 129.1, 128.0, 127.2, 126.4, 115.4 (d, *J* = 20.9 Hz, 2C), 109.2, 62.0, 57.4, 56.2, 53.1, 48.0, 43.6, 42.8, 36.1, 35.9, 35.9, 27.8, 23.8. IR (cast film) cm⁻¹ 3300, 3060, 2931, 1650, 1509. HRMS (+ESI) *m/z* [M+H]⁺ calcd for C₃₉H₄₄FN₄O₃ 635.3392 found 635.3385.



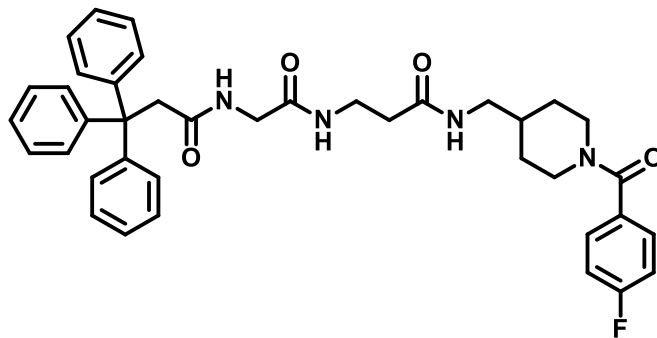
(S)-N-(2-((3-(((1-(4-Fluorobenzyl)piperidin-3-yl)methyl)amino)-3-oxopropyl)amino)-2-oxoethyl)-3,3,3-triphenylpropanamide. Purification by reverse phase HPLC column (30 – 95% MeCN/H₂O) afforded the desired product as a white semi-solid (0.004 g, 63%). ¹H NMR (498 MHz, CDCl₃) σ 7.89 (s, 1H), 7.49 (s, 1H), 7.45 – 7.39 (m, 2H), 7.25 – 7.20 (m, 12H), 7.20 – 7.16 (m, 3H), 7.14 – 7.07 (m, 2H), 6.43 (s, 1H), 4.18 (d, J = 12.7 Hz, 1H), 3.78 (dd, J = 13.1, 5.4 Hz, 1H), 3.68 (d, J = 12.3 Hz, 1H), 3.65 – 3.62 (m, 2H), 3.61 – 3.57 (m, 2H), 3.40 – 3.35 (m, 2H), 3.22 (d, J = 11.9 Hz, 1H), 2.98 (br s, 1H), 2.97 – 2.94 (m, 1H), 2.45 – 2.36 (m, 2H), 2.33 – 2.27 (m, 1H), 2.26 – 2.21 (m, 1H), 2.17 (s, 1H), 1.87 – 1.80 (m, 2H), 1.73 (d, J = 13.4 Hz, 1H), 1.03 – 0.93 (m, 1H). ¹⁹F NMR (468 MHz, CDCl₃) σ -130.72. ¹³C NMR (126 MHz, CDCl₃) σ 172.9, 172.3, 170.3, 146.4, 133.4 (d, J = 6.2 Hz, 1C) 129.1, 127.9, 126.4, 123.9, 116.4 (d, J = 12.4 Hz, 2C), 114.0, 60.5, 57.3, 56.1, 51.2, 47.5, 43.8, 42.2, 36.7, 36.4, 36.1, 26.5, 22.4. IR (cast film) cm⁻¹ 3306, 3059, 2924, 1650, 1509. HRMS (+ESI) m/z [M+H]⁺ calcd for C₃₉H₄₄FN₄O₃ 635.3392 found 635.3388.

General Procedure: Acylation

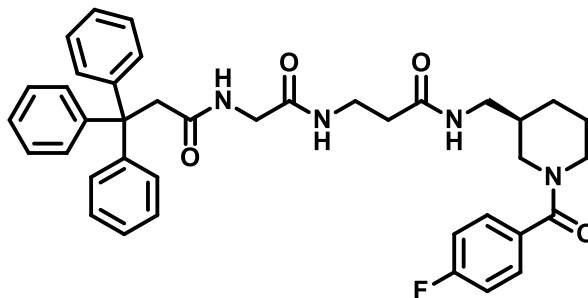
To a solution of piperidine derivative (0.09 mmol) in CHCl_3 (0.5 mL) was added triethylamine (0.45 mmol) and Benzoyl chloride (0.09 mmol) at 0 °C. The reaction was raised to room temperature and stirred for 24 h, monitored by TLC. The mixture was washed with 1 N aqueous HCl (3mL) and brine (3 mL). The organic layers were dried over MgSO_4 , filtered, and concentrated under vacuum. The crude product was purified by silica gel column chromatography (MeOH/ CHCl_3).



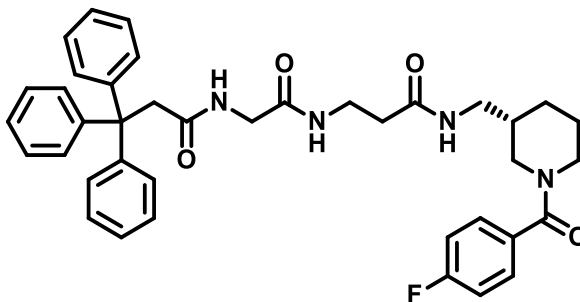
***N*-((1-(4-Fluorobenzoyl)piperidin-4-yl)methyl)-2-phenylacetamide.** Purification by silica gel column chromatography (gradient elution 1 – 7% MeOH/ CHCl_3) afforded the desired product as a pale yellow solid (0.171 g, 60%). ^1H NMR (498 MHz, CD_3OD) σ 7.45 – 7.39 (m, 2H), 7.33 – 7.27 (m, 4H), 7.26 – 7.21 (m, 1H), 7.18 (t, J = 8.6 Hz, 2H), 4.63 – 4.69 (m, 1H), 3.71 – 3.64 (m, 1H), 3.50 (s, 2H), 3.12 (d, J = 6.5 Hz, 2H), 3.04 (d, J = 13.8 Hz, 1H), 2.81 (s, 1H), 1.85 – 1.74 (m, 2H), 1.64 – 1.59 (m, 1H), 1.27 – 1.05 (m, 2H). ^{19}F NMR (468 MHz, CD_3OD) σ -110.37. ^{13}C NMR (126 MHz, CD_3OD) σ 171.2, 169.4, 136.6, 134.9, 132.1 (d, J = 3.9 Hz, 1C), 129.3, 129.1, 127.4, 115.5 (d, J = 33.4 Hz, 2C), 111.3, 45.8, 44.7, 43.8, 42.1, 36.4. IR (cast film) cm^{-1} 3297, 3066, 2921, 1710, 1604, 1552. HRMS (+ESI) m/z $[\text{M}+\text{H}]^+$ calcd for $\text{C}_{21}\text{H}_{24}\text{FN}_2\text{O}_2$ 355.1816 found 355.1819.



***N*-(2-((3-(((1-(4-fluorobenzoyl)piperidin-4-yl)methyl)amino-3-oxopropyl)amino)-2-oxoethyl)-3,3,3-triphenylpropanamide.** Purification by silica gel column chromatography (1 – 8% MeOH/CHCl₃) afforded the desired product as a white semi-solid (0.034 g, 63%). ¹H NMR (498 MHz, CDCl₃) σ 7.40 – 7.32 (m, 2H), 7.27 – 7.24 (m, *m*-, 12H), 7.21 – 7.15 (m, 3H), 7.08 – 7.00 (m, 2H), 6.04 (s, 1H), 5.80 (s, 1H), 5.45 (s, 1H), 3.61 (s, 2H), 3.48 (d, *J* = 5.6 Hz, 2H), 3.36 (q, *J* = 6.1 Hz, 2H), 3.13 (t, *J* = 6.3 Hz, 2H), 2.84 (t, *J* = 12.7 Hz, 2H), 2.29 (t, *J* = 6.1 Hz, 2H), 1.78 – 1.71 (m, 1H), 1.70 – 1.63 (m, 2H), 1.25 (s, 1H), 1.20 – 1.13 (m, 2H), 0.85 – 0.80 (m, 1H). ¹⁹F NMR (468 MHz, CDCl₃) σ -110.73. ¹³C NMR (126 MHz, CDCl₃) σ 171.3, 169.4, 169.1, 162.6, 146.4, 132.1 (d, *J* = 13.5 Hz, 1C), 129.1, 127.9, 127.5, 126.4, 116.7, 115.5 (d, *J* = 27.0 Hz, 2C), 56.1, 47.9, 45.9, 44.5, 43.5, 36.3, 36.0, 35.8, 8.9. IR (cast film) cm⁻¹ 3301, 3058, 1724, 1650, 1543. HRMS (+ESI) *m/z* [M+H]⁺ calcd for C₃₉H₄₂FN₄O₄ 649.3185 found 649.3223.



(S)-N-(2-(((1-(4-Fluorobenzoyl)piperidin-3-yl)methyl)amino)-3-oxopropyl)amino)-2-oxoethyl)-3,3,3-triphenylpropanamide. Purification by silica gel column chromatography (gradient elution 1 – 8% MeOH/CHCl₃) afforded the desired product as a white semi-solid (0.017 g, 73%). ¹H NMR (498 MHz, CDCl₃) σ 7.29 – 7.27 (m, 2H), 7.26 – 7.23 (m, 12H), 7.22 – 7.18 (m, 3H), 7.02 (t, *J* = 8.4 Hz, 2H), 6.84 (s, 1H), 6.73 (s, 1H), 6.66 (s, 1H), 4.20 (d, *J* = 13.0 Hz, 1H), 3.64 – 3.58 (m, 2H), 3.58 – 3.52 (m, 2H), 3.50 (d, *J* = 5.4 Hz, 1H), 3.47 (s, 2H), 3.44 – 3.30 (m, 2H), 3.08 (s, 1H), 2.74 – 2.56 (m, 1H), 2.36 (s, 2H), 1.83 – 1.73 (m, 2H), 1.68 – 1.59 (m, 1H), 1.45 – 1.33 (m, 1H), 1.26 – 1.21 (m, 1H). ¹⁹F NMR (468 MHz, CDCl₃) σ -109.81. ¹³C NMR (126 MHz, CDCl₃) σ 171.7, 171.4, 170.2, 169.5, 146.6, 129.2, 129.0 (d, *J* = 8.7 Hz, 1C), 127.8, 126.3, 115.7 (d, *J* = 21.0 Hz, 2C), 56.2, 48.7, 47.6, 46.4, 43.7, 42.1, 36.5, 36.4, 28.5, 25.2, 18.4. IR (cast film) cm⁻¹ 3308, 3060, 2929, 1654, 1617, 1544. HRMS (+ESI) *m/z* [M+Na]⁺ calcd for C₃₉H₄₁FN₄NaO₄ 671.3004 found 671.3004.



(R)-N-(2-((3-(((1-(4-fluorobenzoyl)piperidin-3-yl)methyl)amino)-3-oxopropyl)amino)-2-oxoethyl)-3,3,3-triphenylpropanamide. Purification by silica gel column chromatography (gradient elution 1 – 8% MeOH/CHCl₃) afforded the desired product as a white semi-solid (0.078 g, 90%). ¹H NMR (498 MHz, CDCl₃) σ 7.25 (t, *J* = 5.7 Hz, 2H), 7.24 – 7.20 (m, *m*-, 12H), 7.20 – 7.15 (m, 3H), 7.08 (s, 1H), 7.00 (t, *J* = 8.4 Hz, 2H), 6.87 (s, 1H), 6.79 (s, 1H), 4.21 (d, *J* = 12.9 Hz, 1H), 3.63 – 3.57 (m, 2H), 3.56 – 3.52 (m, 2H), 3.47 (dd, *J* = 16.2, 5.2 Hz, 1H), 3.41 – 3.29 (m, 2H), 3.06 (s, 2H), 3.04 (s, 1H), 2.65 (dd, *J* = 13.0, 9.6 Hz, 1H), 2.34 (s, 2H), 1.83 – 1.70 (m, 2H), 1.69 – 1.57 (m, 1H), 1.40 (d, *J* = 10.8 Hz, 1H), 1.27 – 1.15 (m, 1H). ¹⁹F NMR (468 MHz, CDCl₃) σ -109.78. ¹³C NMR (126 MHz, CDCl₃) σ 171.8, 171.5, 170.3, 169.5, 164.3, 162.3, 146.6, 129.2, 129.0 (d, *J* = 12.4 Hz, 1C), 127.8, 126.2, 115.7 (d, *J* = 26.1 Hz, 2C), 56.2, 48.7, 47.5, 46.4, 43.6, 42.2, 36.5, 36.5, 36.3, 28.5, 25.2. IR (cast film) cm⁻¹ 3309, 3060, 2933, 1653, 1617, 1544. HRMS (+ESI) *m/z* [M+H]⁺ calcd for C₃₉H₄₂FN₄O₄ 649.3185 found 649.32.

REFERENCES

- [1] Felder, C. C., Muscarinic acetylcholine receptors: signal transduction through multiple effectors, *FASEB*, **1995**, 9, 619–625.
- [2] Bonner, T. I., The molecular basis of muscarinic receptor diversity, *Trends Neurosci.*, **1987**, 12, 148–151.
- [3] Caulfield, M. P., Muscarinic receptors-characterization, coupling and function, *Pharmacol. Ther.* **1993**, 58, 319–379.
- [4] Adlei, B. C., Gregory, P. K., Physiology, cholinergic receptors, *StatPearls*, **2018**.
- [5] Shapiro, R. A., Tietje, K. M., Subers, E. M., Habecker, B. A., Nathanson, N. M., Regulation of muscarinic acetylcholine receptor function in cardiac cells and in cells expressing cloned receptor genes, *Trends Pharmacol. Sci.*, **1989**.
- [6] Enz, A., M4 Muscarinic acetylcholine receptor, *ScienceDirect*, **2007**.
<https://doi.org/10.1016/B978-008055232-3.60213-2>
- [7] Aronstam, R. S., Patil, P., Muscarinic receptors: autonomic neurons, *Encyclop. of Neuroscience*, **2009**. <https://www.sciencedirect.com/topics/neuroscience/muscarinic-acetylcholine-receptor>
- [8] Levey, A. I., Edmunds, S. M., Heilman, C. J., Desmond, C. J., Frey, K. A., Localization of muscarinic M₃ receptor protein and M₃ receptor binding in rat brain, *Neuroscience*, **1994**, 63, 207–221.

[9] Caulfield, M. P., Birdsall, N. J. M., Classification of muscarinic acetylcholine receptors, *ASPET*, **1998**, *50*, 279–290.

[10] Sagara, Y., Sagara, T., Mase, T., Kimura, T., Numazawa, T., Fujikawa, T., Noguchi, K., and Ohtake, N., Cyclohexylmethylpiperidinyltriphenylpropioamide: a selective muscarinic M₃ antagonist discriminating against the other receptor subtypes, *J. Med. Chem.* **2002**, *45*, 984–987.

[11] Lundstrom, K., An overview on GPCRs and drug discovery: structure-based drug design and structural biology on GPCRs, *Methods Mol. Biol.*, **2009**, *552*, 51–66.

[12] Leherte, L., Laaksonen, A., Vercauteren, D. P., Fossépré, M., On the modularity of the intrinsic flexibility of the μ opioid receptor: a computational study, *PLOS ONE*, **2014**, *9(12)*, 1–25.

[13] Baldwin, J. M., Structure and function of receptor coupled to G proteins, *Curr. Opin. Cell Biol.*, **1994**, *6*, 180–190.

[14] Oldham, W. M. and Hamm, H. E., Heterotrimeric G protein activation by G-protein-coupled receptors, *Nat. Rev. Mol. Cell Biol.*, **2008**, *9*, 60–71.

[15] Baltoumas, F. A., Theodoropoulou, M. C., and Hamodrakas, S. J., Interactions of the α -subunits of heterotrimeric G-proteins with GPCRs, effectors and RGS proteins: a critical review and analysis of interacting surfaces, conformational shifts, structural diversity and electrostatic potentials, *J. Struct. Biol.*, **2013**, *182*, 209–218.

[16] Chung, K. Y., Structural aspects of GPCR-G protein coupling, *Toxicol. Res.*, **2013**, 29, 149–155.

[17] Jones, J. C., Duffy, J. W., Machius, M., Temple, B. R., Dohlman, H. G., and Jones, A. M., The crystal structure of self-activating G protein alpha subunit reveals its distinct mechanism of signal initiation, *Sci. Signaling*, **2011**, 4, ra8.

[18] Coleman, D. E., Berghuis, A. M., Lee, E., Linder, M. E., Gilman, A. G., and Sprang, S. R., Structures of active conformations of G_i alpha 1 and the mechanism of GTP hydrolysis, *Science*, **1994**, 265, 1405–1412.

[19] Preininger, A. M., Van Eps, N., Yu, N. J., Medkova, M., Hubbell, W. L., and Hamm, H. E., The myristoylated amino terminus of G_{alpha}(i) (1) plays a critical role in the structure and function of G_{alpha}(i) (1) subunits in solution, *Biochemistry*, **2003**, 42, 7931–7941.

[20] Franco, M., Chardin, P., Chabre, M., and Paris, S., Myristoylation-facilitated binding of G protein ARF1GDP to membrane phospholipids is required for its activation by a soluble nucleotide exchange factor, *J. Biol. Chem.*, **1996**, 271, 1573–1578.

[21] Degtyarev, M. Y., Spiegel, A. M., and Jones, T. L., Palmitoylation of a G protein alpha I subunit requires membrane localization not myristoylation, *J. Biol. Chem.*, **1994**, 269, 30898–30903.

[22] Hamm, H. E., Deretic, D., Arendt, A., Hargrave, P. A., Koenig, B., and Hofmann, K. P., Site of G protein binding to rhodopsin mapped with synthetic peptides from the alpha subunit, *Science*, **1988**, 241, 832–835.

[23] Hu J., Wang Y., Zhang X., Lloyd J. R., Li J. H., Karpiak J., Costanzi S. and Wess J., Structural basis of G protein-coupled receptor-G protein interactions, *Nat. Chem. Biol.*, **2010**, 6, 541–548.

[24] Cai K., Itoh Y., and Khorana H. G., Mapping of contact sites in complex formation between transducing and light-activated rhodopsin by covalent crosslinking: use of a photoactivatable reagent, *Proc. Natl. Acad. Sci. U. S. A.*, **2001**, 98, 4877–4882.

[25] Taylor J. M., Jacob-Mosier G. G., Lawton R. G., Remmers A. E., and Neubig R. R., Binding of an alpha 2 adrenergic receptor third intracellular loop peptide to G beta and the amino terminus of G alpha, *J. Biol. Chem.*, **1994**, 269, 27618–27624.

[26] Itoh Y., Cai K., and Khorana H. G., Mapping of contact sites in complex formation between light-activated rhodopsin and transducing by covalent crosslinking: use of a chemically preactivated reagent, *Proc. Natl. Acad. Sci. U. S. A.*, **2001**, 98, 4883–4887.

[27] Waymire, J. C., Acetylcholine neurotransmission, *Neuroscience Online*, **1997**.
<https://nba.uth.tmc.edu/neuroscience/m/s1/chapter11.html>

[28] Picciotto, M. R., Higley, M. J., and Mineur, Y. S., Acetylcholine as a neuromodulator: cholinergic signaling shapes nervous system function and behavior, *Neuron*. **2012**, 76, 116–129.

[29] Sam, C., and Bordoni, B., Physiology, acetylcholine, *StatPearls*, **2021**.
<https://www.ncbi.nlm.nih.gov/books/NBK557825/>

[30] Ito, H. T., and Schuman, E. M., Frequency-dependent signal transmission and modulation by neuromodulators, *Front. Neurosci.*, **2008**, 2, 138–144.

[31] Hasselmo, M. E., The role of acetylcholine in learning and memory, *Curr. Opin. Neurobiol.*, **2006**, 16, 710–715.

[32] Cherry K., Discovery and functions of acetylcholine, *Biol. Psychology*, **2021**.
<https://www.verywellmind.com/what-is-acetylcholine-2794810>

[33] Colovic M. B., Kristic D. Z., Lazarevic-Pasti T. D., Bondzic A. M., and Vasic V. M., Acetylcholinesterase inhibitors: pharmacology and toxicology, *Curr. Neuropharmacol.*, **2013**, 11(3), 315–335.

[34] Lombardo S., and Maskos U., Role of the nicotinic acetylcholine receptor in Alzheimer's disease pathology and treatment, *Neuropharmacology*, **2015**, 96, 255–262.

[35] Suszkiw, J. B., and Pilar, G., Selective localization of a high affinity choline uptake system and its role in ACh formation in cholinergic nerve terminals, *J. Neurochem.*, **1976**, 26, 1133–1138.

[36] Amenta, F., and Tayebati S. K., Pathways of acetylcholine synthesis, transport and release as targets for treatment of adult-onset cognitive dysfunction, *Current Medicinal Chemistry*, **2008**, 15(5), 488–498.

[37] Jope, R. S., High affinity choline transport and acetylCoA production in the brain and their roles in the regulation of acetylcholine synthesis, *Brain Res.*, **1979**, 180, 313–344.

[38] Tuček, S., The synthesis of acetylcholine: twenty years of progress, *Prog. Brain Res.*, **1990**, *84*, 467–477.

[39] Rylett R. J., and Schmidt, B. M., Regulation of the synthesis of acetylcholine, *Prog. Brain Res.*, **1993**, *98*, 161–166.

[40] George, M. K., Nutritional and herbal therapies for children and adolescents, *Science Direct*, **2010**. <https://www.sciencedirect.com/topics/medicine-and-dentistry/negative-syndrome>

[41] Britannica, The editors of encyclopaedia. “Acetylcholine”, *Encyclopedia Britannica*, **2020**. <https://www.britannica.com/science/acetylcholine>

[42] Han, J., Pluhachkova, K., and Böckmann R. A., The multifaceted role of SNARE proteins in membrane fusion, *Front Physiol.*, **2017**. https://www.researchgate.net/publication/312573222_The_Multifaceted_Role_of_SNARE_Proteins_in_Membrane_Fusion

[43] Hussain, S., and Davanger, S., The discovery of the soluble N-ethylmaleimide-sensitive factor attachment protein receptor complex and molecular regulation of synaptic vesicle transmitter release: the 2010 Kavli Prize in neuroscience, *Neuroscience*, **2011**, *190*, 12–20.

[44] Creative Biomart, Neurotransmitter G-protein coupled receptor, **2021**. https://www.creativebiomart.net/researcharea-neurotransmitter-g-protein-coupled-receptors_2219.htm

[45] Giraudo, C. G., Eng, W. S., Melia, T. J., and Rothman, J. E., A clamping mechanism involved in SNARE-dependent exocytosis, *Science*, **2006**, *313*, 676–680.

[46] Yoon, T. Y., Munson, M., SNARE complex assembly and disassembly, *Curr Biol.*, **2018**, *28(8)*, R397–R401.

[47] Bui, T., and Duong, H., Muscarinic agonist, *StatPearls*, **2020**.
<https://www.ncbi.nlm.nih.gov/books/NBK553130/>

[48] Fetters, L. J., and Matthews, J. I., Methacholine challenge test, *Arch Intern Med.*, **1984**, *144(5)*, 938–940.

[49] Bolton T. B., The depolarizing action of acetylcholine or carbachol in intestinal smooth muscle, *J Physiol.*, **1972**, *220(3)*, 647–671.

[50] Neely G. A., Sabir S., and Kohli A., Neostigmine, *StatPearls*, **2020**.
<https://www.ncbi.nlm.nih.gov/books/NBK470596/>

[51] Santoro, A., Siviero, P., Minicuci, N., Bellavista, E., Mishto, M., Olivieri, F., Marchegiani, F., Chiamenti, A. M., Benussi, L., Ghidoni, R., Nacmias, B., Bagnoli, S., Ginestroni, A., Scarpino, O., Feraco, E., Gianni, W., Cruciani, G., Paganelli, R., Di Lorio, A., Scognamiglio, M., Grimaldi, L. M., Gabelli, C., Sorbi, S., Binetti, G., Crepaldi, G., Franceschi, C., Effects of donepezil, galantamine and rivastigmine in 938 italian patients with Alzheimer's disease: a prospective, observational study, *CNS Drugs*, **2010**, *24(2)*, 163–176.

[52] Tan, C. C., Yu, J. T., Wang, H. F., Tan M. S., Meng, X. F., Wang, C., Jiang, T., Zhu, X. X., and Tan, L., Efficacy and safety of donepezil, galantamine, rivastigmine, and memantine for the treatment of Alzheimer's disease: a systematic review and meta-analysis, *J. Alzheimers Dis*, **2014**, *41(2)*, 615–631.

[53] Naji, A., Gatling, J. W., Muscarinic antagonists, *StatPearls*, **2020**.
<https://www.ncbi.nlm.nih.gov/books/NBK557541/>

[54] Barnes, P. J., Cholinergic control of airway smooth muscle, *Am Rev Respir Dis*, **1987**, *136(4 Pt 2)*, S42–45.

[55] Richardson, J. B., Nerve supply to the lungs, *Am Rev Respir Dis*, **1979**, *119(5)*, 785–802.

[56] Gross, N. J., Ipratropium bromide, *N Engl. J. Med.*, **1988**, *319(8)*, 486–494.

[57] Bajracharya, S. R., Prasad, P. N., Ghimire, R., Management of organophosphorus poisoning, *J. Nepal Health Res. Counc.*, **2016**, *14(34)*, 131–138.

[58] Vanova, N., Pejchal, J., Herman, D., Dlabkova, A., Jun, D., Oxidative stress in organophosphate poisoning: role of standard antidotal therapy, *J. Appl. Toxicol.*, **2018**, *38(8)*, 1058–1070.

[59] Picciotto, M. R., Caldarone, B. J., King, S. L., and Zachariou, V., Nicotinic receptors in the brain. Links between molecular biology and behavior, *Neuropsychopharmacology*, **2000**, *22*, 451–465.

[60] Wess, J., Novel insight into muscarinic acetylcholine receptor function using gene targeting technology, *Trends Pharmacol. Sci.*, **2003a**, 24, 414–420.

[61] McEnery, M. W., Siegel R. E., Encyclopedia of the neurological science, *ScienceDirect*, **2014**. <https://www.sciencedirect.com/topics/medicine-and-dentistry/neurotransmitter-receptor>

[62] Purves, D., Augustine, G. J., Fitzpatrick, D., Katz, L. C., LaMantia, A.-S., and McNamara, J. O., Neurotransmitter receptor and their effects, *NCBI*, **1997**. <https://www.ncbi.nlm.nih.gov/books/NBK10799/>

[63] Dani, J. A., Overview of nicotinic receptors and their roles in the central nervous system, *Biol Psychiatry*, **2001**, 49(3), 166–174.

[64] Ruzafa L. R., Cedillo, J. L., and Hone, A. J., Nicotinic acetylcholine receptor involvement in inflammatory bowel disease and interactions with gut microbiota, *Int. J. Environ. Res. Public Health*, **2021**, 18, 1189.

[65] Lodish, H., Berk, A., Zipursky, S. L., Neurotransmitter receptors, *NCBI*, **2000**. <https://www.ncbi.nlm.nih.gov/books/NBK21586/>

[66] Nieuwenhuys, R., Chemoarchitecture of the brain, *Springer-Verlag, Berlin Heidelberg*, **1985**. <https://link-springer-com.login.ezproxy.library.ualberta.ca/book/10.1007%2F978-3-642-70426-0>

[67] Yamamura, H. I., and Snyder, S. H., Muscarinic cholinergic binding in rat brain, *Proc. Natl. Acad. Sci. U.S.A.*, **1974**, 71, 1725–1729.

[68] Birdsall, N. J. M., and Hulme, E. C., Biochemical studies on muscarinic acetylcholine receptor, *J. Neurochem.*, **1976**, *27*, 7–16.

[69] Haga, T., Molecular properties of muscarinic acetylcholine receptors, *Proc. Jpn. Acad.*, **2013**, *89*, 226–256.

[70] Haga, T., and Noda, H., Choline uptake system of rat brain synaptosomes, *Biochim. Biophys. Acta.*, **1973**, *291*, 564–575.

[71] Kuhar, M. J., Sethy, V. H., Roth, R. H., and Aghajanian, G. K., Choline: selective accumulation by central cholinergic neurons, *J. Neurochem.*, **1973**, *20*, 581–593.

[72] Yamamura, H. I., Kuhar, M. J., Greenberg, D., and Snyder, S. H., Muscarinic cholinergic receptor binding: regional distribution in monkey brain, *Brain Res.*, **1974**, *66*, 541–546.

[73] Haga, K., Kruse, A. C., Asada, H., Yurugi-Kobayashi, T., Shiroishi, M., Zhang, C., Weis, W. I., Okada, T., Kobilka, B. K., Haga, T., and Kobayashi, T., Structure of the human M2 muscarinic acetylcholine receptor bound to an antagonist, *Nature*, **2012**, *482*, 547–551.

[74] Kruse A. C., Hu, J., Pan, A. C., Arlow, D. H., Rosenbaum, D. M., Rosemond, E., Green, H. F., Liu, T., Chae, P. S., Dror, R. O., Shaw, D. E., Weis, W. I., Wess, J., and Kobilka, B. K., Structure and dynamics of the M₃ muscarinic acetylcholine receptor, *Nature*, **2012**, *482*, 552–556.

[75] Liu, H., Hofmann, J., Fish, I., Schaake, B., Eitel, K., Bartuschat, A., Kaindl, J., Rampp, H., Banerjee, A., Hübner, H., Clark, M. J., Vincent, S. G., Fisher, J. T., Heinrich, M. R., Hirata, K., Liu, X., Sunahara, R. K., Shoichet, B. K., Kobilka, B. K., and Gmeiner, P., Structure-guided development of selective M3 muscarinic acetylcholine receptor antagonist, *PNAS*, **2018**, *47*, 12046-12050.

[76] Sales, M. E., Español, A. J., Salem, A. R., Pulido, P. M., Sanchez, Y., and Sanchez, F., Role of muscarinic acetylcholine receptors in breast cancer: design of metronomic chemotherapy, *Current Clinical Pharmacology*, **2019**, *14*(2),91–100.

[77] Song, P., Sekhon, H. S., Lu, A., *et al.*, M3 muscarinic receptor antagonists inhibits small cell lung carcinoma growth and mitogen-activated protein kinase phosphorylation induced by acetylcholine secretion, *Cancer Res.*, **2007**, *67*(8), 3936–3944.

[78] Xu, R., Shang, C., Zhao, J., *et al.*, Activation of M3 muscarinic receptor by acetylcholine promotes non-small cell lung cancer cell proliferation and invasion via EGFR/PI3K/AKT pathway, *Tumour Biol*, **2015**, *36*(6), 4091–4100.

[79] Yang, K., Song, Y., Tang, Y. B., *et al.* mAChRs activation induces epithelial-mesenchymal transition on lung epithelial cells, *BMC Pulm Med*, **2014**, *14*, 53.

[80] Kodira, M., Kajimura M., Takeuchi, K., Lin, S., Hanai, H., and Kaneko, E., Functional muscarinic m3 receptor expressed in gastric cancer cells stimulates tyrosine phosphorylation and MAP kinase, *J. Gastroenterol*, **1999**, *34*(2), 163–171.

[81] Nguyen, P. H., Touchefeu, Y., Durand, T., *et al*, Acetylcholine induces stem cell properties of gastric cancer cells of diffuse type, *Tumour Biol.*, **2018**, *40*(9), 10104283-18799028.

[82] Zhao, C. M., Hayakawa, Y., Kodama, Y., *et al*, Denervatoin suppresses gastric tumorigenesis, *Sci. Transl. Med.*, **2014**, *6*(250), 250ra115.

[83] Von, Rosenvinge, E. C., Cheng, K., Drachenberg, C. B., *et al*, Bedside to bench: role of muscarinic receptor activation in ultrarapid growth of colorectal cancer in a patient with pheochromocytoma, *Mayo Clin. Proc.*, **2013**, *88*(11), 1340–1346.

[84] Rimmaudo, L., de la Torre, E., Sacerdote de Lustig, E., and Sales, M. E., mAChR are involved in murine mammary adenocarcinoma cells LMM3 proliferation and angiogenesis, *Biochem. Biophys. Res. Commun.*, **2005**, *334*, 1360–1365.

[85] Anderson, K. E., Campeau, L., and Olshansky, B., Cardiac effects of muscarinic receptor antagonist used for voiding dysfunction, *Br. J. Clin. Pharmacol.*, **2011**, *72*(2), 186–196.

[86] Sales, M. E., Muscarinic receptors as targets for metronomic therapy in breast cancer, *Curr. Pharm. Des.*, **2016**, *22*(14), 2170–2177.

[87] Fiszman, G. L., Middonno, M. C., de la Torre, E., Farina, M., Español, A. J., and Sales, M. E., Activation of muscarinic cholinergic receptors induces MCF-7 cells proliferation and angiogenesis by stimulating nitric oxide synthase activity, *Cancer Biol. Ther.*, **2007**, *6*(7), 1106–1113.

[88] de la Torre, E., Davel, L., Jasnis, M. A., Gotoh, T., Sacerdote de Lustig, E., and Sales, M. E., Muscarinic receptors participation in angiogenic response induced by macrophages from mammary adenocarcinoma-bearing mice, *Breast Cancer Res.*, **2005**, 7(3), 345–352.

[89] Schmitt, J. M., Abell, E., Wagner, A., and Davare, M. A., ERK activation and cell growth require CaM kinases in MCF-7 breast cancer cells, *Mol. Cell Biochem.*, **2010**, 335, 155–171.

[90] Cancer information, Breast cancer staging, *Canadian Cancer Society*, **2021**.
<https://cancer.ca/en/cancer-information/cancer-types/breast/staging>

[91] The pathologist's role, Staging, *John Hopkins Medicine Pathology*, **2021**.
<https://pathology.jhu.edu/breast/>

[92] Sagara, Y., Sagara, T., Mase, T., Kimura, T., Numazawa, T., Fujikawa, T., Noguchi, K., and Ohtake, N., Cyclohexylmethylpiperidinyltriphenylpropioamide: a selective muscarinic M3 antagonist discriminating against the other receptor subtypes, *J Med Chem.*, **2002**, 45, 984–987.

[93] Wallis, R. M. and Napier, C. M., Muscarinic antagonist in development for disorder of smooth muscle function, *Life Sci.*, **1999**, 64, 395–401.

[94] 4-(4-Formyl-3-methoxyphenoxy)butyryl amino methylated resin (1% divinylbenzene, 100-200 mesh, 0.78 mmol/g) was purchased from Novabiochem.

[95] Coste, J., Le-Nguyen, D., Castro, B., PyBOP: A new peptide coupling reagent devoid of toxic by-product. *Tetrahedron Lett.*, **1990**, *31*, 205–208.

[96] Alexander, M. D., McDonald, J. J., Ni, Y., Niu, D., Petter, R. C., Qiao, L., Singh, J., Wang, T., Zhu, Z., MK2 inhibitors and uses thereof, *United States Patent*, **2018**, *10138256*, 7708–7842.

[97] Chan L. C., and Cox B. G., Kinetics of Amide Formation through Carbodiimide/N-Hydroxybenzotriazole (HOBt) Couplings, *J. Org. Chem*, **2007**, *72*, 8863–8869.

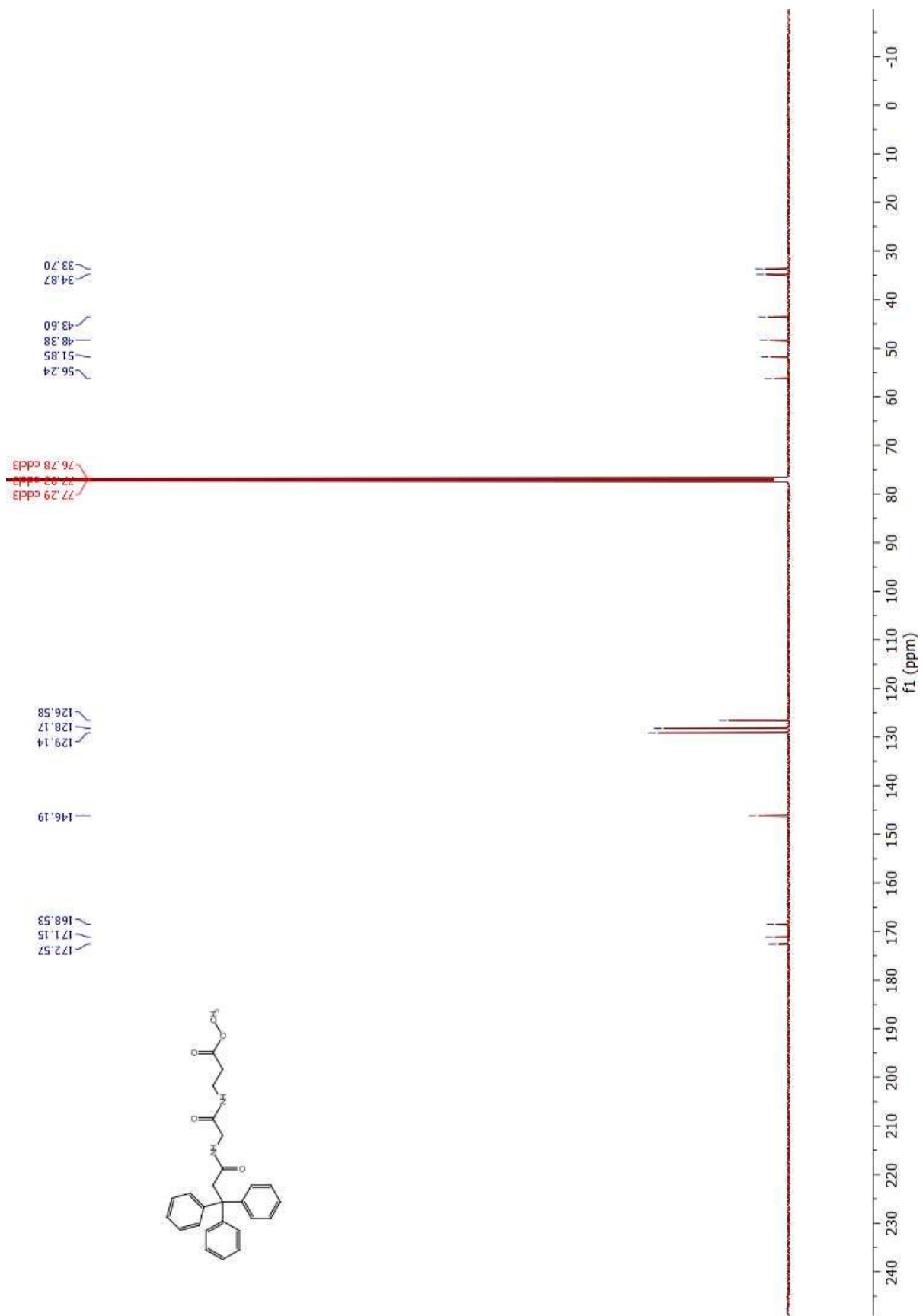
[98] Ye, N., Wu, Q. Q., Zhu, L., Zheng, L., Gao, B., Zhen, X., et al., Further SAR study on 11-O-substituted aporphine analogues: identification of highly potent dopamine D3 receptor ligands, *Bioorg. Med. Chem.*, **2011**, *19*, 1999–2008.

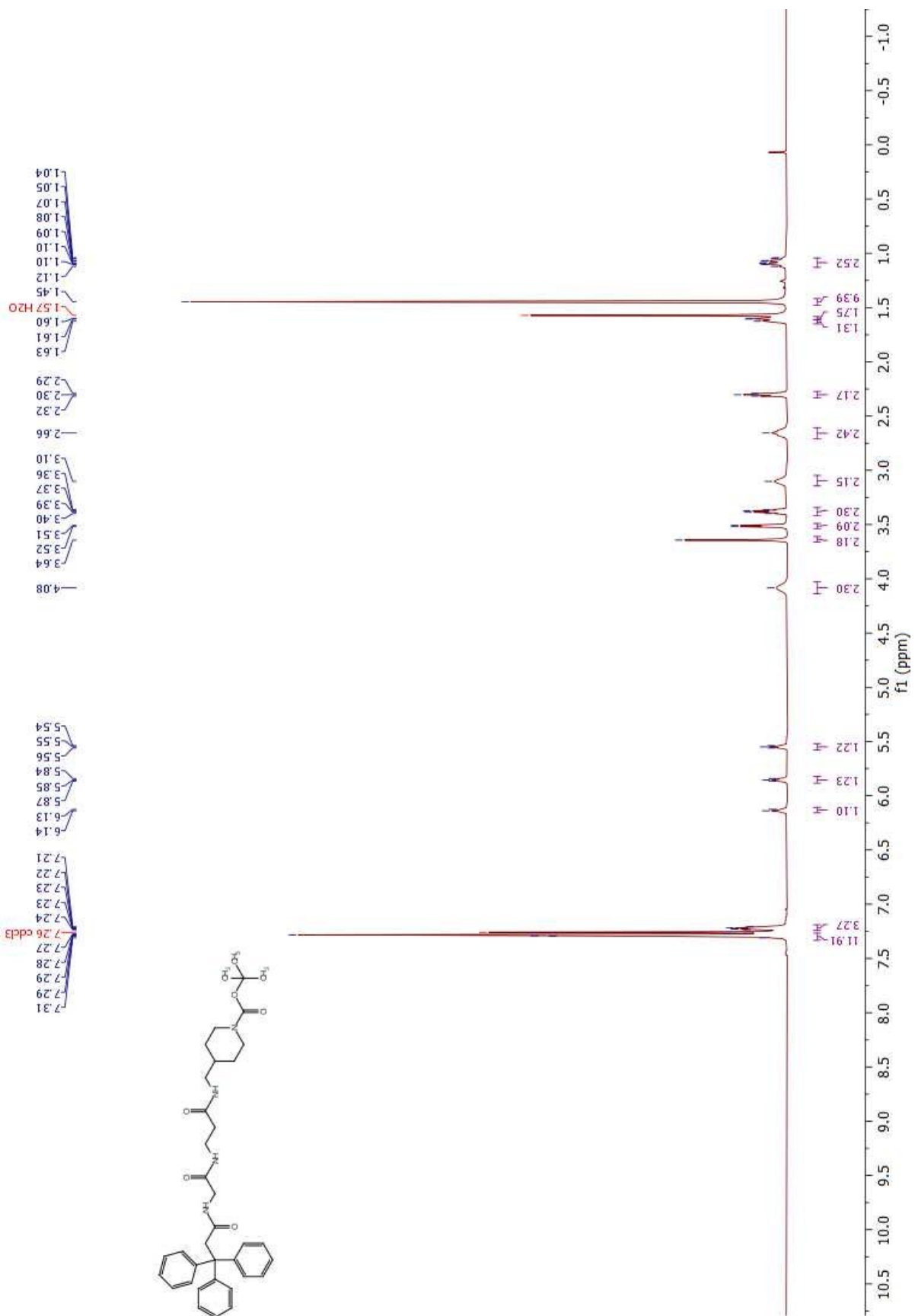
[99] Singh, M., Jadhav, H. R., and Kumar, A., Design, Synthesis and In Vitro Evaluation of Piperazine Incorporated Novel Anticancer Agents, *Letters in Drug Design & Discovery*, **2018**, *15*, 866–874.

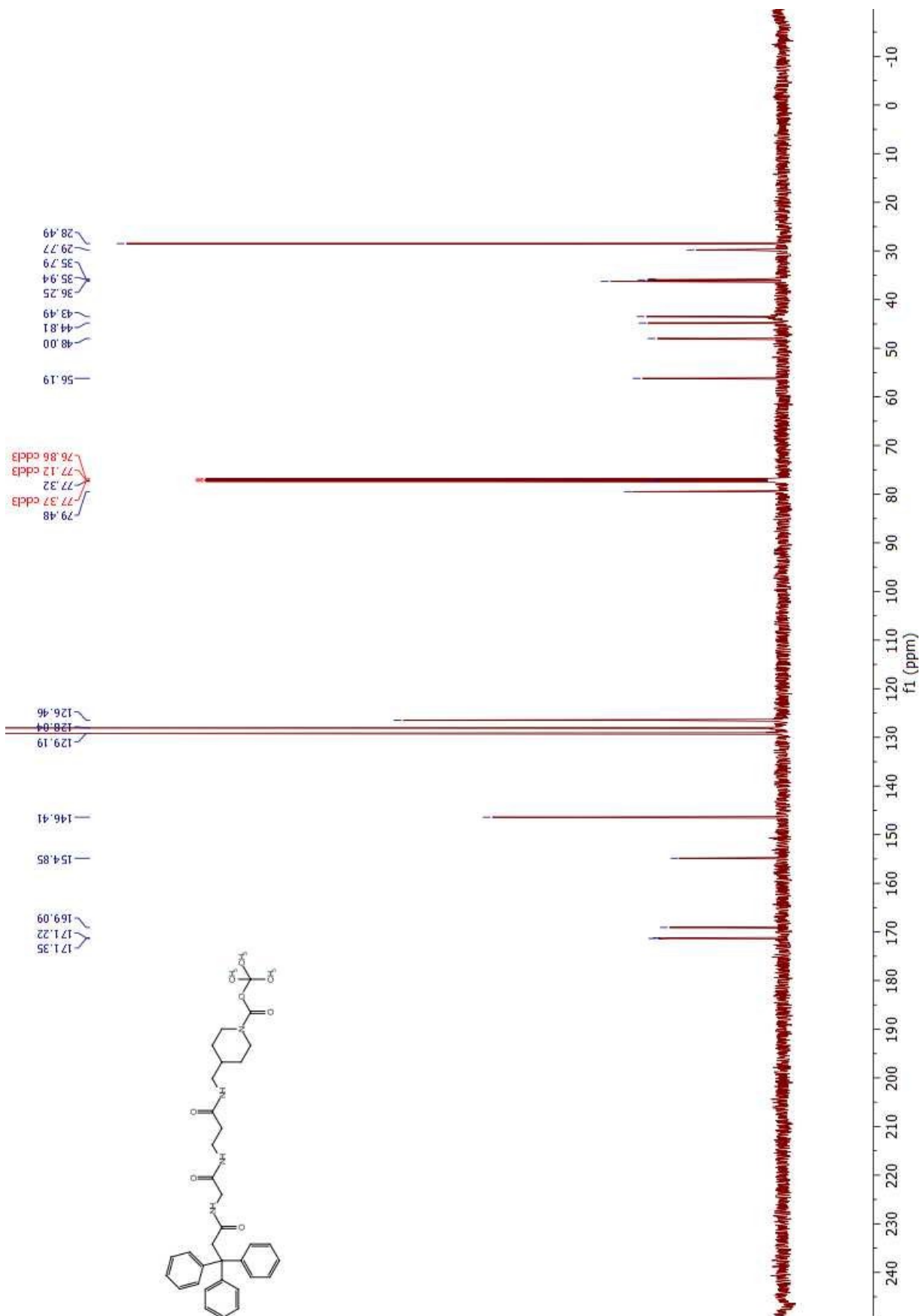
[100] Paccosi, S., Musilli, C., Caporale, R., Grazia Gelli A. M., Guasti, D., Clemente, A. M., Torcia, M. G., Filippelli, A., Romagnoli, P., Parenti, A., Stimulatory Interactions between Human Coronary Smooth Muscle Cells and Dendritic Cells, *PLOS ONE*, **2014**. <https://doi.org/10.1371/journal.pone.0099652>

[101] Kaitsiotou, H., Keul, M., Hardick, J., et al., Inhibitors to overcome secondary mutations in the stem cell factor receptor KIT, *J. Med. Chem.*, **2017**, *60*, 8801–8815.

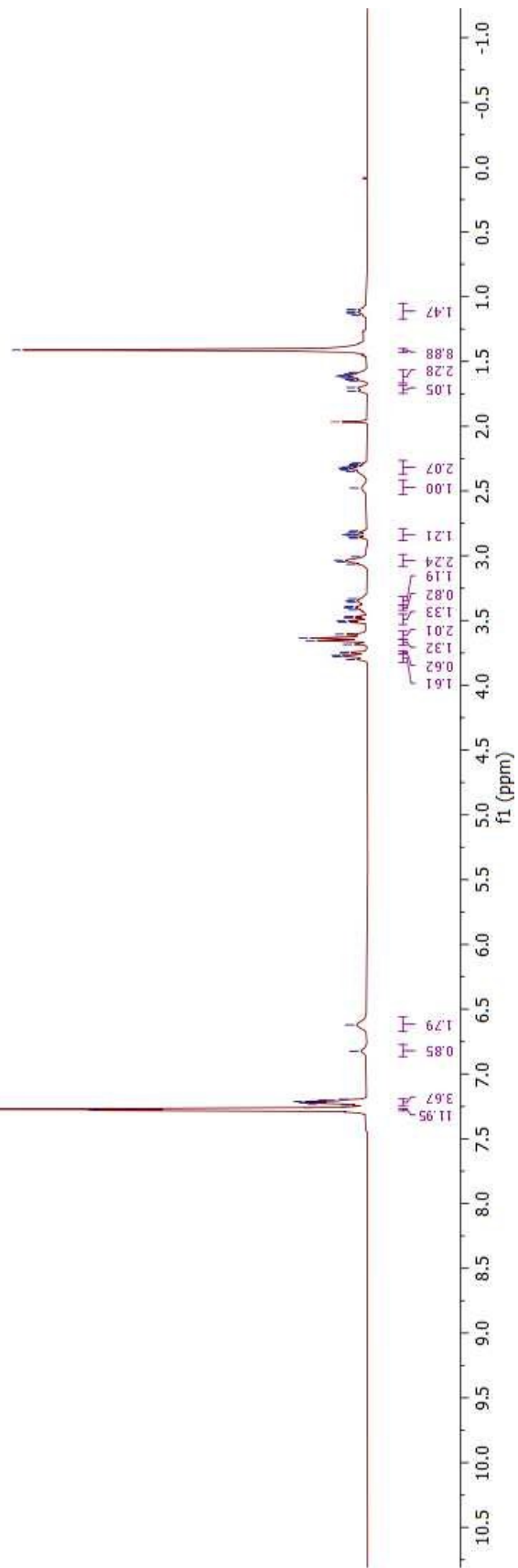
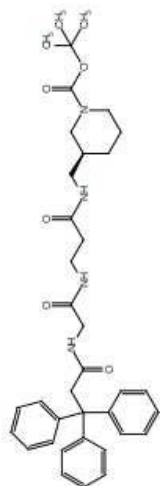
[102] van der Born, D., Pees, A., Poot, A. J., Orru, R. V. A., Windhorst, A. D., and Vugts, D. J., Fluorine-18 labelled building blocks for PET tracer synthesis, *Chem. Soc. Rev.*, **2017**, *46*, 4709.

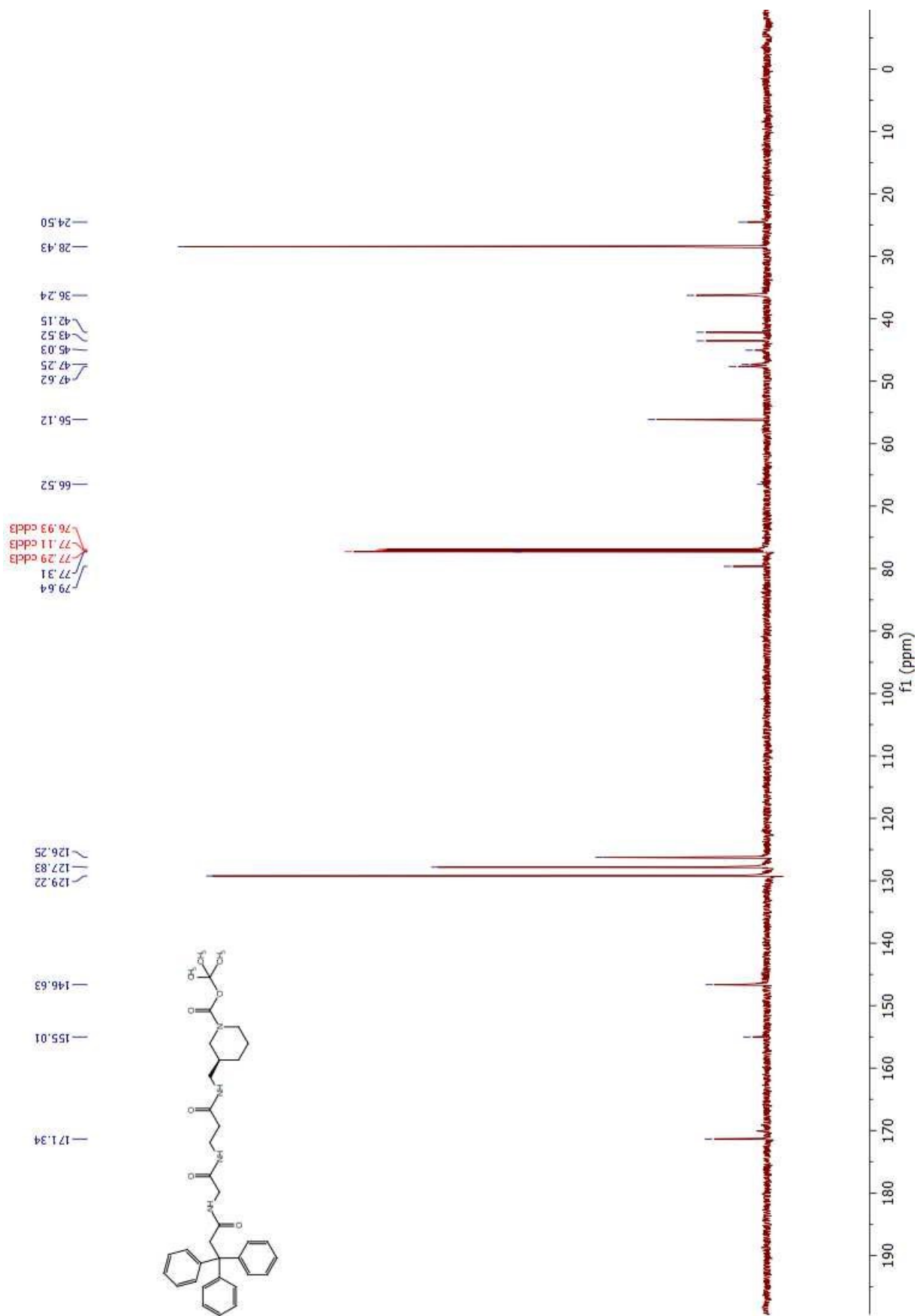


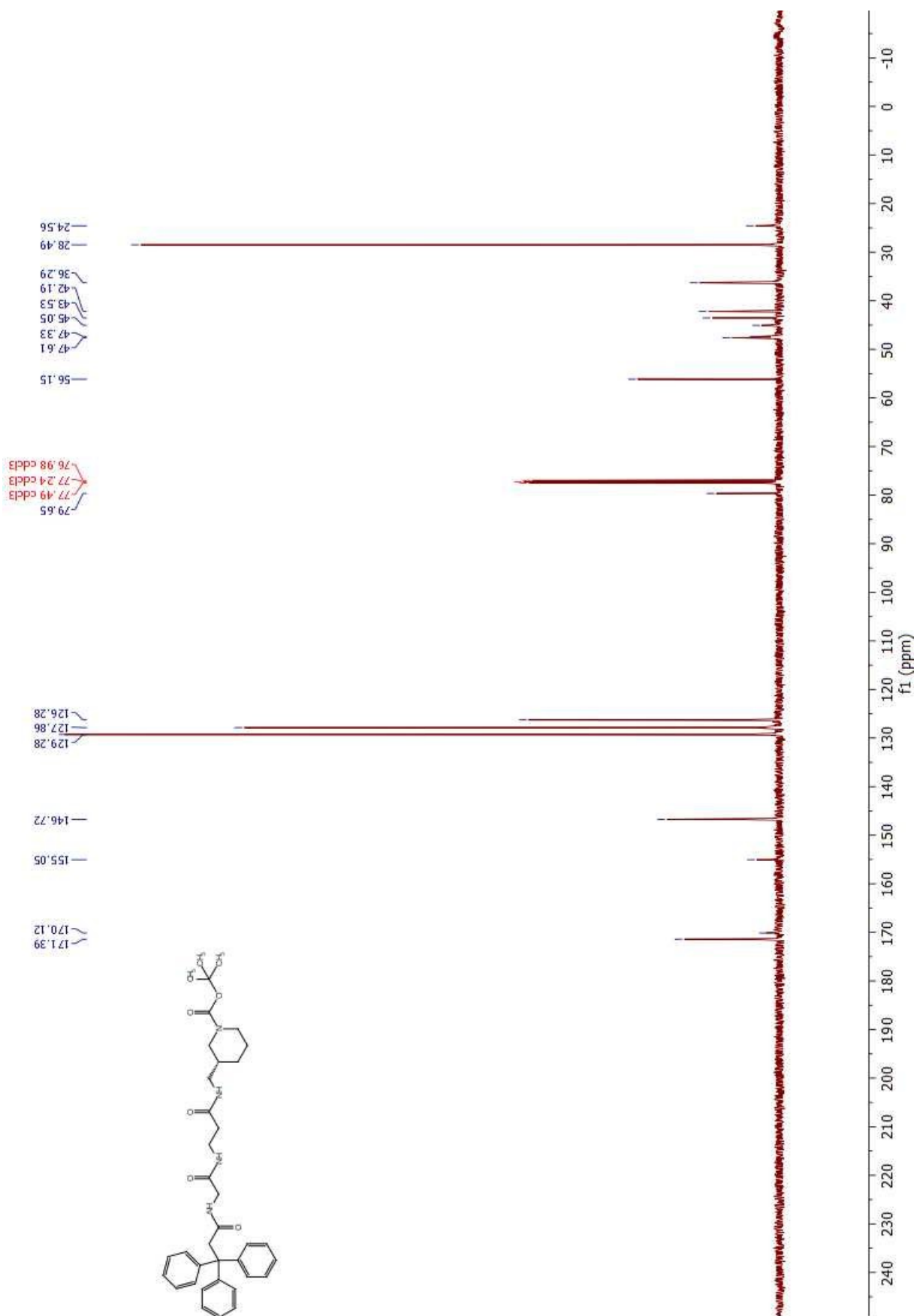


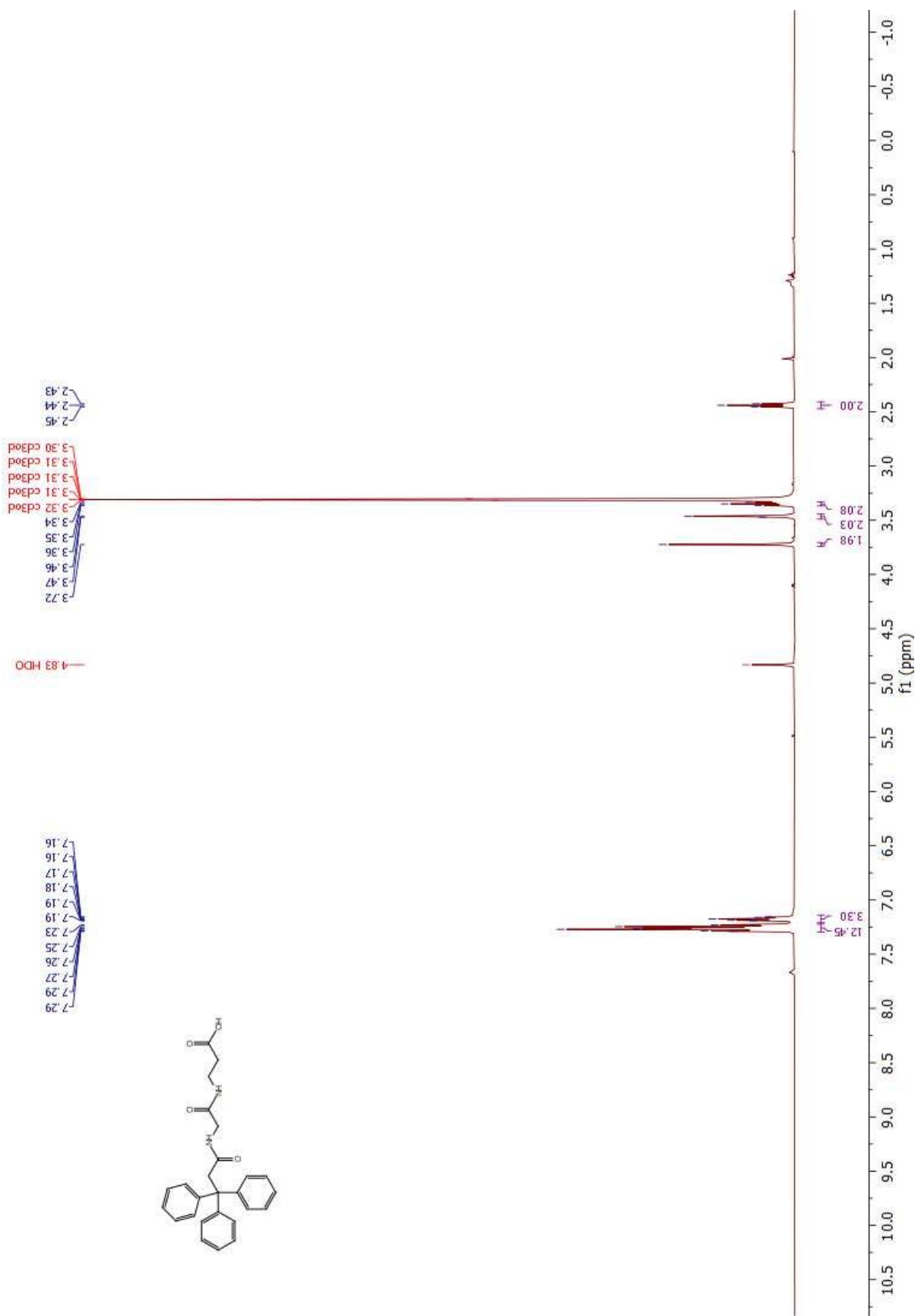


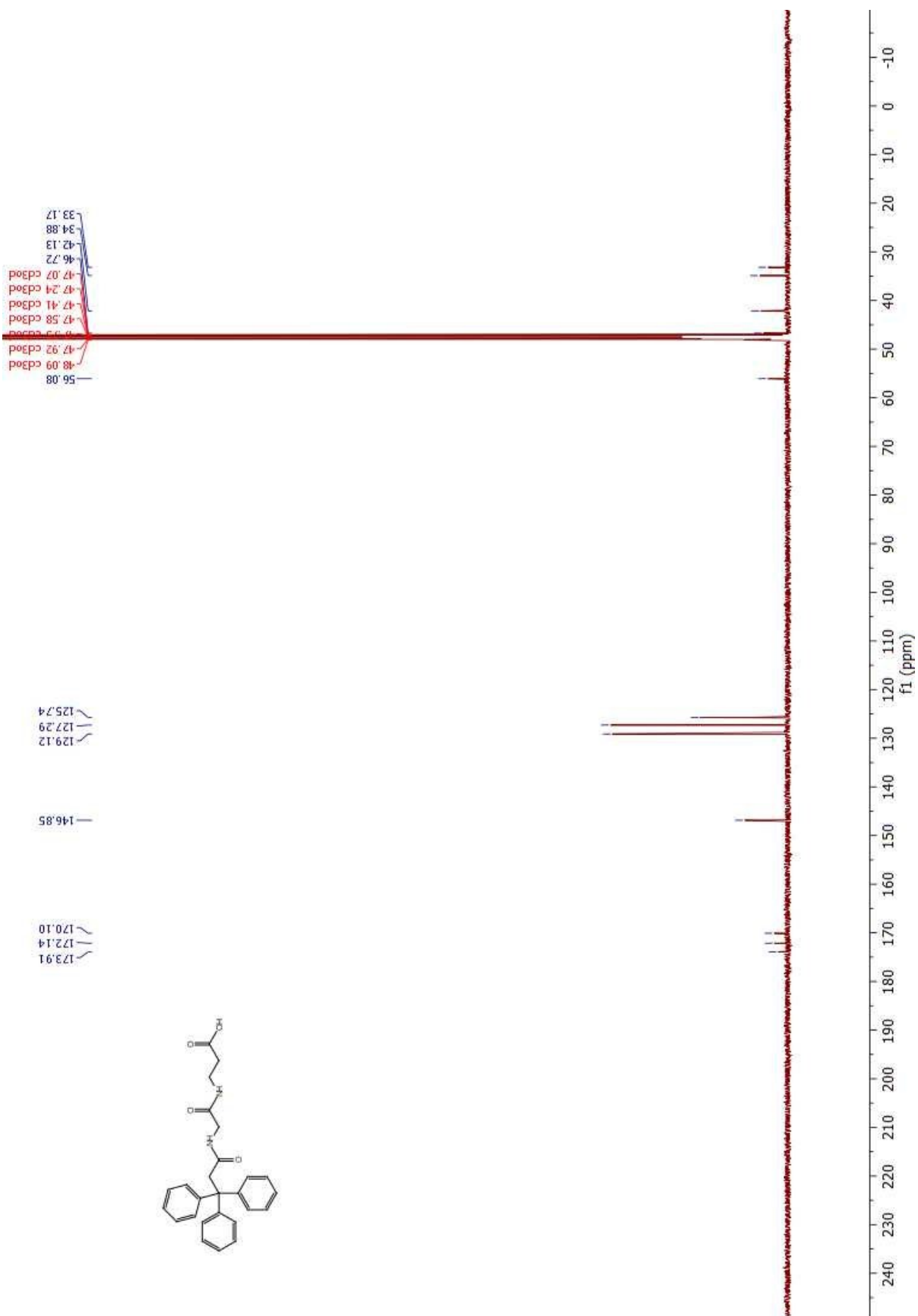
1.10
 1.10
 1.12
 1.13
 1.14
 1.41
 1.58
 1.60
 1.61
 1.61
 1.62
 1.63
 1.64
 1.65
 1.70
 1.73
 1.97 H₂O
 2.28
 2.29
 2.31
 2.31
 2.32
 2.33
 2.34
 2.35
 2.48
 2.81
 2.82
 2.83
 2.84
 2.84
 2.86
 2.86
 3.01
 3.03
 3.05
 3.07
 3.33
 3.35
 3.36
 3.39
 3.40
 3.42
 3.47
 3.48
 3.50
 3.51
 3.61
 3.64
 3.66
 3.69
 3.74
 3.75
 3.77
 3.78
 3.80
 6.62
 6.82
 7.20
 7.20
 7.21
 7.21
 7.21
 7.22
 7.22
 7.22
 7.23
 7.24
 7.26 cddls
 7.27
 7.28
 7.28

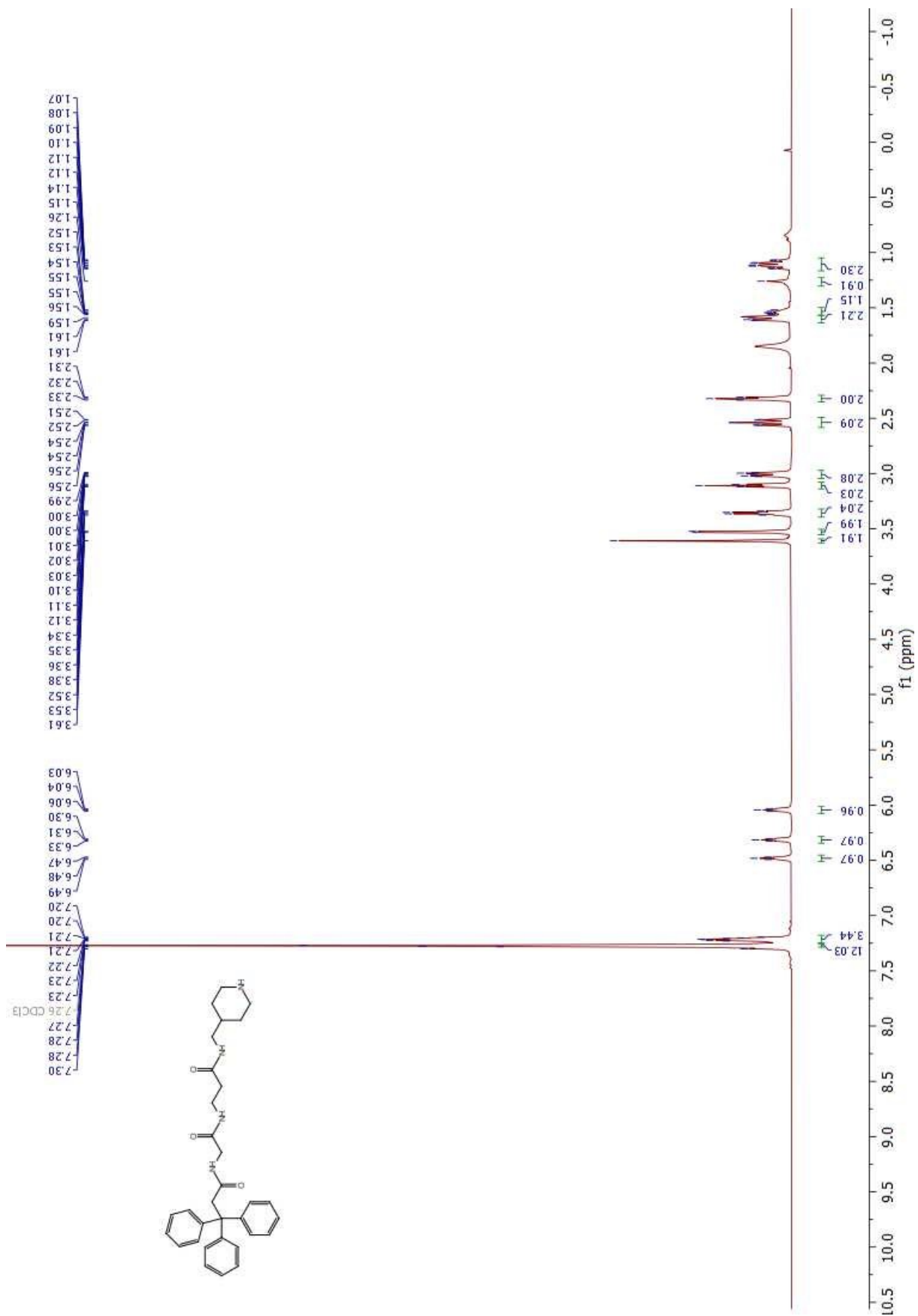


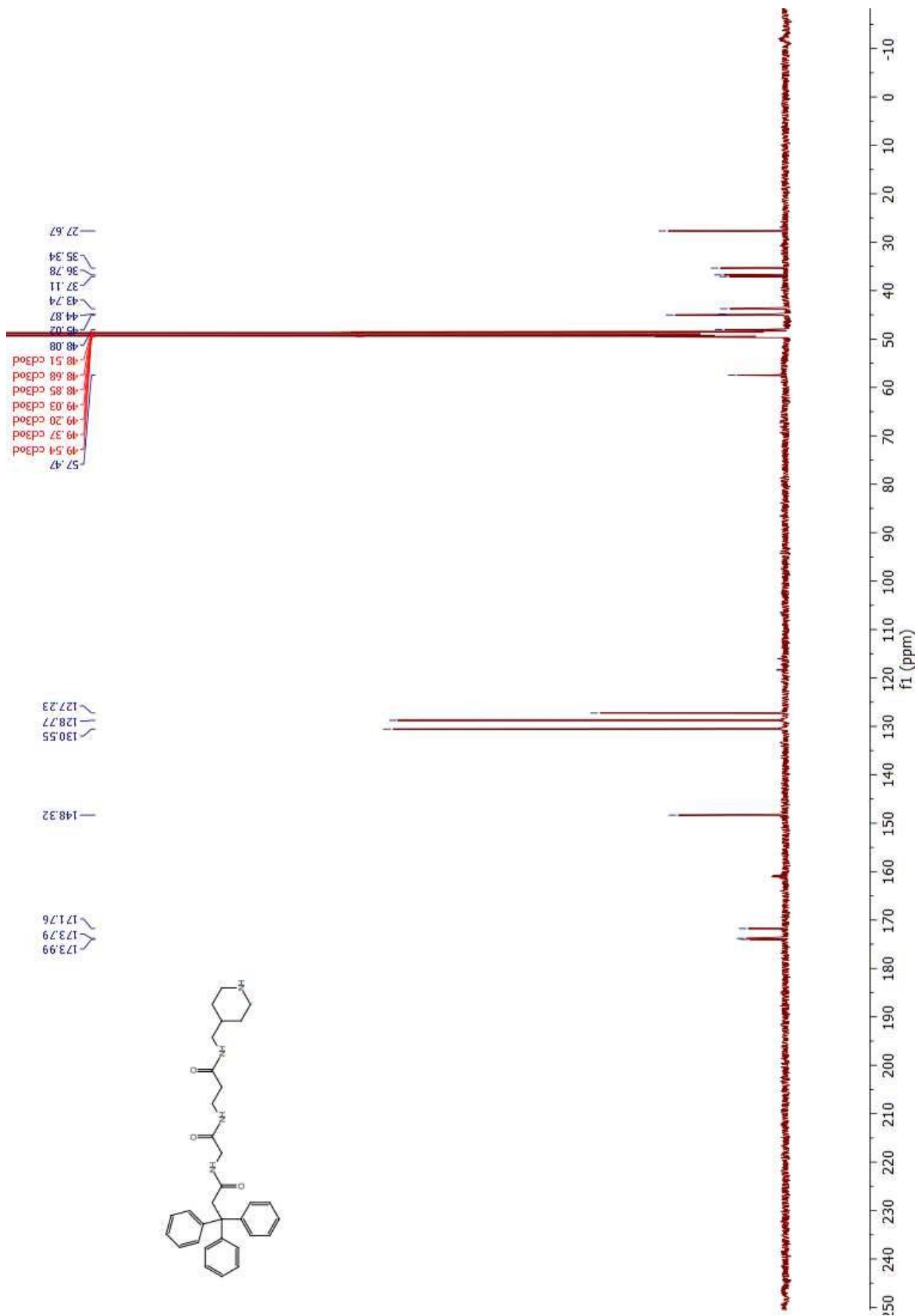


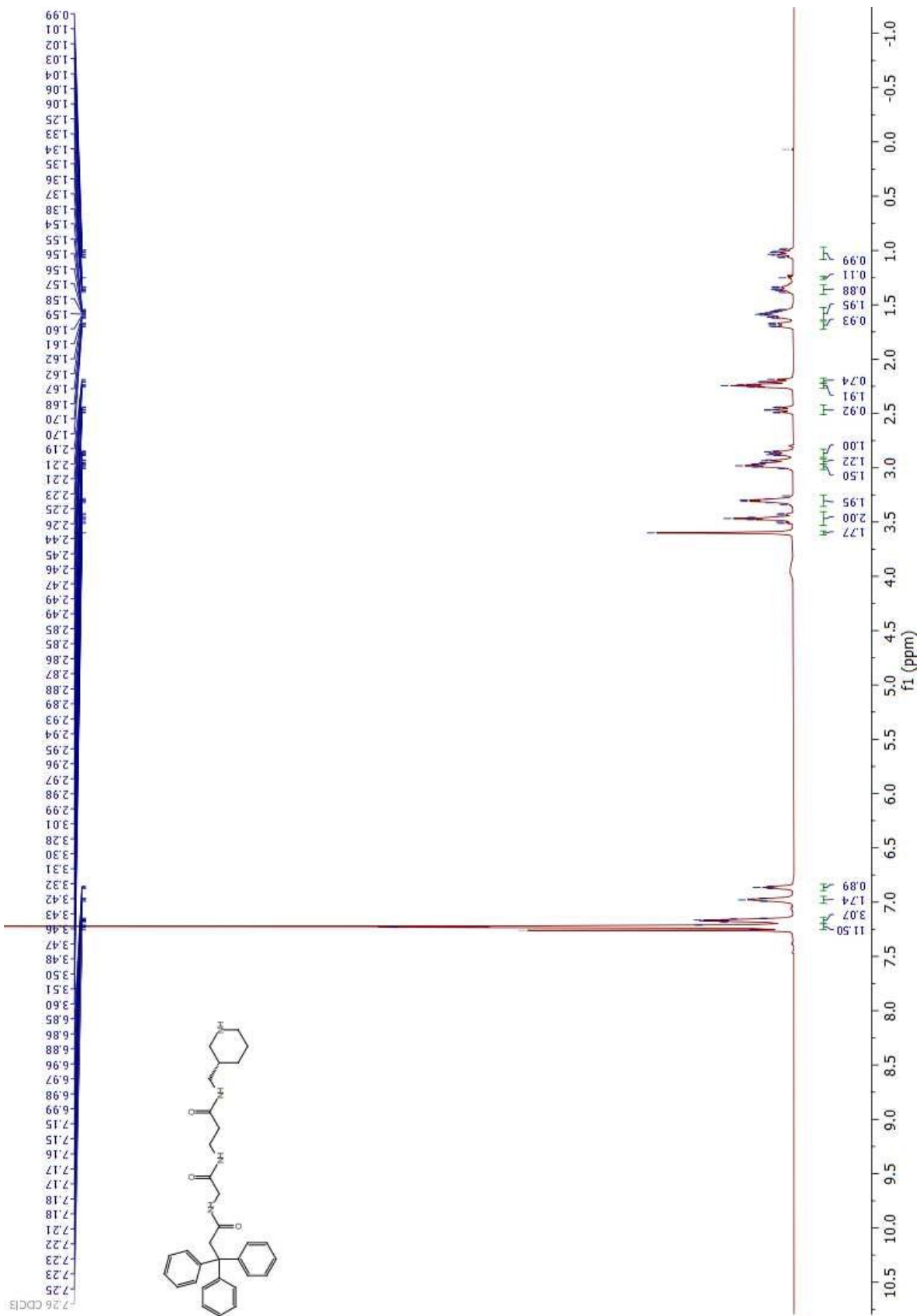


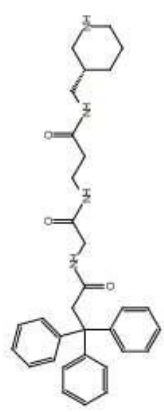
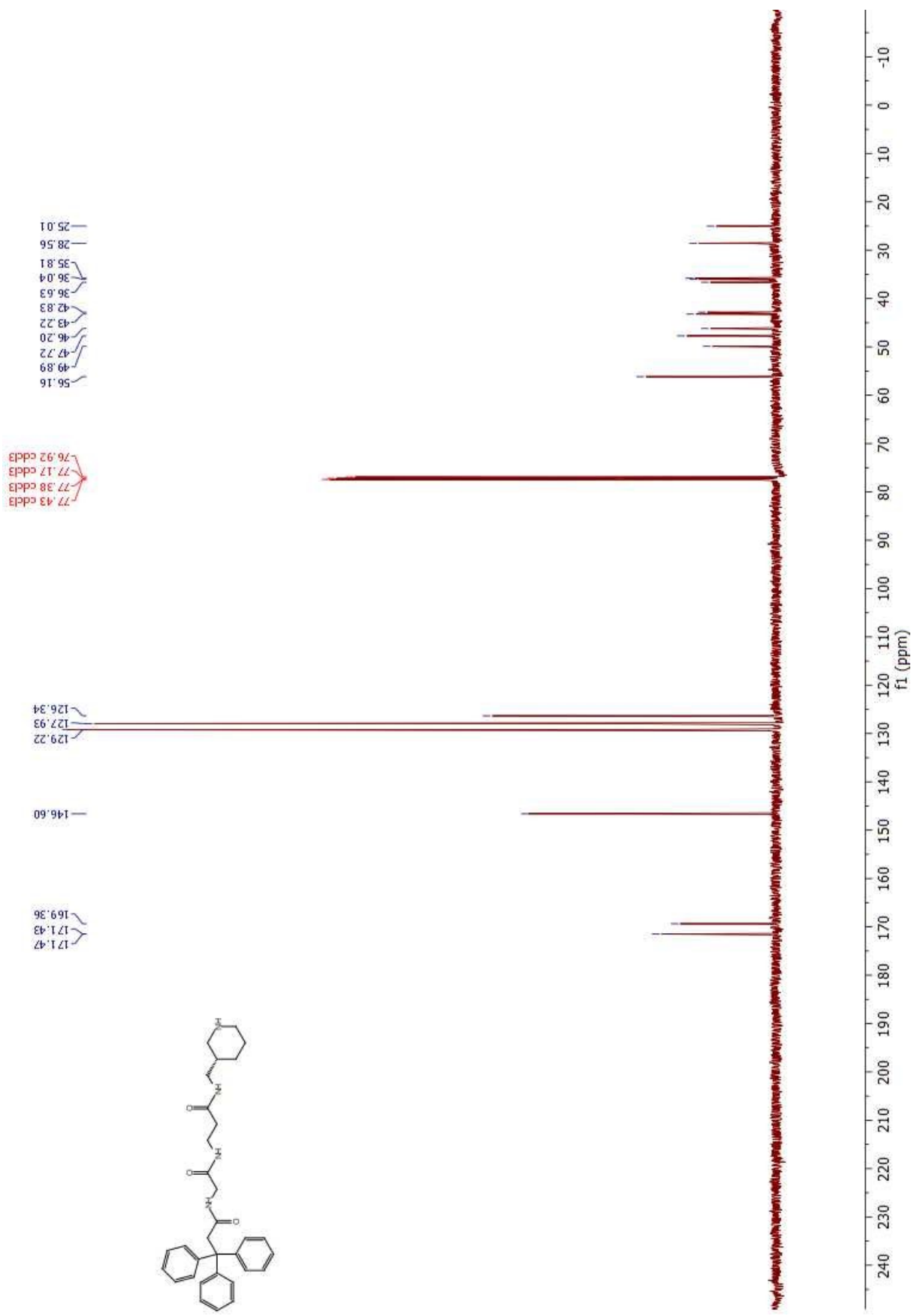


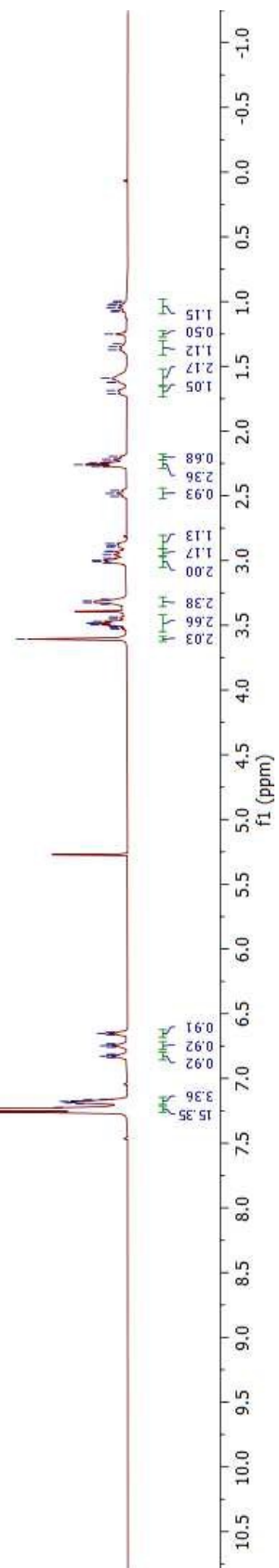
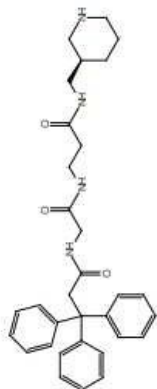


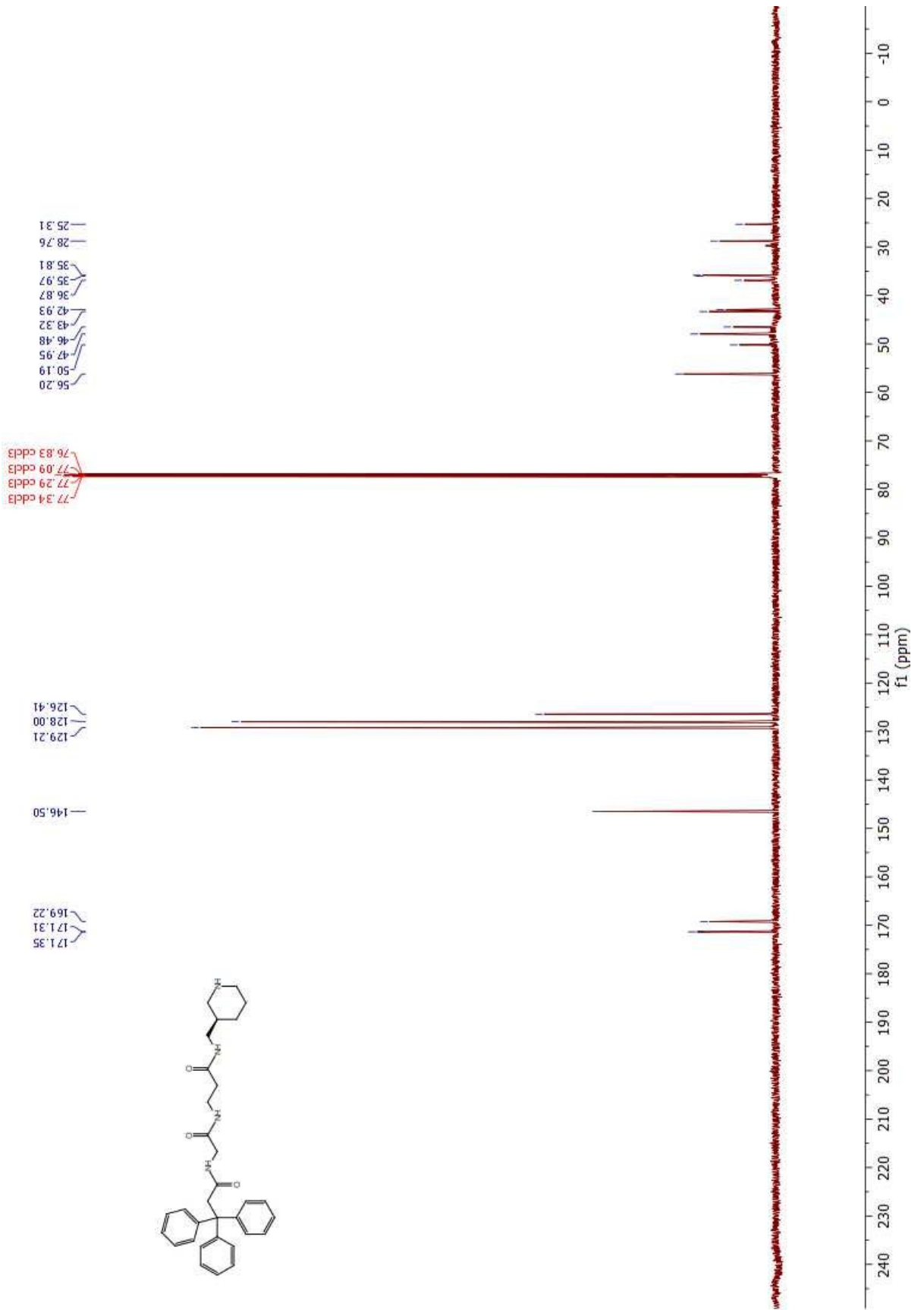


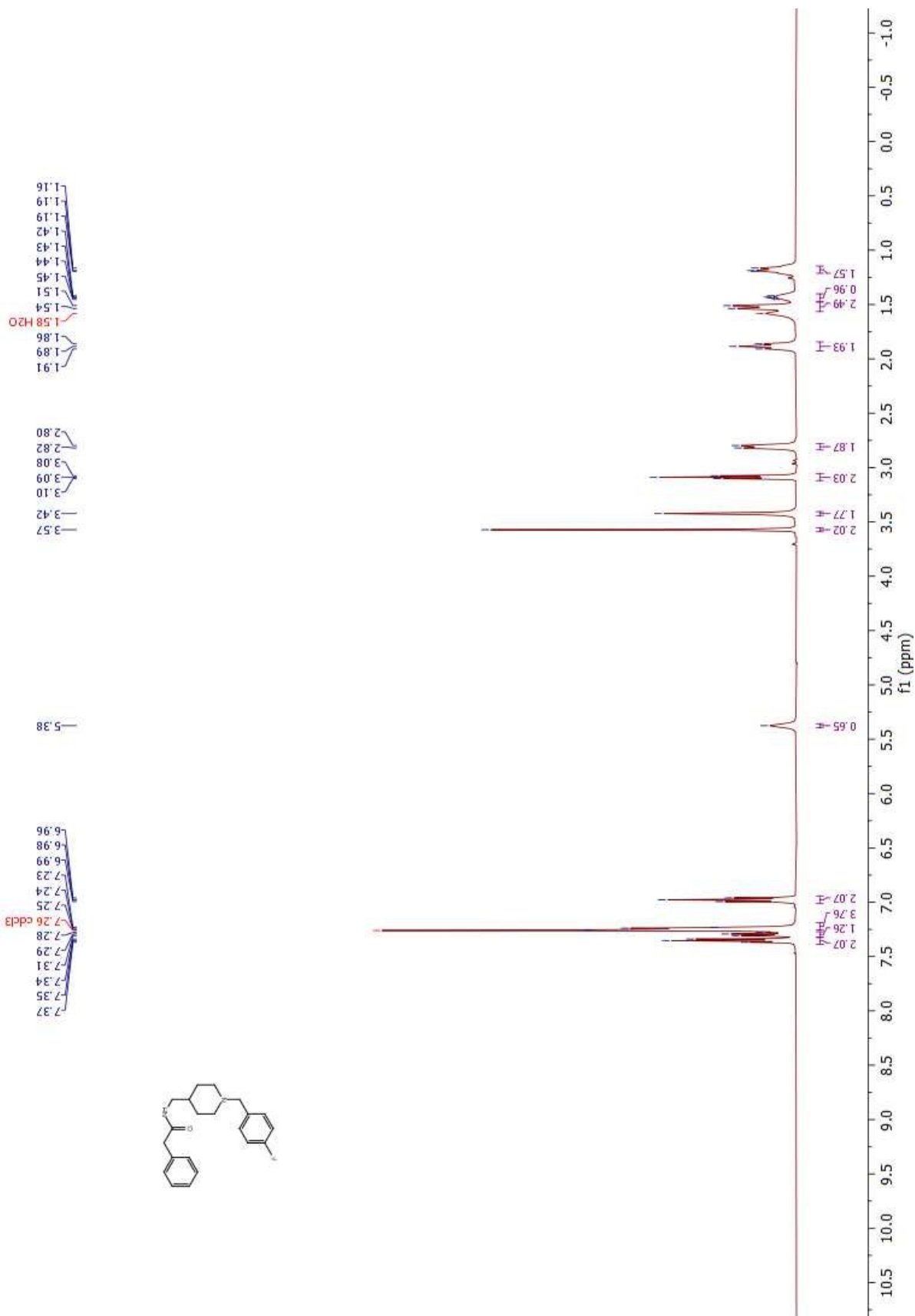






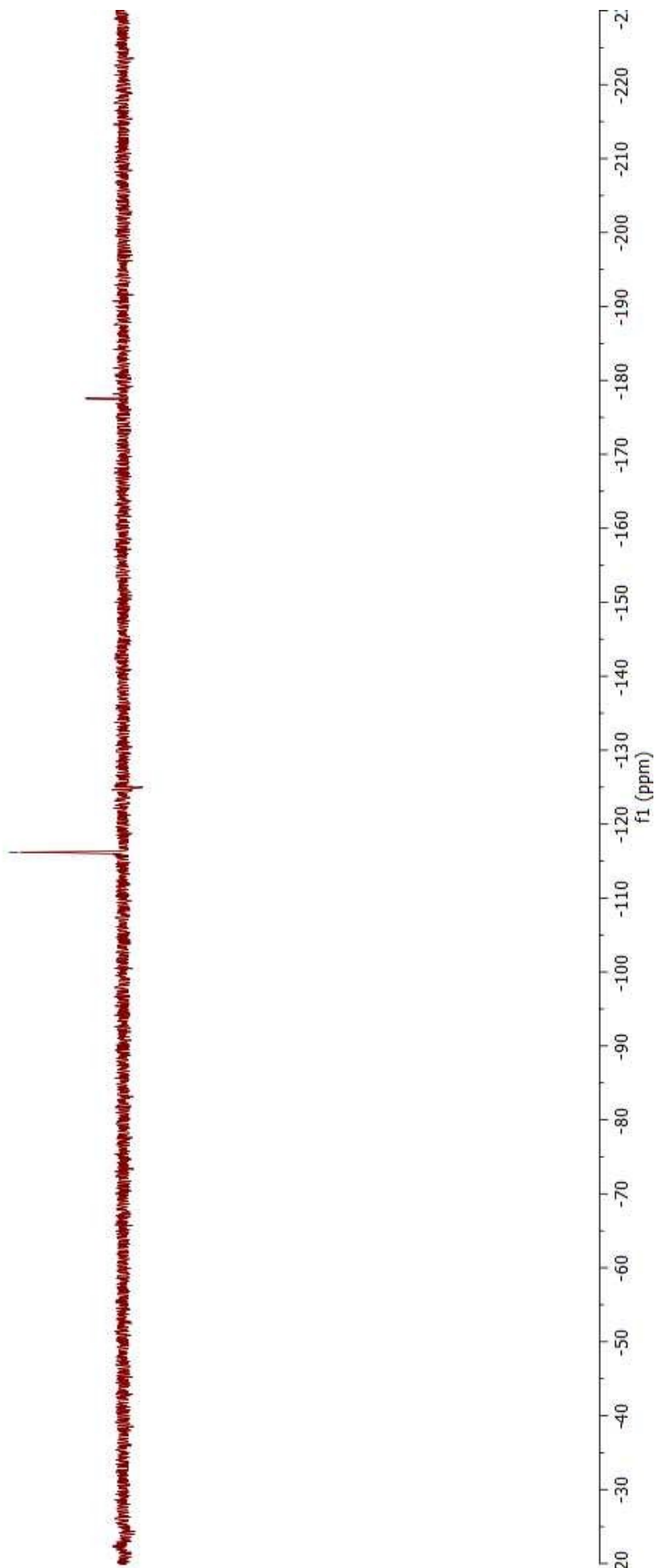


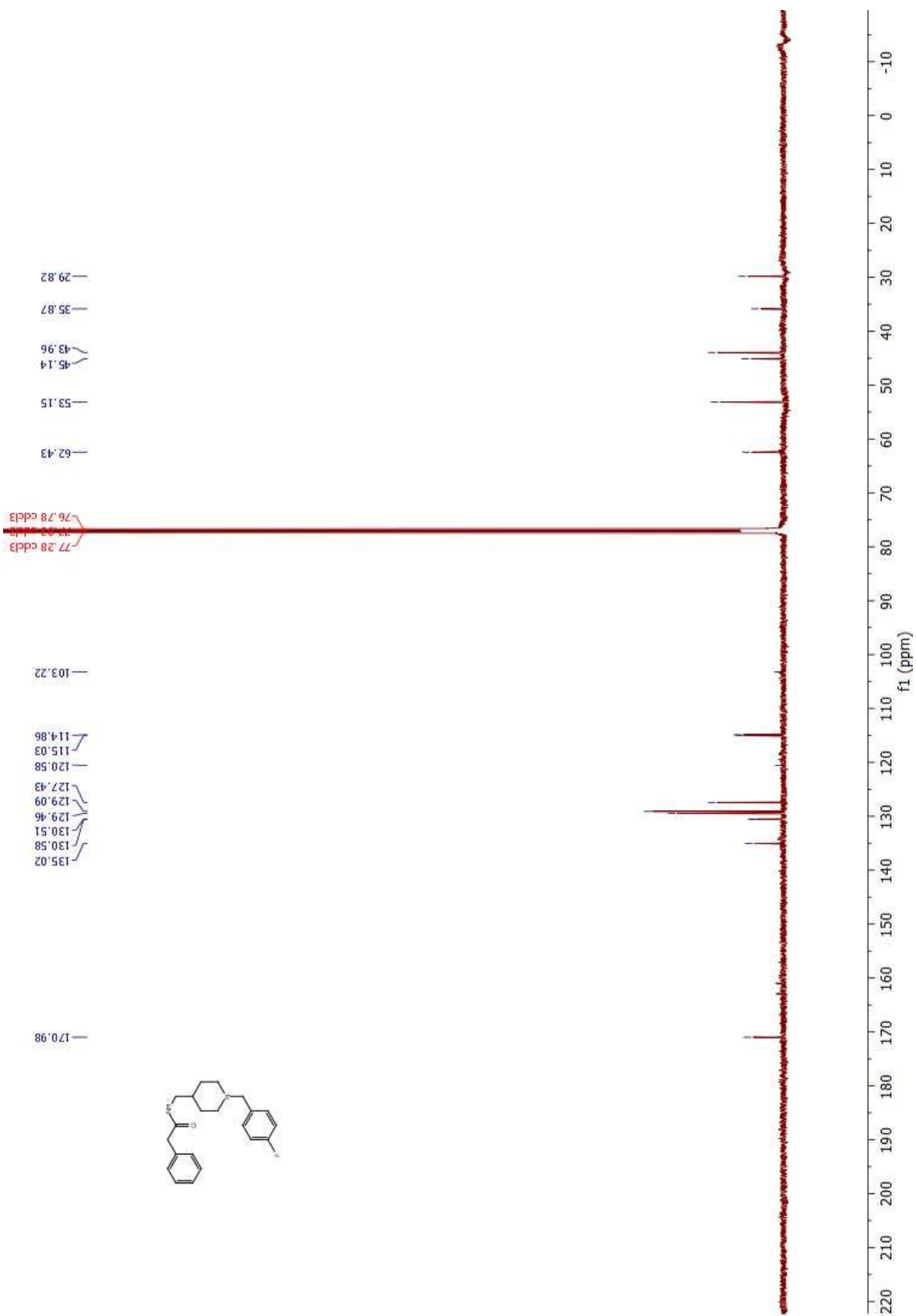


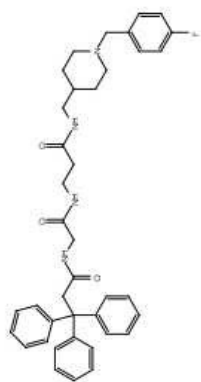




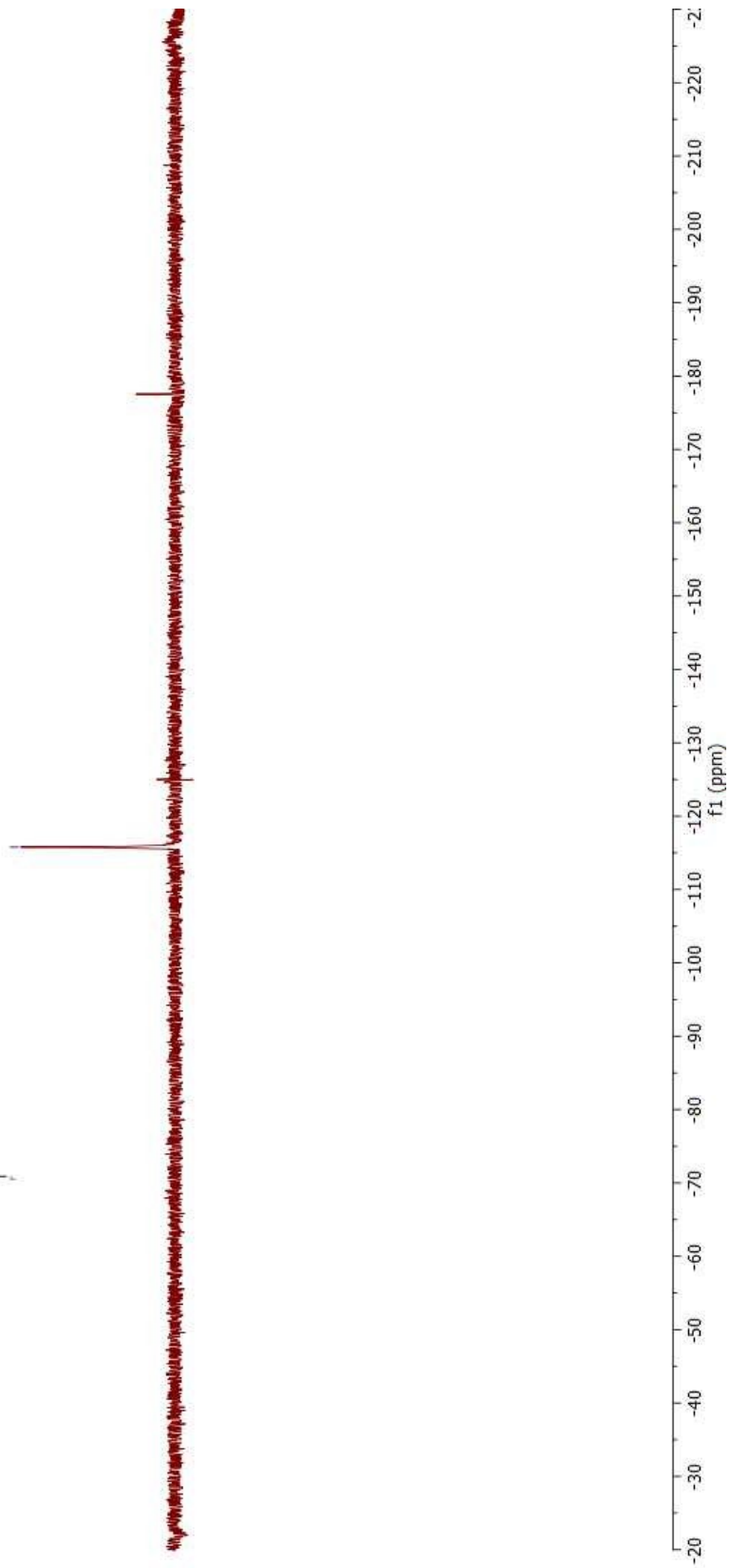
—116.19

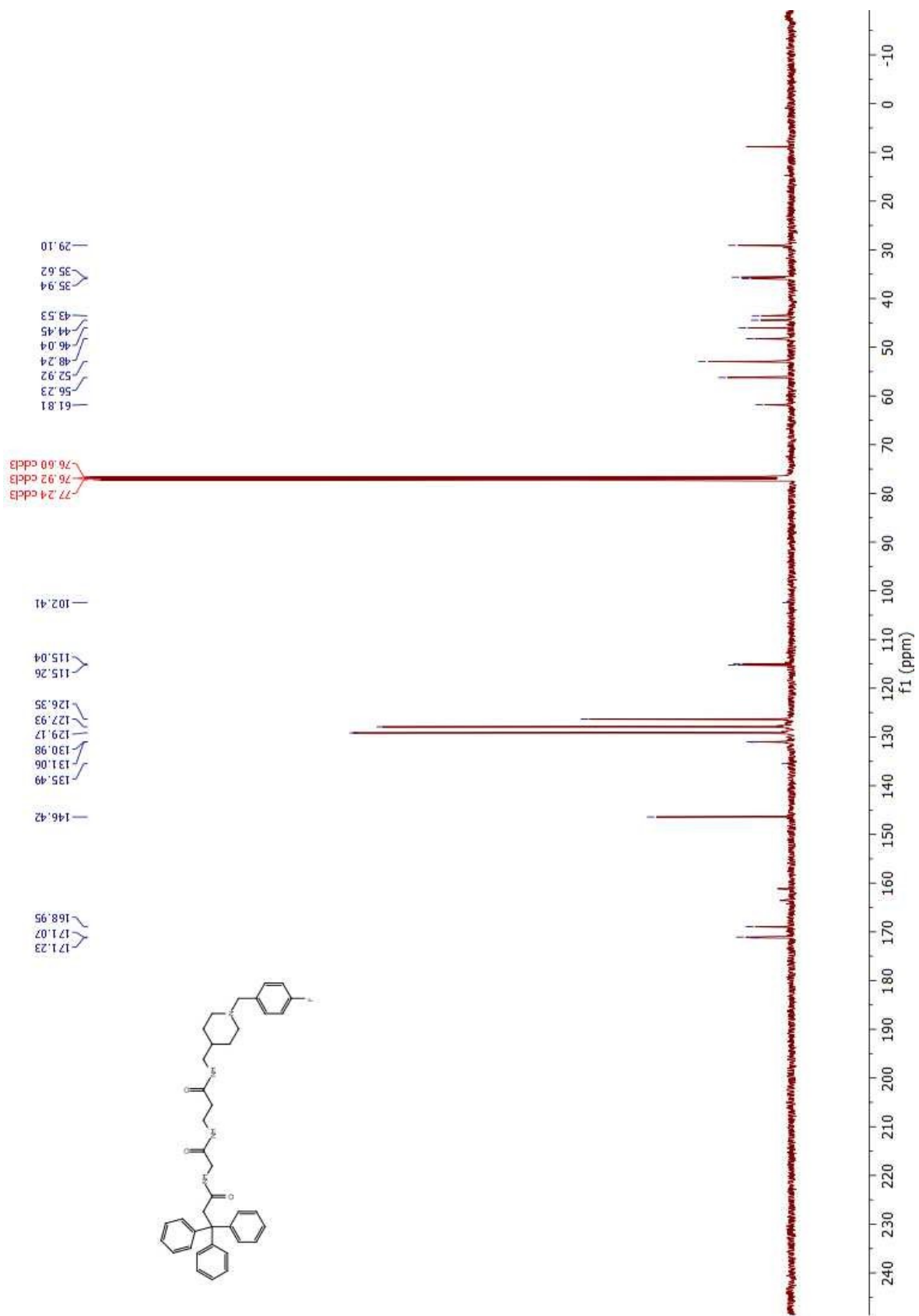


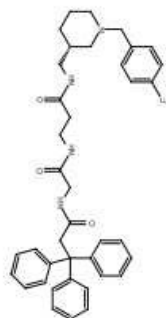




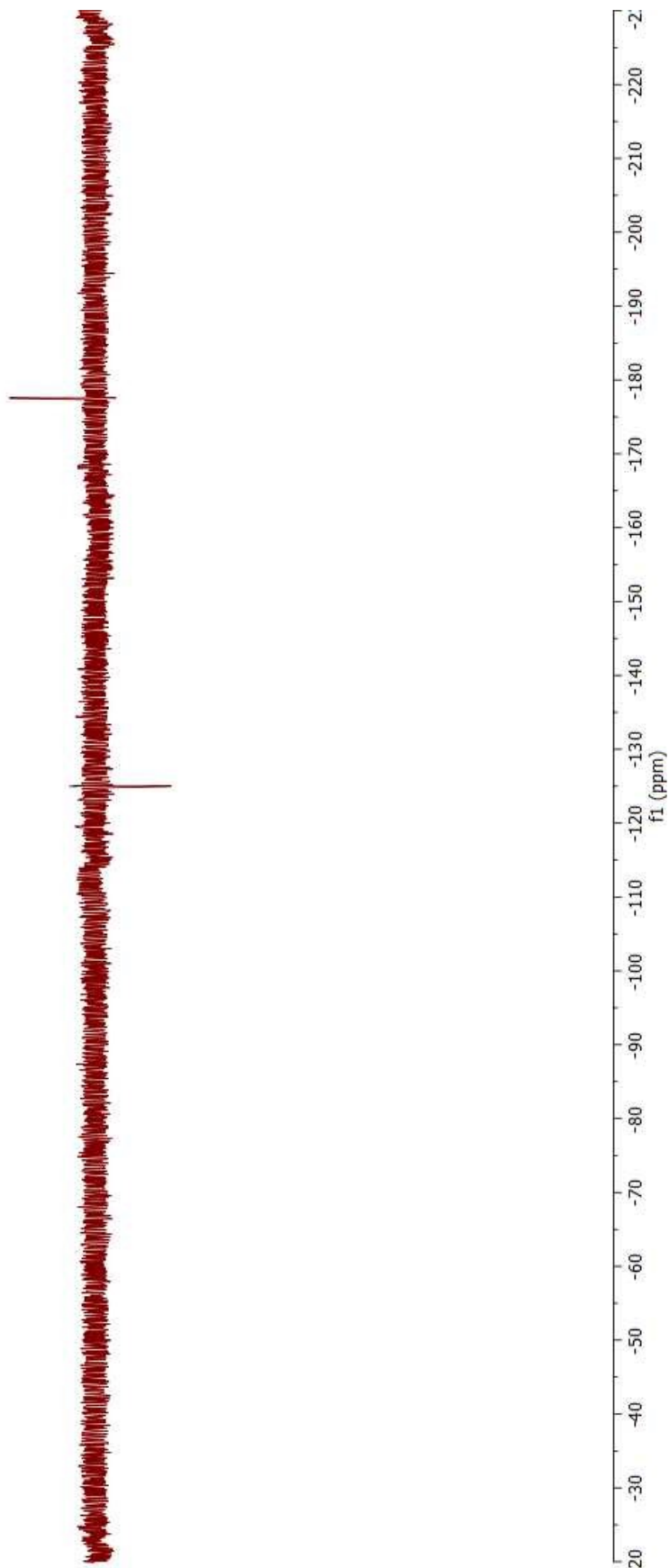
825111

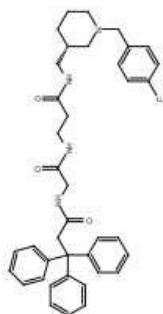
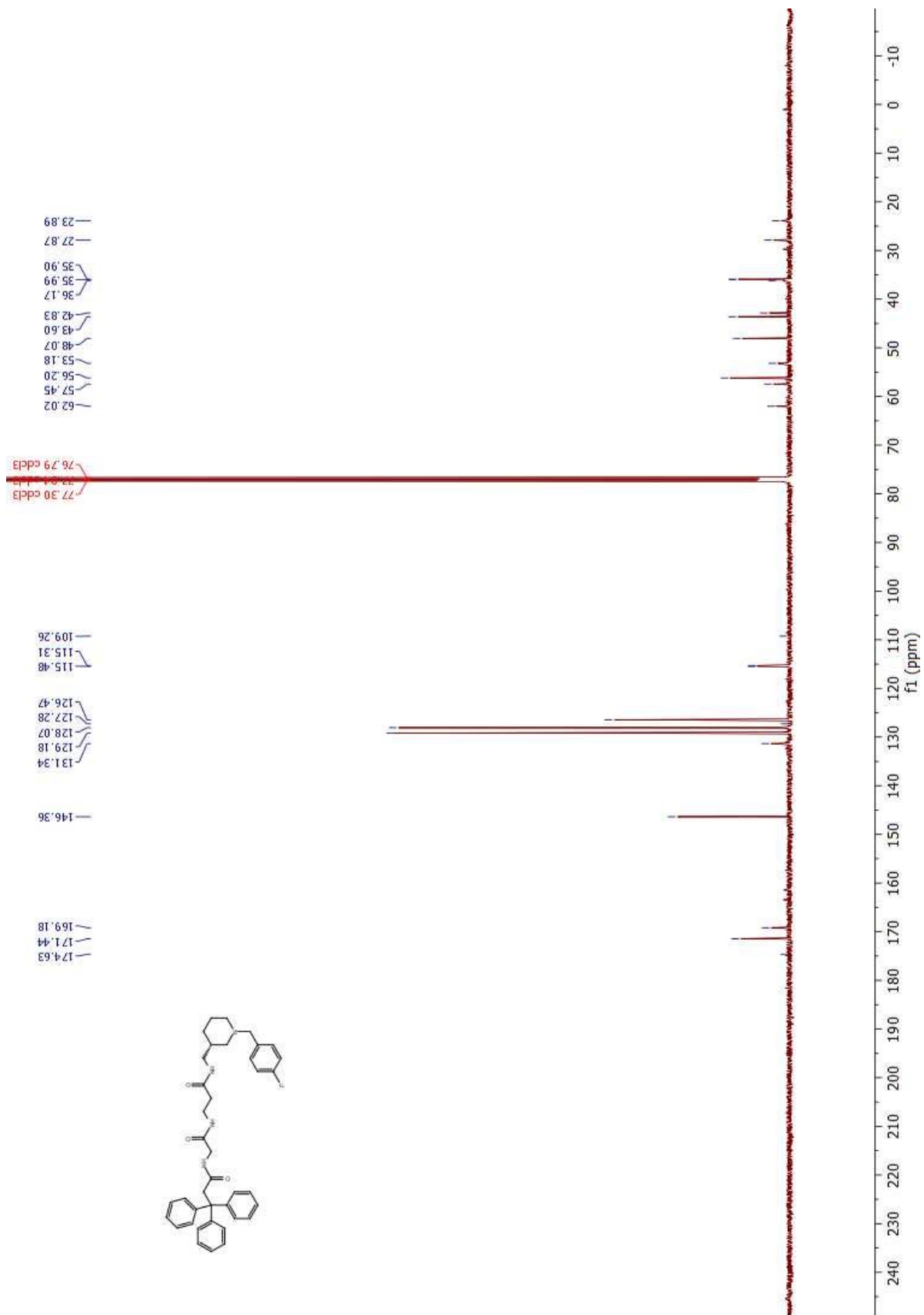


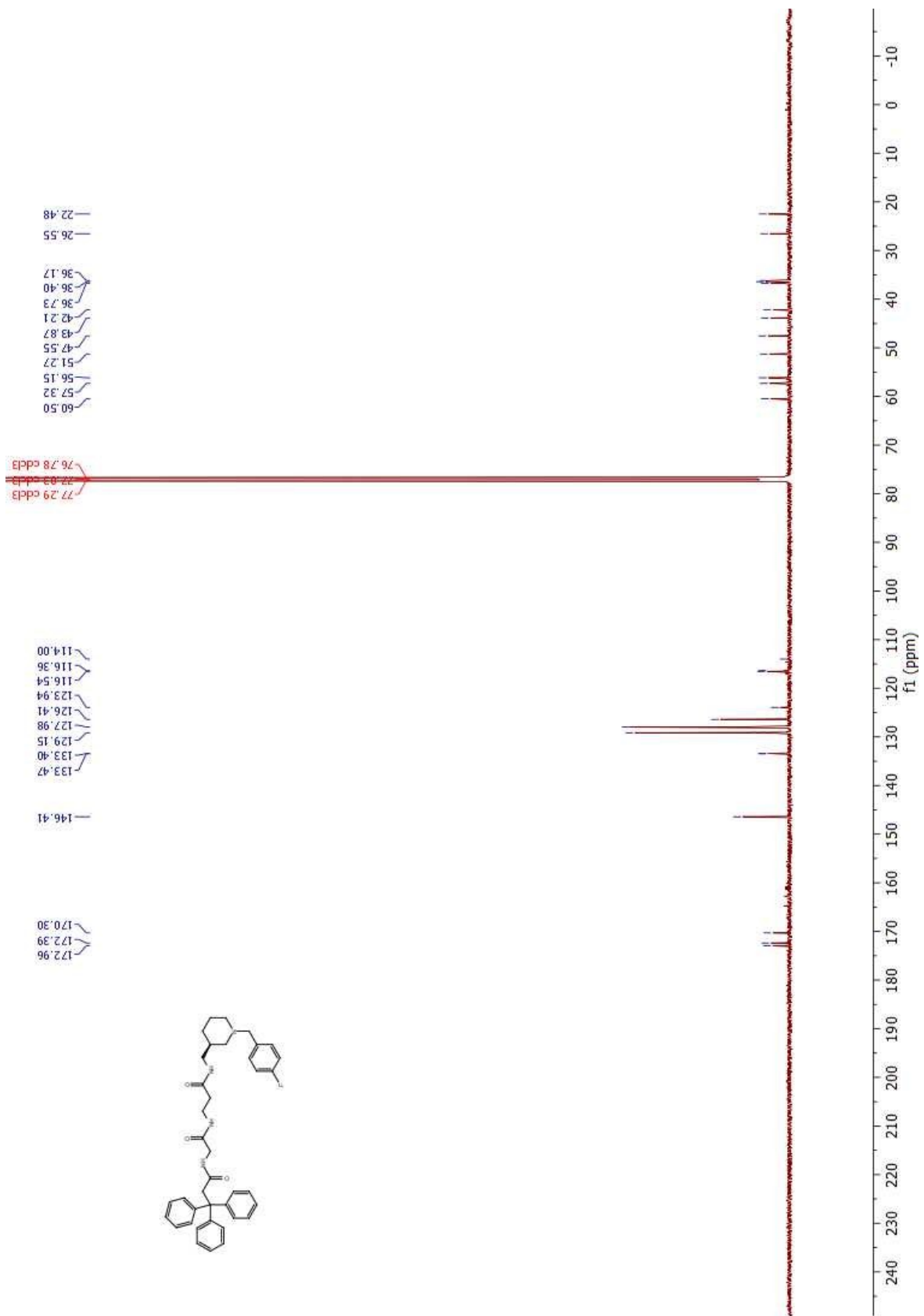


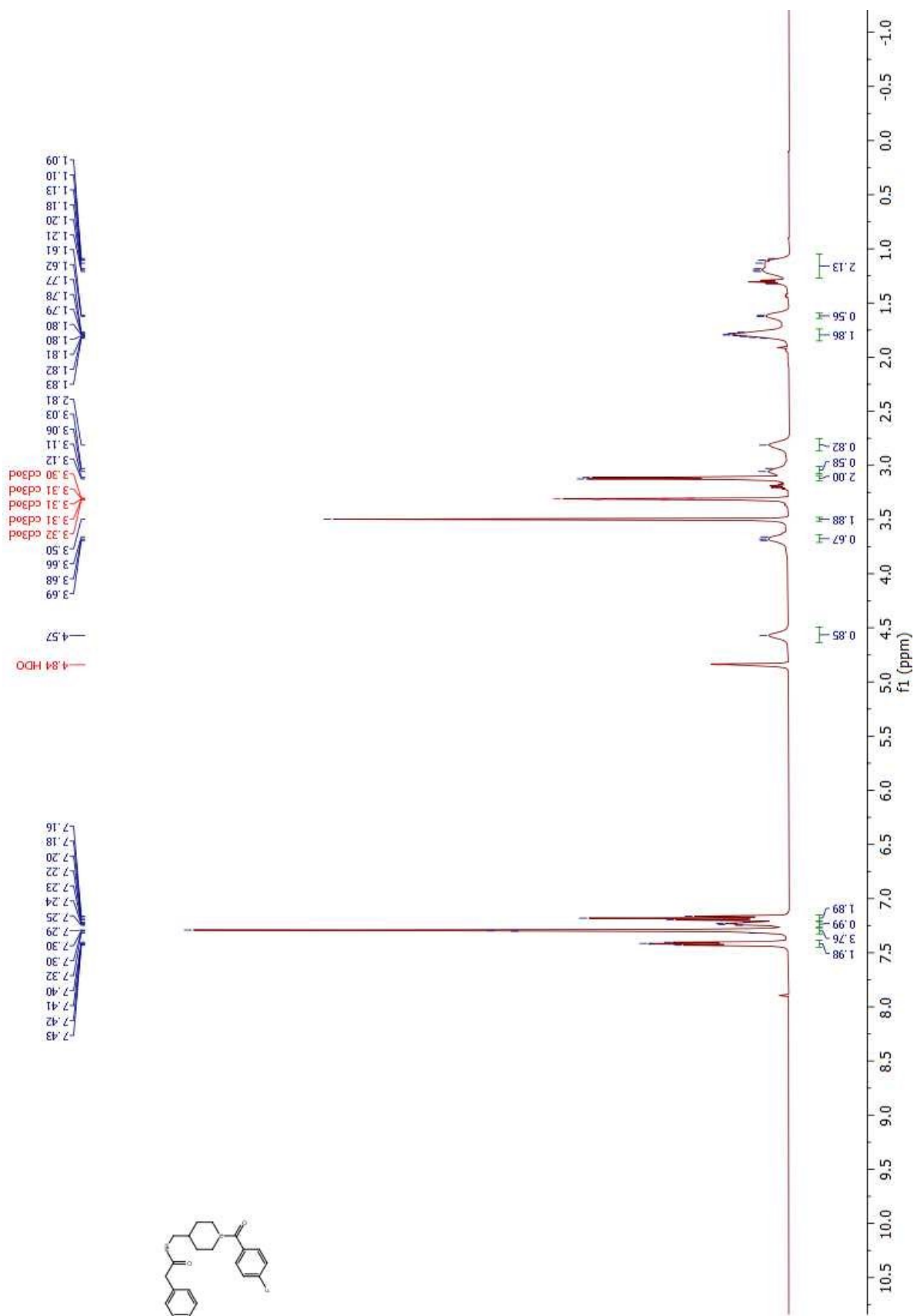


—124.97





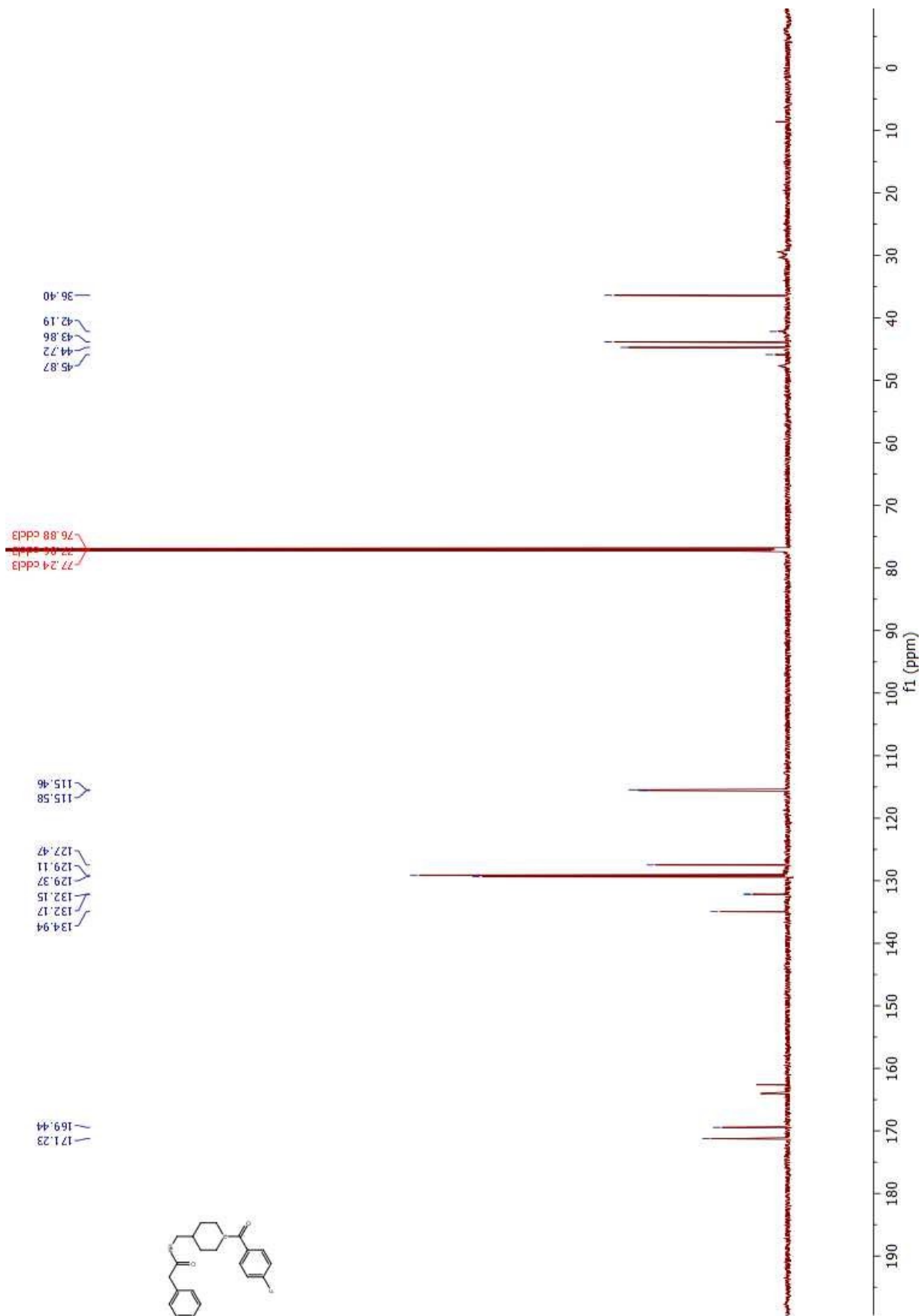


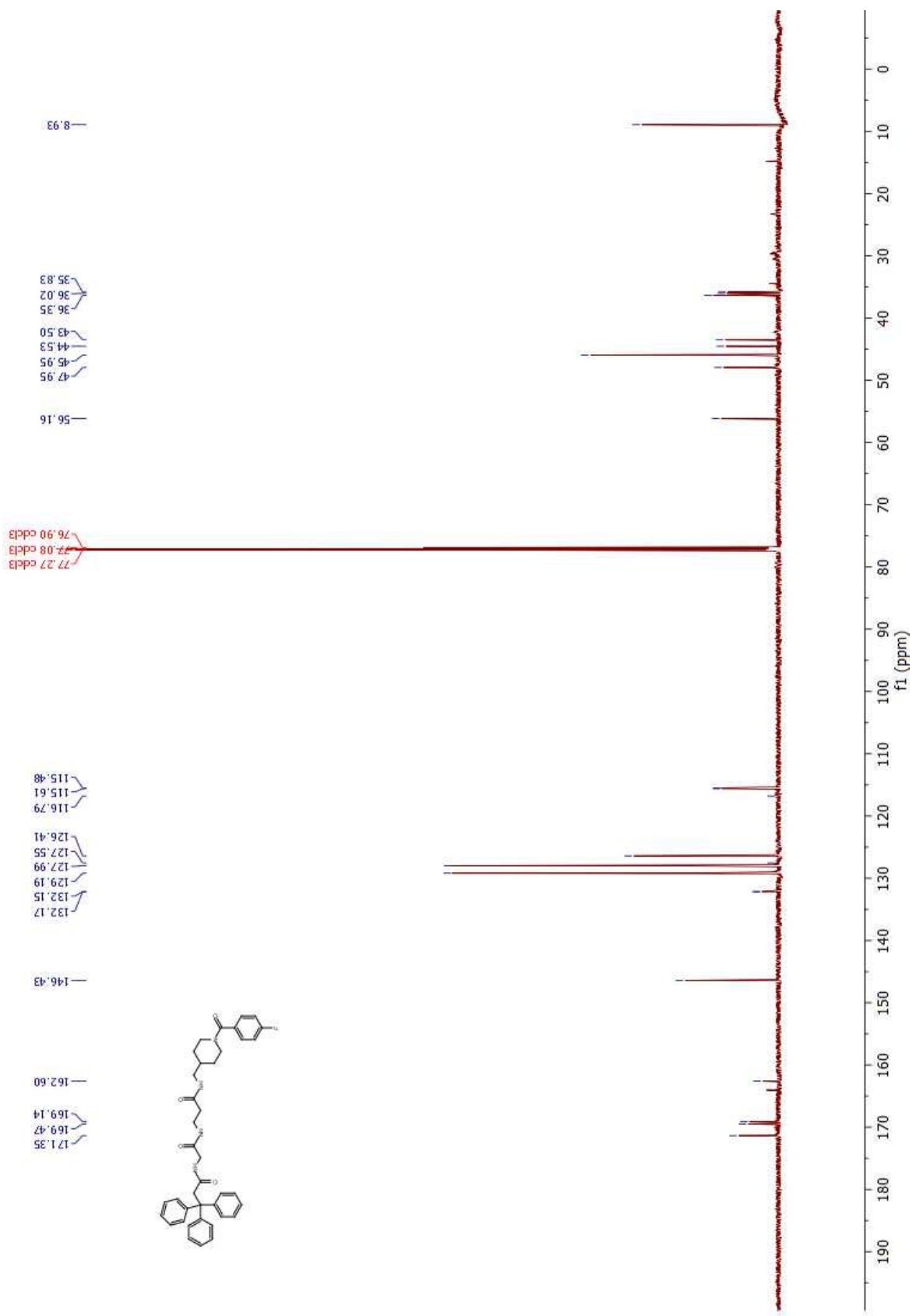


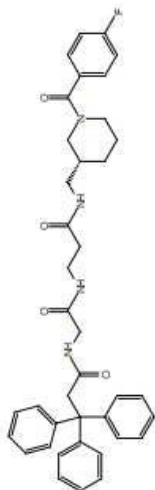


—110.37









—109.78

